CHAINS OF PARTICLES IN SHEAR FLOW

by

Isaac Yung Zung Zia, B.Sc.

A thesis submitted to the Faculty of Graduate Studies and Research of McGill University in partial fulfillment of the requirements for the degree of Doctor of Philosophy

Department of Chemistry
McGill University
Montreal, Canada

October, 1966

ACKNOWLEDGEMENTS

The author wishes to express his sincere thanks to

Dr. S. G. Mason

for his assistance, understanding and guidance as the director of this research.

Among the many others who have contributed in various ways to this thesis project, the author takes special pleasure in expressing his gratitude to the following:

the Pulp & Paper Research Institute of Canada, for financial assistance during the summers of 1962-66 and for the liberal use of its research and service facilities;

the American Chemical Society, for financial support under the Petroleum Research Fund during the session 1964-65;

Canadian Industries Limited for the CIL Fellowship during the session 1965-66;

Mr. C. Ming, Pulp & Paper Research Institute of Canada, for his help in computer programming;

Dr. H. M. Princen for assistance in the theoretical work in Appendix V:

Dr. R. G. Cox for assistance in theoretical derivations in Part II and many valuable suggestions;

Mr. N. Wynn for assistance in film analysis;

Mr. C. P. Henry for experimental assistance in Part III;

and his fellow graduate students of the Physical Chemistry Division, Pulp & Paper Research Institute of Canada, for their encouragement and useful discussions.

ABSTRACT

Based on the creeping motion and lubrication equations, a theory for the behaviour of a straight chain consisting of a number of rigid spheres in shear flow was developed. When the spheres are in contact with one another, the chain should behave like a single rigid rod; quantitative confirmation was provided at low velocity gradients by experiments with chains of spheres formed in an electric field. At high gradients the chains broke. The periodic stretching of chains with non-zero gap width was in qualitative agreement with the theory.

Chains of spheres held together by liquid menisci behaved like flexible threads and formed disordered aggregates at high velocity gradients. Aggregates of discs (rouleaux) behaved like deformable rods and were easily broken as the discs slid apart. Fore-aft symmetrical chains of non-uniform spheres and symmetrical but non-linear aggregates of spheres and aggregates of rods were also studied.

FOREWORD

This thesis describes one of a continuing series of investigations conducted in this laboratory on the behaviour of various suspensions to provide basic knowledge on the rheology and stability of a variety of important suspensions such as fibres in water (used in papermaking) and blood. The present work extends the studies from single particles and their interactions to ordered aggregates of rigid particles possessing various degrees of flexibility in shear flow.

The arrangement of the thesis requires some explanation. The original subject of the thesis research was coalescence and aggregation in two-dimensional dispersions of fluid drops (Appendices III and IV). Unfortunately, this work did not turn out to be as successful as was expected. An interesting experimental technique was developed, nevertheless, and some useful experimental and theoretical work was done; although not considered to be publishable as it now stands it has been written up for record purposes and is presented in Appendices III and IV. The related study (The Measurement of Interfacial Tension from the Shape of a Rotating Drop) is given as Appendix V in which form it is being published in the Journal of Colloid and Interfacial Science.

The main body of the thesis (Parts I to IV) is concerned mainly with chains of particles in shear flow. Parts II and III have been written in a form suitable for publication in a scientific journal with little or no further modification. Thus, each of this two parts is complete with its own abstract, introduction, discussion and references. Certain additional details which will not be published are given in Appendices I and II.

TABLE OF CONTENTS

Page

APPENDIX III (continued)

APPENDIX IV

DETAILS OF APPENDIX III

APPENDIX V

MEASUREMENT OF INTERFACIAL TENSION FROM THE SHAPE OF A ROTATING DROP

Page

APPENDIX V (continued)

LIST OF TABLES

LIST OF FIGURES

PART I

GENERAL INTRODUCTION

Physical properties of suspensions such as their rheology and stability depend on the behaviour of single particles and their interactions with one another. In very dilute suspensions of neutrally buoyant particles, the particles are far apart and there is little particle interaction. With increasing particle concentration, however, the suspensions are influenced both by interactions and by aggregate formation. The main body of this thesis describes theoretical and experimental investigations of ordered aggregates of rigid particles in simple shear Couette flow.

Earlier studies in this laboratory have dealt with the translational and rotary motions and orientations of rigid spheres[1], rods[2,3], and discs[4] in Couette flow. Numerous experiments have confirmed Jeffery's theory[5] for rigid ellipsoids, provided that the true particle axis ratio r_p is replaced by an experimentally determined equivalent ellipsoidal axis ratio r_e. Interactions of rigid spheres[3] and rods[2] and the behaviour of flexible fibres[6-8] and deformable drops[9-11] in Couette flow have also been studied; these works have recently been reviewed in detail by Goldsmith and Mason[12]. The present investigation deals primarily with chains of particles such as spheres and discs suspended in a liquid having zero stiffness and zero tensile strength. These chains were provided with a finite tensile strength by bridging the gaps between the spheres with menisci of a second immiscible liquid. The aggregates thus formed are of interest in connection with various aspects of the flow of suspensions, non-separating doublets of spheres[3], the bending of fibres[8] and breaking of macromolecules[13,14] in shear flow and other rheological properties of such systems.

A theoretical treatment of the behaviour of chains of spheres in shear Couette flow is presented in Part II. The theory is based on the Navier-Stokes equation in the creeping flow regime, where inertial effects are negligible and the fluid is incompressible

$$\nabla p = \eta_o \nabla^2 \underset{\sim}{U}$$

$$\nabla \cdot \underset{\sim}{U} = 0 \ ;$$

p is the pressure in the fluid, η_o the fluid viscosity and $\underset{\sim}{U}$ the fluid velocity. In this regime of flow the equations are also represented by the hydrodynamic lubrication equations[15-17].

If the spheres are in contact with one another, the theory predicts that the chain should rotate as a rigid body, without relative rotation of the spheres and without bending, in a spherical elliptical orbit similar to that predicted by Jeffery[5] for a rigid prolate spheroid. When there are small gaps between the spheres, the chain length should vary periodically between a minimum when the chain is oriented at right angle to the direction of shear flow and a maximum when parallel to it while chain bending should be progressive in general. When a second immiscible liquid is introduced to bridge the gaps, both chain stretching and bending increase with decreasing viscosity of the fluid introduced at any given gap width. No attempt was made, however, to take into account the effect of interfacial tension.

Part III provides an experimental test of the theory of rotation of linear chain of spheres developed in Part II and, in addition, includes studies of more complicated aggregates. Except for the breakage at high velocity gradients, chains of spheres rotated like rigid rods and in accord with the theory developed in Part II. In addition, there was qualitative agreement between the theory and experiment for chain stretching.

Chains of spheres held together by interfacial tension behaved like flexible threads or fibres in Couette flow; the flexibility increased with increasing velocity gradient and the number of spheres in the chain. However, the experiments were limited to low velocity gradients since three-dimensional aggregates formed at high gradients.

Aggregates of discs rotated like deformable cylinders. They were distorted from linearity in shear flow and finally broken as the discs slid apart. Aggregates of rods and non-linear but symmetrical aggregates of spheres were also studied.

General discussion, suggestions for further research and claims to original research form the last section (Part IV) of the main body of the thesis.

REFERENCES

1. Trevelyan, B.J. and Mason, S.G., J. Colloid Sci., 6, 354 (1951).
2. Mason, S.G. and Manley, R.St.J., Proc. Roy. Soc., A238, 117 (1956).
3. Bartok, W. and Mason, S.G., J. Colloid Sci., 12, 243 (1957).
4. Goldsmith, H.L. and Mason, S.G., J. Fluid Mech., 12, 88 (1962).
5. Jeffery, G.B., Proc. Roy. Soc., A102, 161 (1922).
6. Arlov, A.P., Forgacs, O.L. and Mason, S.G., Svensk Papperstidn., 61(3), 61 (1958).
7. Forgacs, O.L. and Mason, S.G., J. Colloid Sci., 14, 457 (1959).
8. Forgacs, O.L. and Mason, S.G., J. Colloid Sci., 14, 473 (1959).
9. Bartok, W. and Mason, S.G., J. Colloid Sci., 13, 293 (1958).
10. Rumscheidt, F.D. and Mason, S.G., J. Colloid Sci., 16, 210 (1961).
11. Rumscheidt, F.D. and Mason, S.G., J. Colloid Sci., 16, 238 (1961).
12. Goldsmith, H.L. and Mason, S.G., "Rheology: Theory and Applications", Vol. IV, Edited by F.R. Eirich, Academic Press, New York. (In Press 1966).
13. Harrington, R.E. and Zimm, B.H., J. Phys. Chem., 69, 161 (1965).
14. Harrington, R.E., J. Polymer Sci., Part A-1, 4, 489 (1966).
15. Goldman, A.J., Cox, R.G. and Brenner, H., Forthcoming Publication.
16. Cox, R.G. and Brenner, H., Forthcoming Publication.
17. Goldman, A.J., Cox, R.G. and Brenner, H., Forthcoming Publication.

PART II

CHAINS OF PARTICLES IN SHEAR FLOW I: RIGID SPHERES (THEORETICAL)

ABSTRACT

It has been shown on the basis of the creeping motion equations and lubrication theory that a straight chain consisting of a number of rigid spheres in contact with one another should behave in plane Couette flow like a single rigid body and that a chain of spheres with non-zero gap width should stretch periodically and in general bend progressively. Such a chain provides an interesting physical model of threads, rouleaux of red blood cells and other linear flexible structures.

1. INTRODUCTION

When an electric field is applied to a suspension of spheres in a dielectric liquid, the spheres become arranged in linear chains aligned in the direction of the field[1,2]. It occurred to us that a study of ordered aggregates of particles, prepared in this and other ways which we subsequently devised, would throw some light on several related problems in suspension rheology such as the behaviour in shear flow of non-separating doublets of spheres[3,4], of rouleaux of red-blood cells[5] and flexible threads[6-8]. Preliminary experiments showed surprisingly that linear chains of spheres rotated in shear flow like single rigid bodies even though such aggregates as a whole have neither tensile strength nor stiffness.

On the basis of the creeping motion equations and lubrication theory we have been able to demonstrate theoretically that a straight chain consisting of a number of spheres in contact with one another should rotate as a rigid body, without relative rotation of the spheres and without bending, in a spherical elliptical orbit similar to that predicted by Jeffery[9] for a rigid prolate spheroid. For chains of spheres with non-zero gap width we have derived equations for chain stretching and bending; the chain length should vary between a minimum when the chain is perpendicular to the direction of shear flow and a maximum when parallel to it, while the bending should generally be progressive. It should be pointed out that although definite equations are obtained for such quantities, the equations contain unknown constants so that some of the conclusions are qualitative.

Tests of the theory and experiments on more complicated particle chains are considered in the following Part[10].

2. THEORETICAL PART

(a) General

Consider the motion of any aggregate of neutrally buoyant particles in plane Couette flow where the creeping motion equations are valid. It then follows from the linearity of these equations that any change in the value of the shear changes proportionately the values of the linear and angular velocities of the particles and that a reversal of the shear reverses these motions. Thus, whether or not the aggregate breaks up depends not on the shear but on the initial positions of its member particles. It can be shown by symmetry that in Couette flow a pair of spheres either separate from each other or form a permanent doublet in periodic motion.

(b) Forces and Couples

Consider a rigid sphere B moving with a linear velocity $\underset{\sim}{u} = (u_1, u_2, u_3)$ at its centre and angular velocity $\underset{\sim}{\omega} = (\omega_1, \omega_2, \omega_3)$ in close proximity to a stationary sphere A (Figure 1a). Then according to lubrication theory[11-13], the force $\underset{\sim}{f} = (f_1, f_2, f_3)$ and couple $\underset{\sim}{g} = (g_1, g_2, g_3)$ acting on sphere B about its centre due to the relative motion are given by

$$f_1 = -\frac{3}{2}\pi\eta_o b^2 u_1 h^{-1}$$

$$f_2 = \pi\eta_o b(u_2 - \omega_3 b)\ln h \qquad (1)$$

$$f_3 = \pi\eta_o b(u_3 + \omega_2 b)\ln h$$

and

$$g_1 = h^o \quad \text{as} \quad h \longrightarrow 0$$

$$g_2 = \pi\eta_o b^2(u_3 + \tfrac{8}{5}\omega_2 b)\ln h \qquad (2)$$

$$g_3 = \pi\eta_o b^2(-u_2 + \tfrac{8}{5}\omega_3 b)\ln h\ ,$$

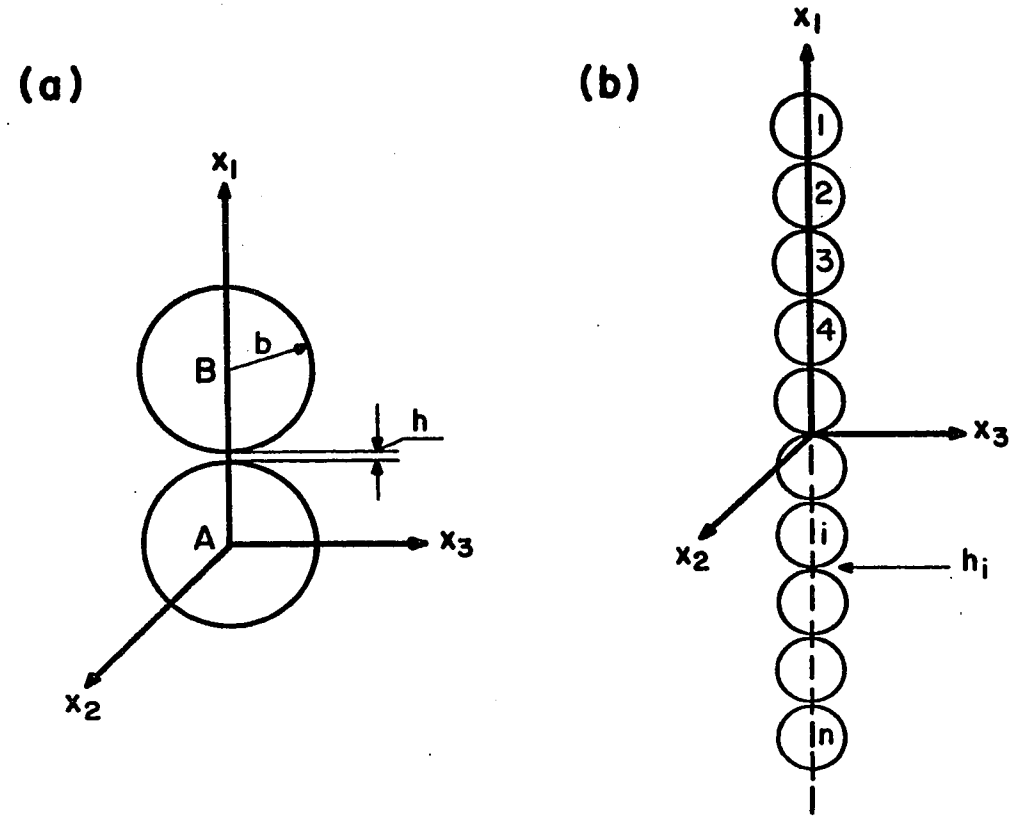

Figure 1 Chain of 2 spheres (a) and n spheres (b).

where b is the radius of the two spheres, η_o the viscosity of the surrounding fluid, and h ($\ll$ b) is the gap width between the two spheres. It follows from (1) and (2) that keeping $\underset{\sim}{f}$ and $\underset{\sim}{g}$ finite and letting $h \to 0$, u_1, u_2, u_3, ω_2 and ω_3 all tend to zero. Thus, for zero gap width there can be no relative motion between the two spheres except possibly a relative rotation of the spheres about a line joining their centres.

Hence for an initially straight chain of any number of spheres (not necessarily all of the same size), if each sphere touches its neighbouring spheres, then in shear or any other flow where the fluid velocity satisfies the creeping motion equations, the chain must remain straight and cannot break up. The only possible relative motion of the spheres is a rotation about the chain axis.

(c) Couette Flow

We now consider a straight chain of n spheres all with the same radius b and take as origin of coordinates its geometric centre (Figure 1b). Such a chain is placed in a fluid undergoing plane Couette flow for which the undisturbed fluid velocity $\underset{\sim}{U} = (U_1, U_2, U_3)$ taken relative to X_1, X_2, X_3 coordinate axes fixed in space is given by

$$U_i = A_{ij} X_j \tag{3}$$

with

$$A_{32} = \Upsilon \quad \text{and otherwise} \quad A_{pq} = 0 \,, \tag{4}$$

Υ being the velocity gradient.

It has been shown above that when h = 0 the only possible relative motion of the spheres is a rotation about the chain axis. We assume now that no such relative rotation exists. A coordinate system

(x_1, x_2, x_3) may now be chosen such that it is fixed in and moving with the chain of spheres, the x_1-axis coinciding with the chain axis (Figure 1b). The spheres in the chain are then labelled 1, 2, 3, ... , n in the negative direction of the chain axis, and the ith gap defined to be the gap between the ith and (i+1)th spheres.

The two coordinate systems (X_1, X_2, X_3) and (x_1, x_2, x_3) are related by

$$X_i = \alpha_{ij} x_j \,, \qquad x_i = \alpha_{ji} X_j \,, \tag{5}$$

where $\alpha_{ip}\alpha_{jp} = \alpha_{pi}\alpha_{pj} = \delta_{ij}$ and

$$\begin{aligned}
\alpha_{11} &= \cos\theta \,, \\
\alpha_{12} &= -\sin\theta\cos\psi \,, \\
\alpha_{13} &= \sin\theta\sin\psi \,, \\
\alpha_{21} &= \sin\theta\cos\phi \,, \\
\alpha_{22} &= -\sin\phi\sin\psi + \cos\theta\cos\phi\cos\psi \,, \\
\alpha_{23} &= -\sin\phi\cos\psi - \cos\theta\cos\phi\sin\psi \,, \\
\alpha_{31} &= \sin\theta\sin\phi \,, \\
\alpha_{32} &= \cos\phi\sin\psi + \cos\theta\sin\phi\cos\psi \,, \\
\alpha_{33} &= \cos\phi\cos\psi - \cos\theta\sin\phi\sin\psi \,;
\end{aligned} \tag{6}$$

θ, ϕ and ψ being the three Euler angles (Figure 2).

The hydrodynamic force $\underset{\sim}{f}^i$ and couple $\underset{\sim}{g}^i$ are defined to be the force and couple acting upon the first to the ith spheres inclusive as a

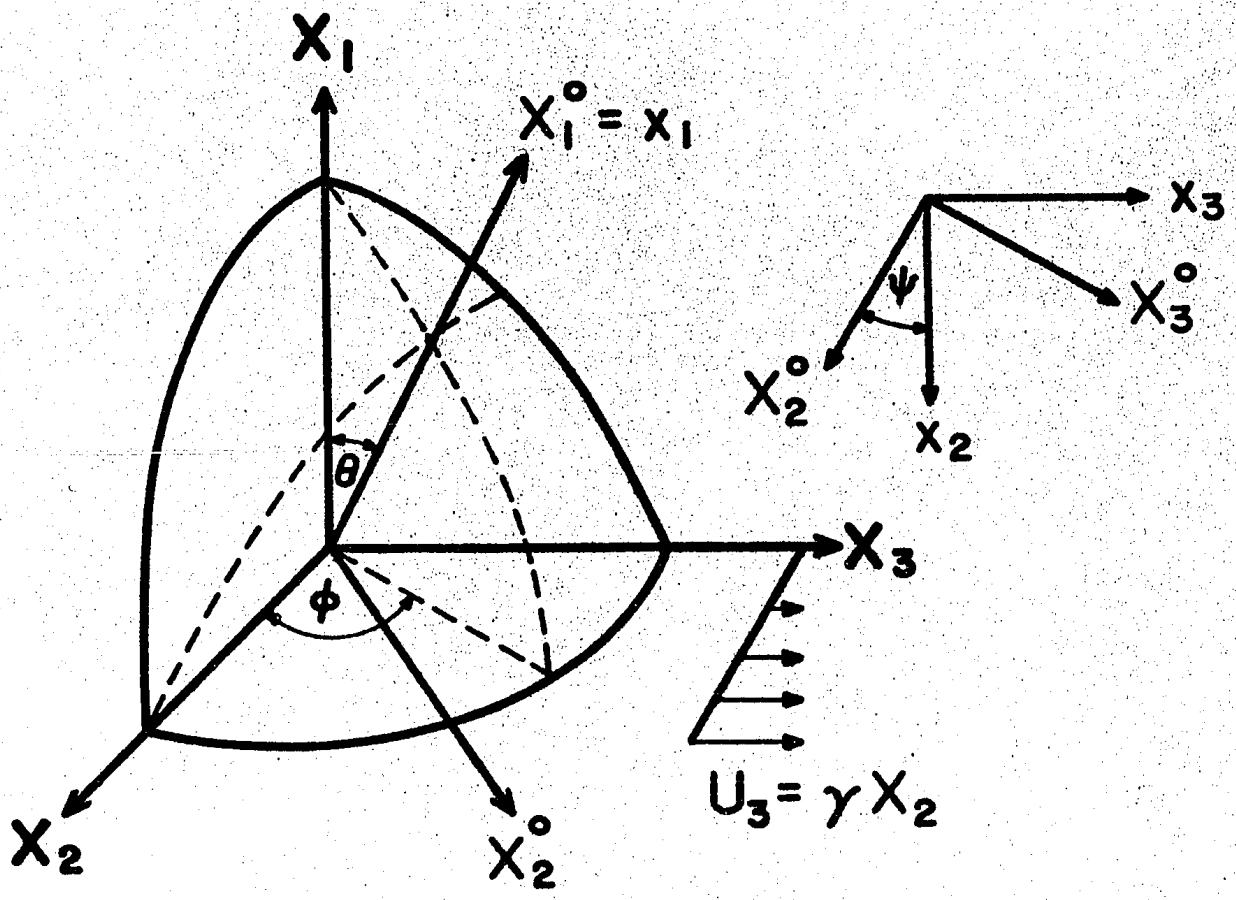

Figure 2 The relative orientations of the fixed coordinate system X_1, X_2, X_3 of the Couette flow field and the particle coordinate systems x_1, x_2, x_3 and X_1°, X_2°, X_3° so chosen that $x_1 = X_1^\circ$ coincides with the axis of symmetry and X_2° axis lies in the X_1x_1 plane. $\emptyset$ and Θ are the polar coordinates with respect to X_1 as the polar axis, while ψ is the angle between x_2 and X_2° axes.

result of the fluid motion where local forces and couples in the neighbourhood of the ith gap (i.e., those forces and couples arising from the relative motion of the ith and (i+1)th spheres) have been omitted. The couple $\underset{\sim}{g}^i$ is taken relative to the point of "contact" at the ith gap. It may then be shown[14] from the linearity of the creeping motion equations that relative to the x_1, x_2, x_3 axes, the force $\underset{\sim}{f}^i$ and couple $\underset{\sim}{g}^i$ are given by

$$
\begin{aligned}
f_1^i &= \gamma \eta_o b^2 \left[C^i_{111}(\alpha_{31}\alpha_{21}) + C^i_{122}(\alpha_{32}\alpha_{22} + \alpha_{33}\alpha_{23}) \right] \\
f_2^i &= \eta_o b^2 \left\{ \gamma \left[C^i_{212}(\alpha_{31}\alpha_{22}) + C^i_{221}(\alpha_{32}\alpha_{21}) \right] + L^i_{23}\omega_3 \right\} \\
f_3^i &= \eta_o b^2 \left\{ \gamma \left[C^i_{212}(\alpha_{31}\alpha_{22}) + C^i_{221}(\alpha_{33}\alpha_{21}) \right] - L^i_{23}\omega_2 \right\}
\end{aligned}
\tag{7}
$$

and

$$
\begin{aligned}
g_1^i &= \eta_o b^3 \left[\gamma D^i_{123}(\alpha_{32}\alpha_{23} - \alpha_{33}\alpha_{22}) + M^i_{11}\omega_1 \right] \\
g_2^i &= \eta_o b^3 \left\{ \gamma \left[D^i_{231}(\alpha_{33}\alpha_{21}) - D^i_{312}(\alpha_{31}\alpha_{23}) \right] + M^i_{22}\omega_2 \right\} \\
g_3^i &= \eta_o b^3 \left\{ \gamma \left[D^i_{312}(\alpha_{31}\alpha_{22}) - D^i_{231}(\alpha_{32}\alpha_{21}) \right] + M^i_{22}\omega_3 \right\} ,
\end{aligned}
\tag{8}
$$

where ω_1, ω_2, ω_3 are the components of the angular velocity of the chain along the x_1, x_2, x_3 axes and where the tensors $\underset{\sim}{C}^i$, $\underset{\sim}{D}^i$, $\underset{\sim}{L}^i$ and $\underset{\sim}{M}^i$ [14] depend on i and n only.

If the inertia of the chain is neglected then the total force and couple on the entire chain must vanish:

$$
\underset{\sim}{f}^n = \underset{\sim}{g}^n = \underset{\sim}{0} . \tag{9}
$$

Substituting (8) into (9) gives the following expressions for the three angular velocities:

$$M^n_{11}\omega_1 + \gamma D^n_{123}(\alpha_{32}\alpha_{23} - \alpha_{33}\alpha_{22}) = 0$$

$$M^n_{22}\omega_2 + \gamma(D^n_{231}\alpha_{33}\alpha_{21} - D^n_{312}\alpha_{31}\alpha_{23}) = 0 \qquad (10)$$

$$M^n_{22}\omega_3 + \gamma(D^n_{312}\alpha_{31}\alpha_{22} - D^n_{231}\alpha_{32}\alpha_{31}) = 0 \ .$$

Eliminating α_{ij} and ω_i from (7) and (8) by using (6) and (10) and introducing a new coordinate system X^o_1, X^o_2, X^o_3 such that

$$X^o_1 = x_1$$

$$X^o_2 = x_2\cos\psi - x_3\sin\psi \qquad (11)$$

$$X^o_3 = x_2\sin\psi + x_3\cos\psi$$

lead to the final equations for the components of the hydrodynamic force $\underset{\sim}{F}^i$ and couple $\underset{\sim}{G}^i$ (about the point of contact at the ith gap) along X^o_1, X^o_2, X^o_3 axes:

$$F^i_1 = \eta_o \gamma b^2 A^i_1 \sin^2\theta\sin\phi\cos\phi \qquad (12a)$$

$$F^i_2 = \eta_o \gamma b^2 A^i_2 \sin\theta\cos\theta\sin\phi\cos\phi \qquad (12b)$$

$$F^i_3 = \eta_o \gamma b^2 \sin\theta(A^i_3 \sin^2\phi + A^i_4 \cos^2\phi) \qquad (12c)$$

and

$$G^i_1 = \eta_o \gamma b^3 A^i_5 \cos\theta \qquad (13a)$$

$$G^i_2 = \eta_o \gamma b^3 \sin\theta(A^i_6 \sin^2\phi + A^i_7 \cos^2\phi) \qquad (13b)$$

$$G^i_3 = \eta_o \gamma b^3 A^i_8 \sin\theta\cos\theta\sin\phi\cos\phi \ , \qquad (13c)$$

where the A^i's depend on i and n only[14].

In plane Couette flow a chain at $\Theta = 0$ rotates about the x_1-axis with angular velocity $\gamma/2$, the couple G_1^i then being zero for all i since the shear is equivalent to a rotation of $\gamma/2$ together with a flow which cannot produce any couple on any sphere in the chain. Thus from (13a)

$$A_5^i = 0 \tag{14}$$

and hence

$$G_1^i = 0 \quad \text{for all } \Theta \text{ and } i. \tag{15}$$

This shows that the assumption made earlier that there is no relative rotation of the spheres about the chain axis is indeed correct.

It should be observed that while (10) was obtained for a chain of equal sized spheres, the arguments could nevertheless be used to prove (10) for general axisymmetric bodies with fore-aft symmetry. Similarly, (12), (13), (14) and (15) can also be shown to apply to straight chains of spheres of different sizes so long as the chain as a whole possesses fore-aft symmetry.

(d) Rotation of Chain

Since the position of the chain with respect to the X_1, X_2, X_3 axes is determined by the angles Θ, ϕ and ψ, it is convenient to express the chain's equation of motion in terms of these quantities alone. Thus, upon differentiating (6) with respect to time t and expressing $d(\alpha_{ij})/dt$ in terms of ω_i one may transform[14] (10) into the form

$$\frac{d\Theta}{dt} = \frac{\gamma(D^n_{231} - D^n_{312})}{M^n_{22}} \sin\Theta\cos\Theta\sin\phi\cos\phi \tag{16a}$$

$$\frac{d\phi}{dt} = \frac{\gamma}{M^n_{22}} (D^n_{231}\cos^2\phi + D^n_{312}\sin^2\phi) \tag{16b}$$

$$\frac{d\psi}{dt} = \gamma\cos\theta\left[\frac{D^n_{123}}{M^n_{11}} - \frac{1}{M^n_{22}}(D^n_{312}\sin^2\phi + D^n_{231}\cos^2\phi)\right] . \qquad (16c)$$

The spin of the chain about x_1-axis is given by

$$\omega_1 = d\psi/dt + \cos\theta(d\phi/dt) = \frac{\gamma D^n_{123}}{M^n_{11}}\cos\theta . \qquad (17)$$

It can be shown further[14] that the above equations of motion may be put in the form

$$\frac{d\theta}{dt} = \gamma B_1 \sin\theta\cos\theta\sin\phi\cos\phi , \qquad (18a)$$

$$\frac{d\phi}{dt} = \gamma(B_2\sin^2\phi + B_3\cos^2\phi) , \qquad (18b)$$

$$\omega_1 = \frac{\gamma}{2}\cos\theta , \qquad (18c)$$

where

$$B_1 = \frac{D^n_{231} - D^n_{312}}{M^n_{22}} , \qquad B_2 = \frac{D^n_{312}}{M^n_{22}} , \qquad B_3 = \frac{D^n_{231}}{M^n_{22}} . \qquad (19)$$

If we let

$$B_3/B_2 = r_e^2 , \qquad (20)$$

then it can be shown[14] that

$$B_1 = \frac{r_e^2 - 1}{r_e^2 + 1} , \qquad B_2 = \frac{1}{r_e^2 + 1} , \qquad B_3 = \frac{r_e^2}{r_e^2 + 1} . \qquad (21)$$

The equation of motion (18) for the chain then becomes identical to Jeffery's equations[9] for an ellipsoid of axis ratio r_e. One therefore refers to this quantity r_e as the equivalent ellipsoidal axis ratio of the chain of spheres. Like (10), (18) also applies to general axisymmetric bodies with fore-aft symmetry.

(e) Chain Stretching and Bending

We now consider a straight chain of spheres in which the member spheres are separated by small but finite gaps. We let $h_i (\ll b)$ be the gap width between the ith and (i+1)th spheres. If the inertia of the chain is neglected, there can be no net force or couple acting on the chain or any part of it and therefore the hydrodynamic force $\underset{\sim}{F}^i$ and couple $\underset{\sim}{G}^i$ acting on any section of the chain from the first to the ith spheres must be balanced by the force $\underset{\sim}{\mathcal{F}}^i$ and couple $\underset{\sim}{\mathcal{G}}^i$ (about the point of "contact" at the ith gap) due to the relative motion between the ith and the (i+1)th spheres:

$$\underset{\sim}{F}^i + \underset{\sim}{\mathcal{F}}^i = 0$$

and (22)

$$\underset{\sim}{G}^i + \underset{\sim}{\mathcal{G}}^i = 0 \,.$$

The forces and couples along the X_1^o, X_2^o, X_3^o axes due to the relative motion of the ith and the (i+1)th spheres are known from lubrication theory[11-13]:

$$\mathcal{F}_1^i = -\frac{3}{2}\pi\eta_o b^2 (V_1^i - V_1^{i+1})(h_i)^{-1} \tag{23a}$$

$$\mathcal{F}_2^i = \pi\eta_o b\left[(V_2^i - V_2^{i+1}) - b(\Omega_3^i + \Omega_3^{i+1})\right] \ln h_i \tag{23b}$$

$$\mathcal{F}_3^i = \pi\eta_o b\left[(V_3^i - V_3^{i+1}) + b(\Omega_2^i + \Omega_2^{i+1})\right] \ln h_i \tag{23c}$$

and

$$\mathcal{G}_1^i = O(h_i)^o \qquad \text{as} \qquad h_i \longrightarrow 0 \tag{24a}$$

$$\mathcal{G}_2^i = \frac{3}{5}\pi\eta_o (\Omega_2^i - \Omega_2^{i+1}) b^3 \ln h_i \tag{24b}$$

$$\mathcal{G}_3^i = \frac{3}{5}\pi\eta_o (\Omega_3^i - \Omega_3^{i+1}) b^3 \ln h_i \,, \tag{24c}$$

where V_1^i, V_2^i, V_3^i and Ω_1^i, Ω_2^i, Ω_3^i are the respective X_1^o, X_2^o, X_3^o components of the additional linear and angular velocities of the ith sphere (taken at its centre) due to the relative motion of spheres in the chain.

The forces $\underset{\sim}{F}^i$ and couples $\underset{\sim}{G}^i$ acting on a chain with zero gap width have already been given by (12) and (13), but they can also be used as a good approximation for chains with small gap width. Thus, by substituting (12) (13) and (23) (24) into (22) one obtains sets of equations which determine the state of the chain.

By balancing the forces F_1^i and $\mathfrak{F}_1^i$ given by (12a) and (23a) respectively, and noting that the gap width h_i is related to the relative velocity of the ith and (i+1)th spheres along the X_1^o-axis, i.e.,

$$\frac{dh_i}{dt} = V_1^i - V_1^{i+1} , \tag{25}$$

one can show[14] that

$$h_i = (h_o)_i \left[\frac{1}{C^2+1} + \frac{C^2 B_3}{(C^2+1)(B_3\cos^2\phi + B_2\sin^2\phi)} \right]^{\frac{A_1^i}{3\pi B_1}} , \tag{26}$$

where $(h_o)_i$ is h_i at $\phi = 0$ and C is a constant of integration identical to the orbit constant in Jeffery's theory[9] for rigid ellipsoidal particles. It follows from (26) that the chain length for $\theta = \pi/2$ or $C = \infty$ is given by

$$\ell = 2nb + \sum_{i=1}^{n-1} (h_o)_i \left(\frac{B_3}{B_3\cos^2\phi + B_2\sin^2\phi} \right)^{\frac{A_1^i}{3\pi B_1}} \tag{27}$$

with

$$\ell_{min} = 2nb + \sum_{i=1}^{n-1} (h_o)_i \quad \text{at} \quad \phi = m\pi \tag{28}$$

where V_1^i, V_2^i, V_3^i and Ω_1^i, Ω_2^i, Ω_3^i are the respective X_1^o, X_2^o, X_3^o components of the additional linear and angular velocities of the ith sphere (taken at its centre) due to the relative motion of spheres in the chain.

The forces $\underset{\sim}{F}^i$ and couples $\underset{\sim}{G}^i$ acting on a chain with zero gap width have already been given by (12) and (13), but they can also be used as a good approximation for chains with small gap width. Thus, by substituting (12) (13) and (23) (24) into (22) one obtains sets of equations which determine the state of the chain.

By balancing the forces F_1^i and $\mathcal{F}_1^i$ given by (12a) and (23a) respectively, and noting that the gap width h_i is related to the relative velocity of the ith and (i+1)th spheres along the X_1^o-axis, i.e.,

$$\frac{dh_i}{dt} = V_1^i - V_1^{i+1} , \tag{25}$$

one can show[14] that

$$h_i = (h_o)_i \left[\frac{1}{C^2+1} + \frac{C^2 B_3}{(C^2+1)(B_3\cos^2\phi + B_2\sin^2\phi)} \right]^{\frac{A_1^i}{3\pi B_1}} , \tag{26}$$

where $(h_o)_i$ is h_i at $\phi = 0$ and C is a constant of integration identical to the orbit constant in Jeffery's theory[9] for rigid ellipsoidal particles. It follows from (26) that the chain length for $\Theta = \pi/2$ or $C = \infty$ is given by

$$\ell = 2nb + \sum_{i=1}^{n-1} (h_o)_i \left(\frac{B_3}{B_3\cos^2\phi + B_2\sin^2\phi} \right)^{\frac{A_1^i}{3\pi B_1}} \tag{27}$$

with

$$\ell_{min} = 2nb + \sum_{i=1}^{n-1} (h_o)_i \quad \text{at} \quad \phi = m\pi \tag{28}$$

and

$$\ell_{max} = 2nb + \sum_{i=1}^{n-1} (h_o)_i (r_e)^{\frac{2A_1^i}{3\pi B_1}} \qquad \text{at} \qquad \phi = \frac{2m+1}{2}\pi \,. \tag{29}$$

A simpler alternative model is to consider the chain to behave as a rigid prolate spheroid and to calculate the axial force f_1^i from Jeffery's equations, and from this to calculate in turn the rate of approach of the ith and (i+1)th spheres using the lubrication equation for this case[15]. However, although such a method gives a value for A_1^i, it possesses a number of rather arbitrary assumptions.

From the balance of the X_2^o and X_3^o components of forces given by (12) and (23) and of couples given by (13) and (24), the equations for chain bending may be deduced[14]. Thus it may be shown that in general there exists bending in both the X_2^o and X_3^o directions. For the particular case of

$$C = \infty \qquad \text{or} \qquad \theta = \pi/2$$

and

$$\left|\ln(h_o)_j\right| \gg \left| \frac{A_1^j}{3\pi B_1} \ln\left(\frac{B_3}{B_3\cos^2\phi + B_2\sin^2\phi}\right)\right| \quad \text{for all } \phi \,, \tag{30}$$

it can be shown[14] that

$$\frac{d(\Delta X_2^o)^i}{dt} = 0 \tag{31}$$

and

$$\frac{1}{b}\cdot\frac{d(\Delta X_3^o)^i}{dt} = \sum_{j=1}^{m} \frac{T_{ij}\sin^2\phi + U_{ij}\cos^2\phi}{\ln(h_o)_j (B_2\sin^2\phi + B_3\cos^2\phi)} \,, \tag{32}$$

where $(\Delta X_2^o)^i$ and $(\Delta X_3^o)^i$ are the relative displacements of the ith sphere with respect to the (i+1)th sphere in the X_2^o and X_3^o directions respectively

and T_{ij} and U_{ij} are (m x m) matrices[14], m being n/2 for n even and (n-1)/2 for n odd. Finally, it can be shown that (32) has the following solution:

$$\frac{(\Delta X_3^o)^i}{b} = P^i \tan^{-1}(r_e \tan\phi) + Q^i\phi \ , \tag{33}$$

where P^i and Q^i [14] depend on i, n and $(h_o)_i$ only.

When there is a second fluid of viscosity η filling the gaps between the spheres, (27) and (33) become

$$\ell = 2nb + \sum_{i=1}^{n-1} (h_o)_i \left(\frac{B_3}{B_3\cos^2\phi + B_2\sin^2\phi} \right) \frac{\eta_o}{\eta} \cdot \frac{A_1^i}{3\pi B_1} \tag{34}$$

and

$$\frac{(\Delta X_3^o)^i}{b} = \frac{\eta_o}{\eta} \left[P^i \tan^{-1}(r_e \tan\phi) + Q^i\phi \right] \ . \tag{35}$$

However, for such a case one would expect (34) and (35) to be modified as a result of the forces between spheres arising from interfacial tension effects.

3. DISCUSSION

It is shown above for a general aggregate of particles in Couette flow that on the basis of the creeping motion equations (1) the motion is reversible under a reversal of shear and (2) the existence or non-existence of aggregate break-up is independent of the shear.

The motion of a straight chain of spheres with zero gap widths is shown on the basis of lubrication theory to be identical to that for a single rigid body except for a possible relative rotation of the spheres

about the chain axis. However, from symmetry considerations and from the linearity of the creeping motion equations it is seen that even such relative rotation is impossible.

When the gap widths are not zero, the chain is then capable of stretching and bending. Equation (27) indicates that stretching is periodic with a frequency twice that of the rotation about X_1-axis and that the chain length reaches a maximum when the chain is parallel to the direction of flow and a minimum when perpendicular to it.

In contrast to chain stretching, the chain bending as given by (33) is generally progressive, since $(\Delta X_3^o)^i/b$ increases by $2\pi(P^i + Q^i)$ when ϕ increases by 2π. If for all i, $P^i + Q^i = 0$, however, the chain then bends periodically, each sphere coming back to its exact original position when ϕ changes by 2π. In another special case: $P^i = Q^i = 0$ for all i, there is no bending at all. On the other hand, (31) shows that if a chain is originally in the X_2X_3 plane ($\theta = \pi/2$), it will always remain there.

Because of the variation of h_i, there must exist large pressures within the gaps. These pressures, positive or negative (relative to the pressure at infinity) according to whether the chain is under compression or tension, may be calculated from lubrication theory by making use of (26). Thus it may be shown that the order of magnitude of such a pressure p_p is given by

$$p_p \sim \frac{\eta_o \gamma b}{h_o} , \tag{36}$$

where h_o is a typical value of $(h_o)_i$. Similarly it may be shown from lubrication theory that due to the relative rotation of the spheres and of the velocity of the spheres normal to the chain axis large pressures p_n are produced whose order of magnitude is given by

$$p_n \sim \frac{\eta_o \pi_b^{3/2}}{h_o^{3/2} \ln(h_o/b)} \cdot \qquad (37)$$

For very small h_o, p_n is much greater than p_p, showing that the greatest positive or negative pressures in the gaps are of an order of magnitude given by (37). It is seen that as $h_o \longrightarrow 0$, this pressure tends to infinity, indicating that for very small gap widths, one might expect the above theory to be no longer valid as a result of cavitation taking place in the gaps between spheres.

When there is a second immiscible fluid between the spheres, chain bending should increase with decreasing viscosity η of that fluid if the gap widths are assumed constant.

REFERENCES

1. Winslow, W.M., J. Appl. Phys., 20, 1137 (1949).
2. El-Tantawy, Y. and Mason, S.G., Forthcoming Publication.
3. Bartok, W. and Mason, S.G., J. Colloid Sci., 12, 243 (1957).
4. Manley, R.St.J. and Mason, S.G., Can. J. Chem., 33, 763 (1955).
5. Goldsmith, H.L., Science (In Press 1966).
6. Arlov, A.P., Forgacs, O.L. and Mason, S.G., Svensk Papperstidn., 61(3), 61 (1958).
7. Forgacs, O.L. and Mason, S.G., Tappi, 41, 695 (1958).
8. Forgacs, O.L. and Mason, S.G., J. Colloid Sci., 14, 473 (1959).
9. Jeffery, G.B., Proc. Roy. Soc., A102, 161 (1922).
10. This Thesis, Part III.
11. Goldman, A.J., Cox, R.G. and Brenner, H., Forthcoming Publication.
12. Cox, R.G. and Brenner, H., Forthcoming Publication.
13. Goldman, A.J., Cox, R.G. and Brenner, H., Forthcoming Publication.
14. This Thesis, Appendix I.
15. Allan, R.S. and Mason, S.G., J. Colloid Sci., 17, 383 (1962).

LIST OF SYMBOLS

A_1^i, A_2^i, ... = defined by (I-15)

A_{ij}, a_{ij} = second-order tensors which define the flow in (X_1, X_2, X_3) and (x_1, x_2, x_3) coordinates

B_1, B_2, B_3 = defined by (19) and (21)

b = radius of sphere

C = orbit constant

F_1, F_2, F_3 = hydrodynamic forces in (X_1, X_2, X_3) coordinates

f_1, f_2, f_3 = hydrodynamic forces in (x_1, x_2, x_3) coordinates

$\mathcal{F}_1$, $\mathcal{F}_2$, $\mathcal{F}_3$ = forces along X_1^o, X_2^o, X_3^o axes due to the relative motion of spheres when $h_i > 0$

G_1, G_2, G_3 = hydrodynamic couples about X_1, X_2 and X_3 axes

g_1, g_2, g_3 = hydrodynamic couples about x_1, x_2 and x_3 axes

$\mathcal{G}_1$, $\mathcal{G}_2$, $\mathcal{G}_3$ = couples about X_1^o, X_2^o and X_3^o axes due to the relative motion of spheres when $h_i > 0$

h_i, $(h_o)_i$ = gap width between the ith and the (i+1)th spheres at $\phi = \phi$ and $\phi = 0$

ℓ = chain length

$\Delta\ell$ = $\ell(\phi) - \ell(\pi/4)$

n = total number of spheres in a chain

p_n, p_p = pressures in the gap generated by relative motion of spheres in the directions normal, and parallel to the chain axis

P^i, Q^i = defined by (I-34)

r_e, r_p = equivalent ellipsoidal, and true axis ratio

t = time

T = period of rotation of the chain about X_1 axis

U_1, U_2, U_3 = fluid velocity along X_1, X_2 and X_3 axes

V_1, V_2, V_3 = additional linear velocity along X_1^o, X_2^o and X_3^o axes when $h_i > 0$

X_1, X_2, X_3 = coordinates fixed in space

X_1^o, X_2^o, X_3^o = particle coordinates with X_1^o as the axis of symmetry, see (11)

x_1, x_2, x_3 = coordinates fixed in particle with x_1 as the axis of symmetry

$(\Delta X_2^o)^i, (\Delta X_3^o)^i$ = relative displacements between the ith and (i+1)th spheres in X_2^o and X_3^o directions

a_{ij} = a tensor relating (X_1, X_2, X_3) and (x_1, x_2, x_3) coordinates, see (6)

γ = velocity gradient

η_o, η = viscosity of suspending medium, of a second immiscible fluid in the gaps

θ, ϕ, ψ = Euler angles

σ = interfacial tension

$\Omega_1, \Omega_2, \Omega_3$ = additional angular velocity about X_1^o, X_2^o and X_3^o axes when $h_i > 0$

$\omega_1, \omega_2, \omega_3$ = angular velocity about x_1, x_2 and x_3 axes

PART III

CHAINS OF PARTICLES IN SHEAR FLOW II: SPHERES, DISCS AND RODS (EXPERIMENTAL)

ABSTRACT

The behaviour of ordered aggregates of rigid spheres, discs and rods in plane Couette flow was studied.

Chains of spheres formed in an electric field behaved like rigid rods and good agreement with theory was obtained except for breakage of the chains at high velocity gradients. Chains of spheres held together by liquid menisci behaved like flexible threads and formed disordered aggregates at high gradients.

Aggregates of discs (rouleaux) behaved like deformable rods and were easily broken as the discs slid apart. Symmetrical but non-linear aggregates of spheres rotated like single spheres at low velocity gradients.

It is shown that breakage of the chains of spheres may result from cavitation of the liquid between spheres.

1. INTRODUCTION

On the basis of the creeping motion equations, it has been shown in the preceding paper[1] that a straight chain consisting of n spheres in contact with each other behaves in shear flow like a single rigid body even when there is no force holding the spheres together. Its motion is described by the equations*

$$\frac{d\theta}{dt} = \gamma B_1 \sin\theta\cos\theta\sin\phi\cos\phi \ , \tag{1}$$

$$\frac{d\phi}{dt} = \gamma(B_2\sin^2\phi + B_3\cos^2\phi) \ , \tag{2}$$

$$\omega_1 = \frac{\gamma}{2}\cos\theta \tag{3}$$

with

$$B_1 = \frac{r_e^2 - 1}{r_e^2 + 1} \ , \qquad B_2 = \frac{1}{r_e^2 + 1} \ , \qquad B_3 = \frac{r_e^2}{r_e^2 + 1} \ . \tag{4}$$

For comparison with experiment, however, it is more convenient to use the integrated forms of (1) and (2):

$$\tan\theta = \frac{Cr_e}{(r_e^2\cos^2\phi + \sin^2\phi)^{1/2}} \ , \tag{5}$$

$$\tan\phi = r_e\tan\left(\frac{2\pi t}{T}\right) \ , \tag{6}$$

where C, the spherical elliptical orbit constant, takes values from zero to infinity as θ changes from 0 to $\pi/2$ and where T, the period of rotation about the X_1-axis, is given by

$$T = \frac{2\pi}{\gamma}\left(r_e + \frac{1}{r_e}\right) \ . \tag{7}$$

---

*All symbols have the same definition as in reference (1).

A chain with non-zero gap width is also capable of stretching and bending. The stretching of the chain at $\Theta = \pi/2$ ($C = \infty$) is given by

$$\ell = 2nb + \sum_{i=1}^{n-1} (h_o)_i \left(\frac{B_3}{B_3 \cos^2\phi + B_2 \sin^2\phi} \right) \frac{\eta_o}{\eta} \cdot \frac{A_1^i}{3\pi B_1} \qquad (8)$$

and the bending by

$$\frac{(\Delta X_3^o)^i}{b} = \frac{\eta_o}{\eta} \left[P^i \tan^{-1}(r_e \tan\phi) + Q^i \phi \right] . \qquad (9)$$

Equation (8) applies to small stretching only (i.e., $(\ell - 2nb) \ll 2nb$) whilst (9) applies only to small chain bending[1]. It should also be pointed out that although A_1^i depends on i and n only and P^i and Q^i depend on i, n and $(h_o)_i$ only, they are all unknown.

A number of ordered aggregates of spheres, discs and rods was studied in plane shear Couette flow. First, straight chains of metal coated spheres were formed in an electric field to provide thread-like particles of zero stiffness and zero tensile strength. The chains of spheres were then given some tensile strength by introducing a liquid immiscible in the suspending medium such as water so that a meniscus bridged the gaps between the spheres. The chains formed in an electric field rotated in Couette flow like a rigid body[2,3] and good agreement with the theory[1,4] was obtained, though they were broken at sufficiently high velocity gradients. The chains held together by interfacial tension, however, behaved like flexible threads[5-7] except that, instead of breaking at high velocity gradients, they formed three-dimensional aggregates. While the theoretical equations did not allow quantitative comparison with experiment for chain

stretching and bending because of unknown quantities in the equations, they nevertheless provided a qualitative explanation.

Stacks of discs rotated like deformable rods; they bent easily and finally broke apart by the sliding of their faces over one another. Aggregates of rods also behaved like rigid bodies. Some non-linear but symmetrical aggregates of spheres rotated about the X_1-axis at an angular velocity of $\gamma/2$ as for single rigid spheres[2].

2. EXPERIMENTAL PART

Most of the experiments were conducted in the Couette Mark 2 apparatus[3], consisting of two steel concentric cylinders, electrically insulated from one another and rotating in opposite directions to establish a known γ in the liquid in the annulus[2]. The cylinder speeds could be adjusted so that there was no translational motion of the aggregate centre. Observations were made by viewing along the X_1-axis and photographing the field with a still or a ciné camera; when necessary a microscope was also used.

The aggregates formed with polystyrene spheres and discs[8] and nylon rods were suspended in a solution of Dow Corning silicone fluid (density 0.97 g/cm.^{3}) and Du Pont Freon-113 (1.56 g/cm.^{3}) whose density was matched to that of the particles (ca. 1.05 g/cm.^{3}) so that there was no appreciable sedimentation in the course of an experiment; the viscosity η_o of the solution was about 30 poises.

3. RESULTS AND DISCUSSION

(a) Rigid Chains of Spheres

(i) General

By applying an electric field of about 2 kv./cm. across the Couette apparatus with the cylinders stopped, spheres moved towards one another as a result of mutual electrostatic attraction and became aligned parallel to the X_2-axis; the process was facilitated by coating the spheres with aluminium to give them a large electrical conductivity and by using a 60 c.p.s. alternating field to prevent electrophoretic movement. In this way straight chains of up to 20 spheres formed. With the electric field off and shear field on, the chains rotated at low Υ as rigid bodies[2,3] in accordance with the theory presented earlier[1]; when Υ was increased the chains broke (Figure 1). Most experiments were carried out with the chains in the horizontal X_2X_3 plane ($\Theta = \pi/2$) and at values of Υ at which the chains did not break.

(ii) Rotation

The angular velocity of the chain $d\phi/dt$ reached a maximum when the chain was perpendicular to the direction of flow, i.e., $\phi = m\pi$ and a minimum when parallel to it, i.e., $\phi = (2m+1)\pi/2$, as can be seen from Figure 2a where the curve represents (6), r_e being calculated from (7) with experimentally measured T and Υ. When $\tan\phi$ was plotted against $\tan(2\pi t/T)$, a straight line was obtained with its slope equal to r_e, giving experimental verification of (6). This shows that such chains of spheres behave very similarly to rigid rods.

The relationship between the two angles Θ and ϕ for a chain of 6 spheres not in the X_2X_3 plane is shown by Figure 3 where the curve was calculated from (5) with r_e determined from (7). Fairly good agreement

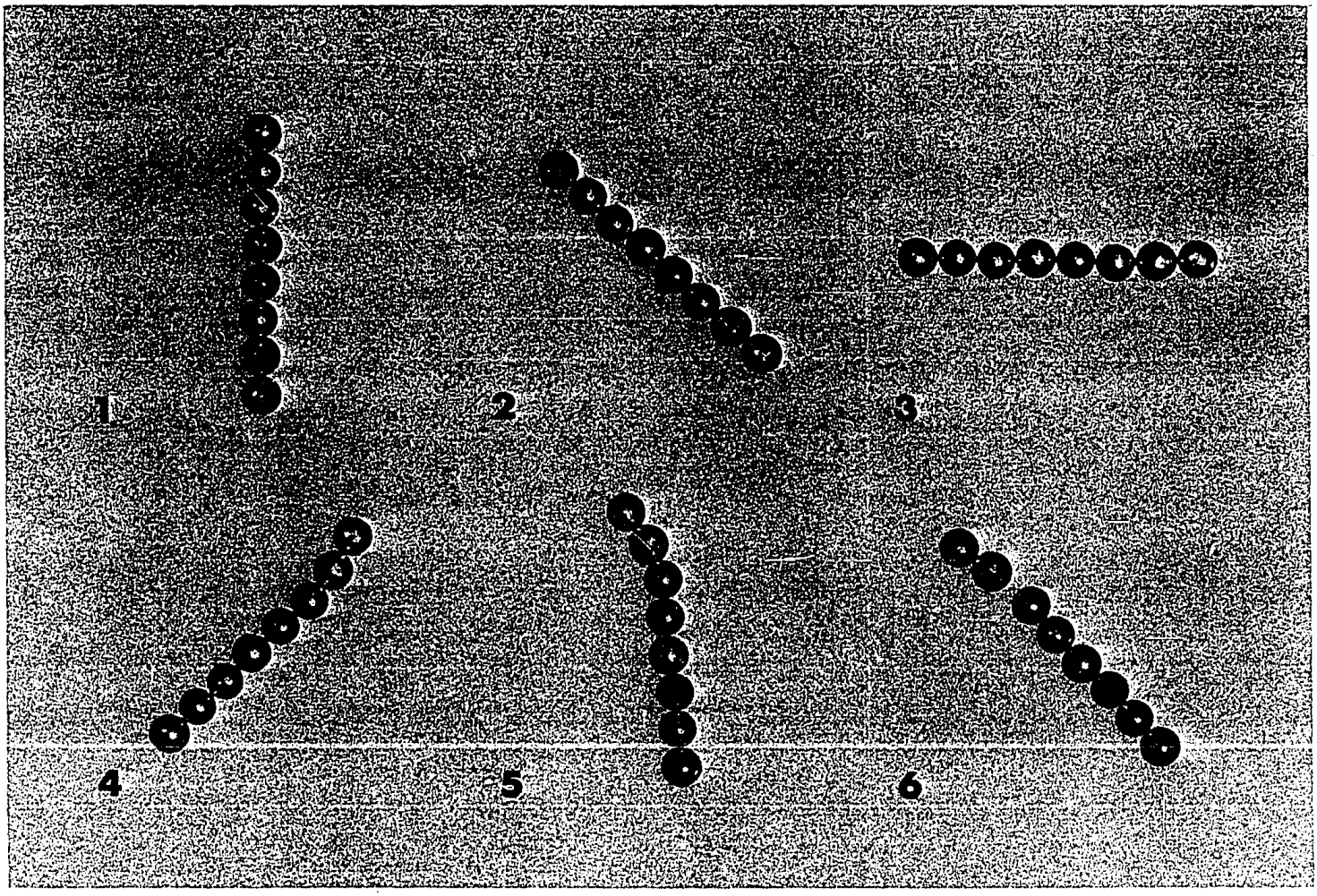

Figure 1 Linear aggregate of spheres formed by applying an electric field in the vertical (X_2) direction (1). After removing the field and starting Couette flow, the aggregate rotates counterclockwise (2,3); at a sufficiently high value of Υ (0.6 $sec.^{-1}$) it buckles (4,5) and breaks apart when $0 \leqslant \phi \leqslant \pi/2$ (6). $n = 8$, $b = 0.48$ mm.

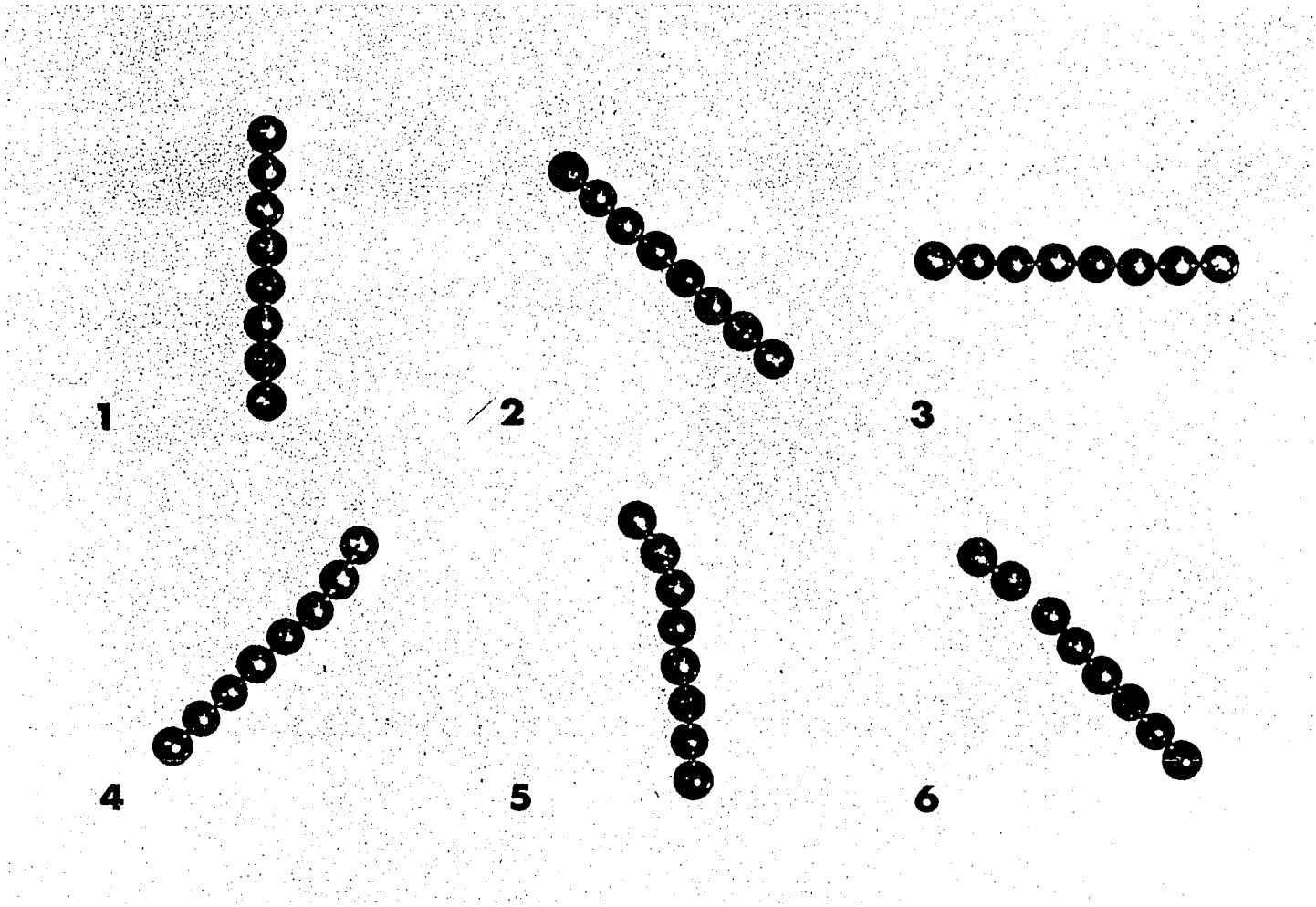

Figure 1 Linear aggregate of spheres formed by applying an electric field in the vertical (X_2) direction (1). After removing the field and starting Couette flow, the aggregate rotates counterclockwise (2,3); at a sufficiently high value of Υ (0.6 $sec.^{-1}$) it buckles (4,5) and breaks apart when $0 \leqslant \phi \leqslant \pi/2$ (6). n = 8, b = 0.48 mm.

Figure 2 The variation of ϕ with t for various aggregates.

curve	aggregate type	n	γ $sec.^{-1}$	T sec.	legend
a	chain of spheres formed in electric field	8	0.263	158.6	▼
			0.520	81.5	▽
b	ordered aggregates of spheres	3(triangular)	0.108	122.8	○
		4(tetrahedral)	0.0795	166.1	●
		6(triangular)	0.125	91.8	△
		7(hexagonal)	0.104	117.6	▲
c	rouleau	12	0.0547	259.0	□

The curves represent (6) with r_e = 6.52, 1.00 and 1.65 for a, b and c, respectively.

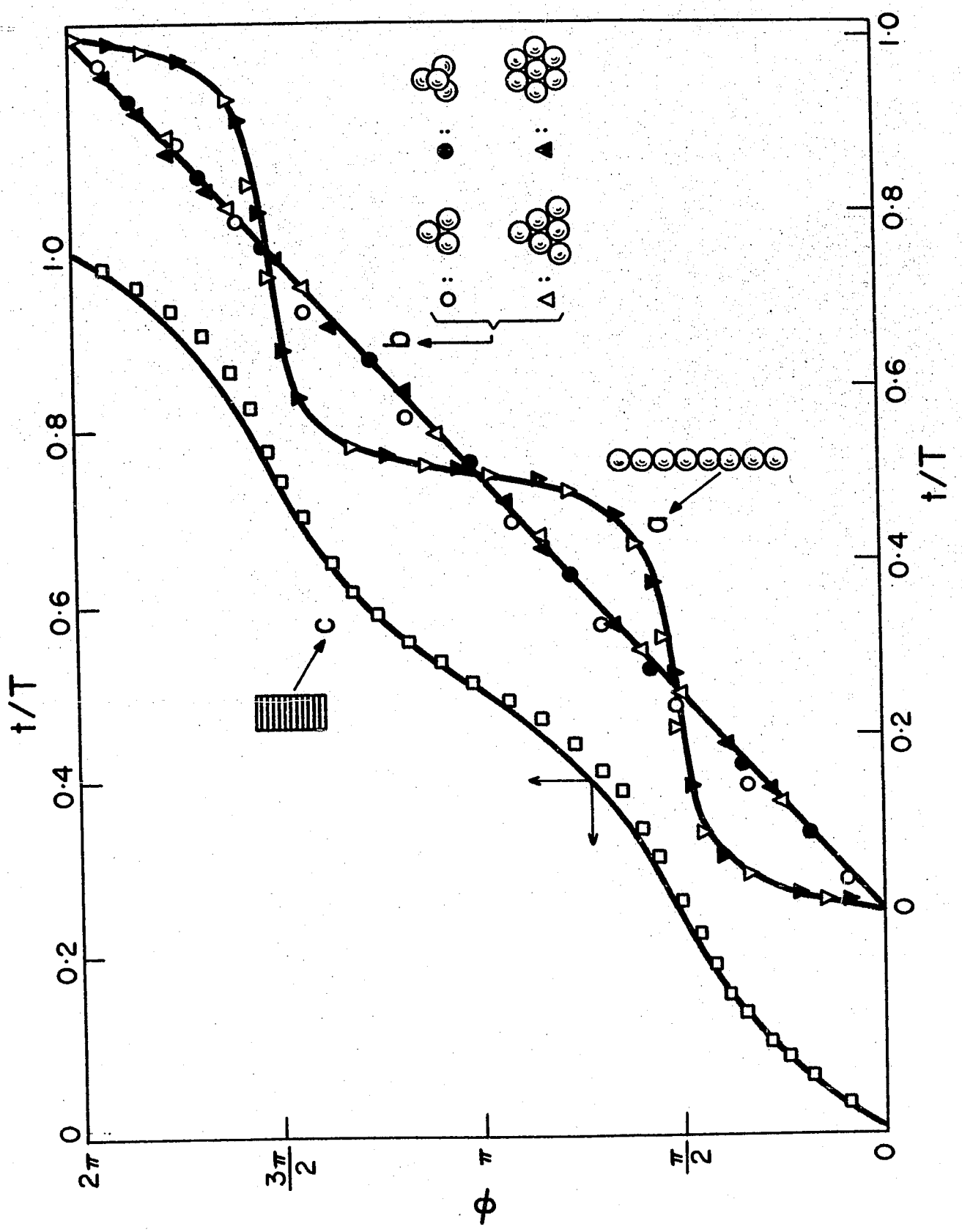
t/T
0
0·2
0·4
0·6
0·8
1·0
2π
3π/2
π
π/2
0
φ
a
b
c
t/T
0
0·2
0·4
0·6
0·8
1·0

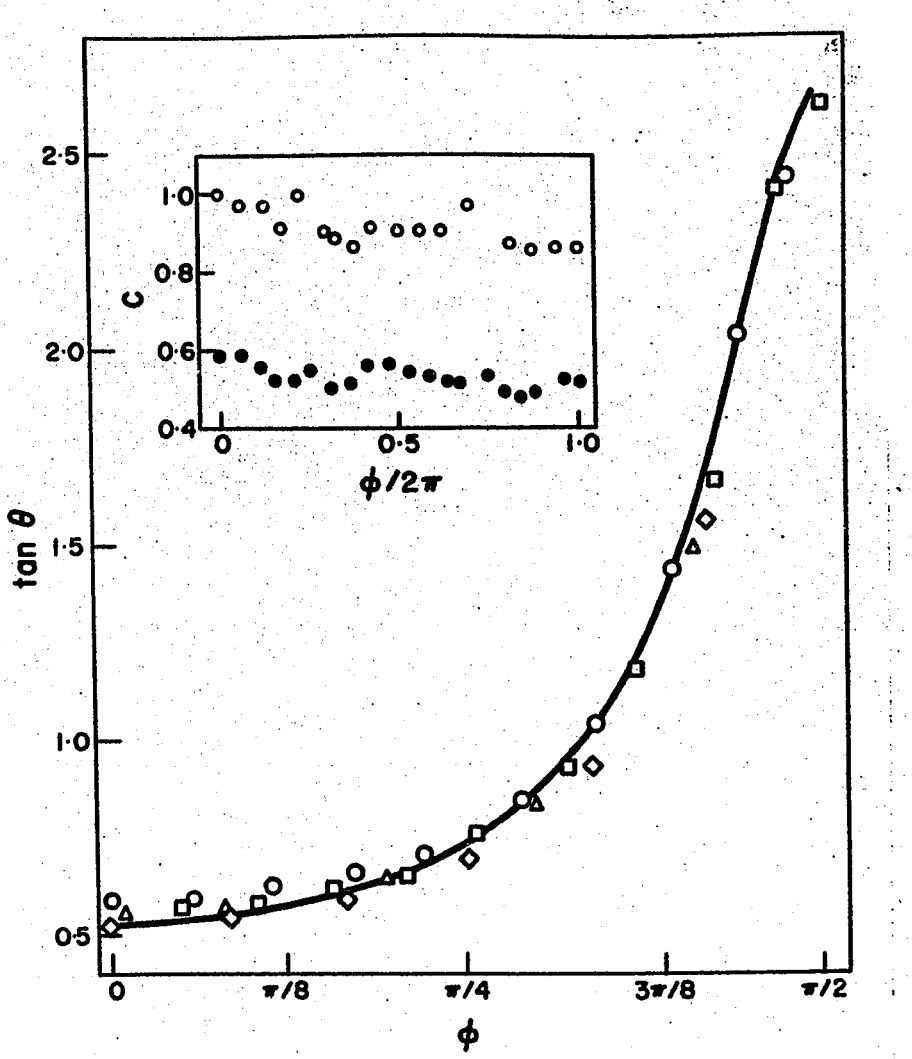

Figure 3 The variation of θ with ϕ for a chain of spheres not in the X_2X_3 plane ($\theta \neq \pi/2$). $n = 6$, $r_e = 5.05$, $\gamma = 0.170$ sec.$^{-1}$ and $C \doteq 0.53$. The curve for $C = 0.53$ was calculated from (5) with r_e from (7). Different symbols (circles, triangles, squares and diamonds for the four quadrants) were used to show the trend of decreasing C; this is further illustrated in the inset where the open circles ($C \doteq 0.93$) were obtained at several revolutions earlier than the closed circles ($C \doteq 0.53$) for the same chain and under otherwise identical conditions.

between the theory and the experiments was obtained, although the orbit constant C calculated from (5) showed a tendency to decrease (Figure 3). It is known[5] that for a single rigid rod, C is constant whereas for a flexible thread C drifts to either zero or infinity. Thus, in this respect the chain of spheres is rather similar to a flexible thread, although no noticeable bending of the chain was observed. It should be pointed out that any periodical chain stretching can only cause a periodical change of C.

For such a chain not in the X_2X_3 plane, it was found that the variation of ϕ with t satisfied (6) and that a spin ω_1 of the chain about its axis existed. The theoretical prediction that $\omega_1 = 0$ for a chain in the X_2X_3 plane ($\theta = \pi/2$) was confirmed by experiments using partially aluminium coated spheres.

(iii) Equivalent axis ratio

For a general axisymmetric body the true axis ratio r_p is defined as the ratio of the maximum body dimensions measured parallel to its axis of symmetry to that measured perpendicular. For the chain of spheres, the relation between the equivalent ellipsoidal axis ratio r_e and r_p, equalling n, is shown in Figure 4 where every point stands for an average value of r_e. Some results obtained for rigid cylinders by others[9] are included for comparison.

(iv) Chain length

As expected from (8), the chain length varied periodically between the maxima at $\phi = (2m+1)\pi/2$ and the minima at $\phi = m\pi$, when the chain lay in the X_2X_3 plane. Since the change in length was small (Table I) the data are presented in a plot of $\Delta\ell(\phi)/\Delta\ell(0)$ against ϕ to illustrate the periodical variation of the chain length with ϕ (Figure 5a). However since the quantities $(h_o)_i$ and A_1^i in (8) are unknown, no quantitative comparison with experiments

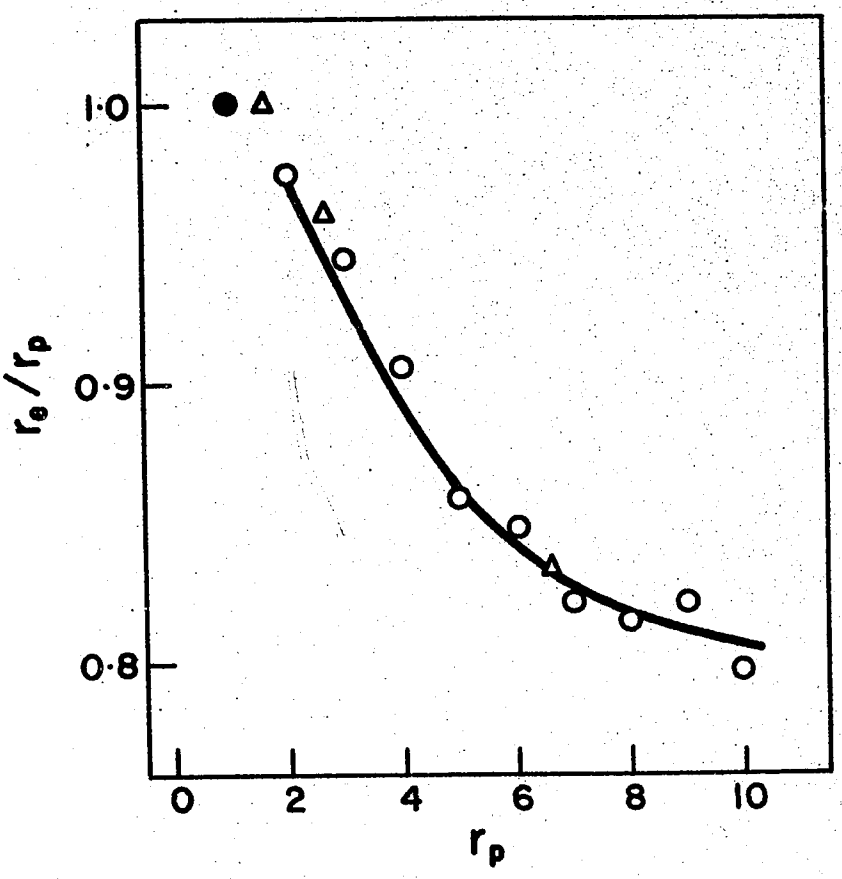

Figure 4 The relation between r_e (calculated from (7) using the measured T and γ) and $r_p (= n)$ for chains of spheres of equal size formed in electric field. All points are mean values with standard deviations less than 3%. The solid circle represents a single sphere. For comparison, the data for rigid cylinders[9] (triangles) are shown, including the value ($r_p = 1.7$) at which $r_e/r_p = 1$.

TABLE I

Variation of length of linear chain of spheres

n	γ $sec.^{-1}$	$(\ell_{max} - \ell_{min})/\ell_{min}$ %
5	0.245	4.3
	1.248	5.8
	2.263	5.5
6	0.231	3.8
7	0.271	2.3
	0.514	2.4
	0.592	3.7
8	0.263	3.1
	0.347	2.8
	0.440	3.3
	0.520	3.8
9	0.246	3.6
	0.654	5.9

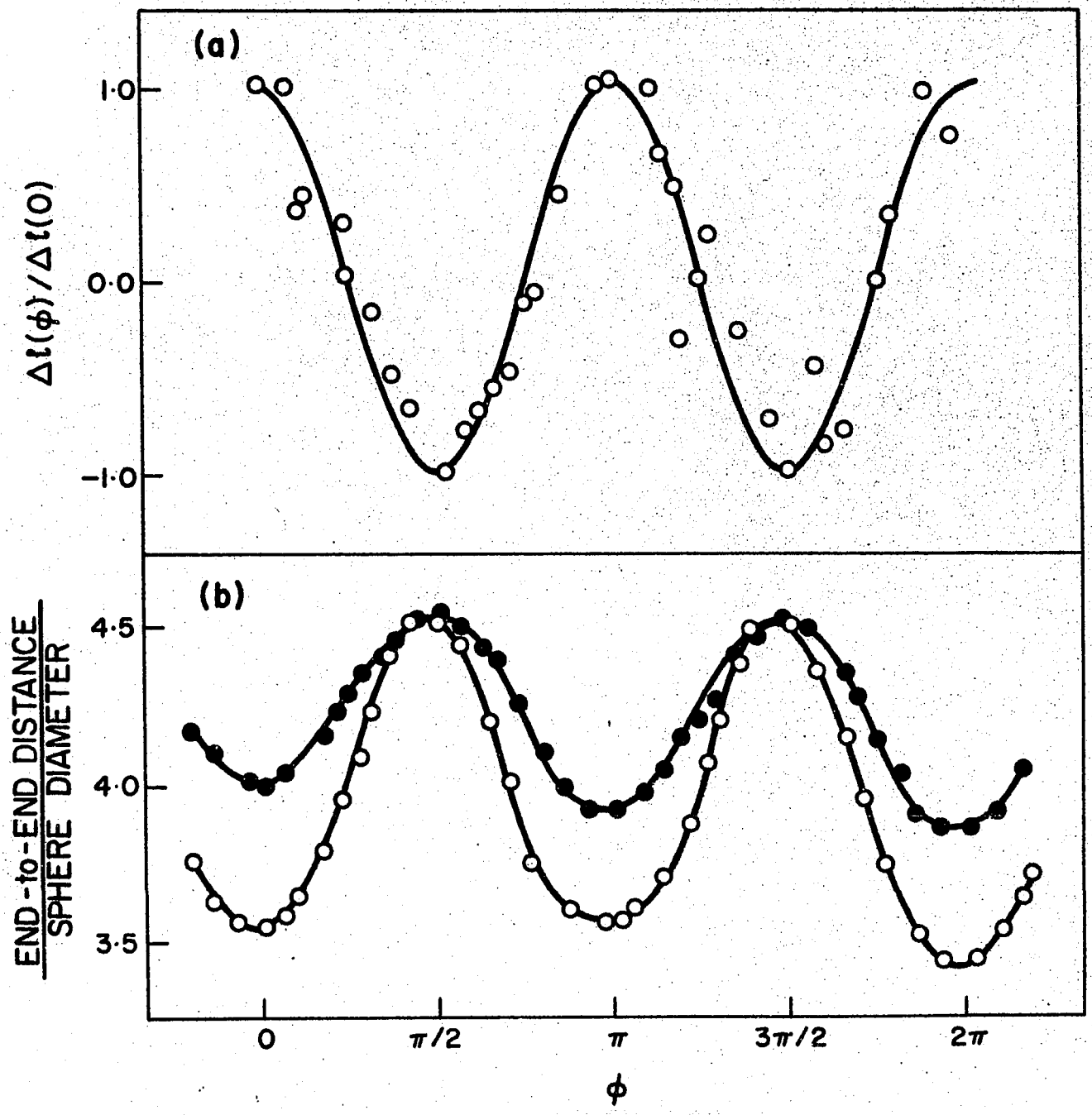

Figure 5 (a) The periodic change in length for a chain of spheres formed in an electric field. $\Delta\ell(\phi) = \ell(\phi) - \ell(\pi/4)$, $n = 8$, $\Upsilon = 0.263 - 0.520$ sec^{-1}.

(b) The variation of chain length with ϕ for a chain of four spheres held together by 0.1% Aerosol AY solution. Closed circles for $\Upsilon = 0.226$ sec^{-1}, $T = 101.3$ sec, $r_e = 3.34$ and open circles for $\Upsilon = 0.479$ sec^{-1}, $T = 50.7$ sec, $r_e = 3.59$. Increased bending reduced the chain length (end-to-end distance) at higher Υ.

can be made. These experiments were performed in the Couette Mark 4 apparatus[10] arranged for simultaneous viewing along the X_2 and X_3 directions to ensure that the chain was indeed horizontal ($\theta = \pi/2$, $C^{-1} = 0$), and that the change in length was real and not merely due to foreshortening at $\theta < \pi/2$, as the particle rotated in the orbit given by (5).

Equation (8) also predicts that for given $(h_o)_i$ chain stretching is independent of Υ. This was confirmed experimentally in the sense that no definite correlation between the variation of the chain length and Υ was found (Table I).

For a rigid particle the product $T\Upsilon$ is independent of Υ by (7). However, since deformation varies with Υ for a flexible particle, $T\Upsilon$ (if the motion of the particle is periodic to make T meaningful) may also vary with Υ. The constancy of $T\Upsilon$ was therefore used by Mason et al[5-7] as a test for the flexibility of the particle. For all the chains of spheres studied, the standard deviations for both r_e and $T\Upsilon$ were found to be less than 3%, offering another indication that such chains behaved like rigid particles.

However, the chains broke at sufficiently high Υ, the breaking always being preceded by chain bending as a rule near the centre. Although bending started when the chain was under compression ($-\pi/2 \leqslant \phi \leqslant 0$), breakup always occurred when it was under tension, i.e., when $0 \leqslant \phi \leqslant \pi/2$. Longer chains were more easily broken.

Bending was neither gradual nor smooth. The chain rotated without any noticeable bending until immediately before its breakage when a segment suddenly bent away from the chain axis (Figure 1). Such chain

breakage cannot be explained on the basis of the creeping motion equations since it has been shown[1] that the absence of breakage at low Υ would imply that there would be no breakage for any value of Υ. It was further observed that if the shear was reversed after the breaking of a chain, the motion was not reversible in that the two parts of the chain did not reattach themselves. The absence of bending in rigid chains at low Υ despite the appreciable chain stretching would suggest that in (9), P^i and Q^i are very small for all i.

(v) Fore-aft symmetry

Several fore-aft symmetrical chains (Table II) formed in an electric field with two sizes of aluminium coated spheres were also studied. They rotated in Couette flow like a rigid rod; good agreement with theory and plots similar to Figure 2 were obtained. Thus the experimental results confirmed the theoretical prediction that a fore-aft symmetrical chain consisting of unequal sized spheres should behave like a chain of uniform spheres, if the spheres are all in contact with one another. It is noted however that the ratio r_e/r_p for these fore-aft symmetrical chains (Table II) was very close to unity as they (especially the last 3 in the table) resembled prolate spheroids more closely than chains of uniform spheres.

(b) Flexible Chains of Spheres

(i) General

When a liquid immiscible with the suspending medium was introduced in the gaps to bind the spheres together by interfacial tension, the chains became very flexible. The large bending probably resulted from (1) the low viscosity of the fluid introduced, (2) a possible increase of the gap width and (3) the interfacial tension causing the chain, once bent, to

TABLE II

Linear chains with fore-aft symmetry

sphere diameters: 0.92 mm. (B) and 0.58 mm. (s)

chain structure	range of γ $sec.^{-1}$	r_p*	$\bar{r}_e$	$\bar{r}_e/r_p$
BssssB	0.0701 - 0.1008	4.53	4.54	1.00
sBs	0.0252 - 0.5461	2.26	2.22	0.98
ssBss	0.0334 - 0.6747	3.52	3.98	1.13
sBsBs	0.0666 - 0.5001	3.89	3.95	1.01

* r_p: (end-to-end distance)/(diameter of big sphere)

bend even more. Large stretching or breakage was, however, impeded by interfacial tension. The effectiveness of the interfacial tension σ in holding the chain together is determined by the size of the dimensionless parameter $\sigma/\eta_0 b\Upsilon$, which was of the order of 10^1 for the experimental conditions.

Unless otherwise stated the fluid used to hold the spheres together was a 0.1% aqueous Aerosol AY (American Cyanamid) solution, chosen to promote good wetting of the spheres. Only chains consisting of from 2 to 6 spheres were studied in detail, as large aggregates tended to become three-dimensional.

Short chains ($n=2$ or 3) were observed to be quite stiff and showed reasonably good agreement with the theory for rigid particles, a plot similar to Figure 2 being obtained. For $n \geqslant 4$ the chains bent so much that the measurement of ϕ became meaningless.

The distance between adjacent spheres in a flexible chain was seen to vary whilst the chain length as measured by its end-to-end distance varied with ϕ (Figure 5b) in a manner similar to that for a rigid chain. However, for large Υ, a greater variation of chain length (Figure 5b) resulted from larger chain bending.

(ii) Period of rotation

The orbit of a flexible chain depended on both n and Υ, the latter being limited by the formation of non-linear aggregate and chain breakage. Mason et al[5-7] have termed the orbits of flexible fibres as "rigid, springy, snake or S-turn and complex" in order of increasing fibre flexibility. According to their terminology and within the range of Υ limited by the formation of the three-dimensional non-linear aggregate, the orbits of the flexible chains were always rigid for $n = 2$, but could be springy for $n = 3$.

Snake turns (Figure 6) became possible when $n \geq 4$ and S-turns when $n \geq 5$. Thus, the flexibility increased remarkably with n.

For increasing $\dot{\gamma}$, the flexible chains with $n = 2$ showed an increase in the product $T\dot{\gamma}$ (Figure 7) similar to that for flexible threads[5-7]. For longer chains, however, either at higher $\dot{\gamma}$ or after prolonged shearing at low $\dot{\gamma}$, a point could easily be reached where the non-neighbouring spheres were brought so closely together by the bending of the chain that they were united by water and never separated again (Figure 8). The formation of such non-linear aggregate made it impossible to test the constancy of $T\dot{\gamma}$ for longer chains of spheres.

(iii) Effect of an electric field

In some cases (for $n > 4$) an electric field was superimposed on the shear field. The electric field helped to keep the chains in the horizontal X_2X_3 plane and to prevent the formation of non-linear aggregates (Figure 9). At a low electric field strength, the rotation of the chains was retarded in the first and third quadrants and speeded up in the second and fourth quadrants. The net effect, however, was an increase of the period of rotation[11]. At sufficiently high electric field strength, the rotation of the chains could be impeded so that they no longer executed complete rotations. Further increase of the field strength could cause the water bridges between the spheres to burst and split the chain.

(iv) Other bridging liquids

Chains of spheres held together by Ucon lubricant 50HB260 ($\eta = 1$ poise, Union Carbide and Carbon Corporation), glycerol (8 poise) and cyclohexanol phthalate (230 poise) were formed in the same way, though with greater difficulty, as those held together by water. Surprisingly, these chains all exhibited flexibility comparable to those with water. The more

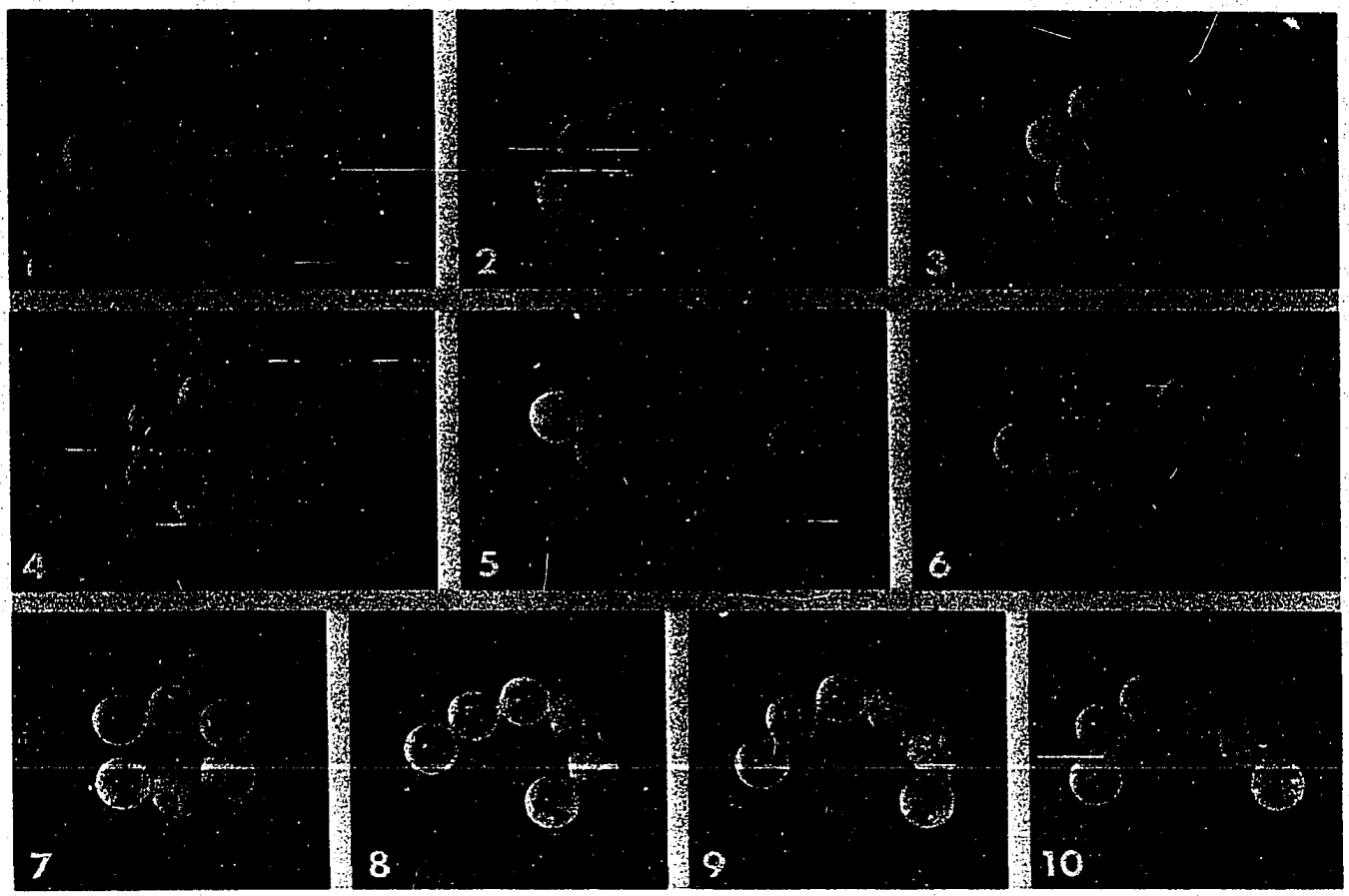

Figure 6 Rotation of a long flexible chain of spheres bridged by aqueous menisci which can be seen in the photograph. The capability of independent movement by the two ends of the chain is characteristic of the snake turn[6]. $n = 6$, $\Upsilon = 0.0986$ $sec.^{-1}$.

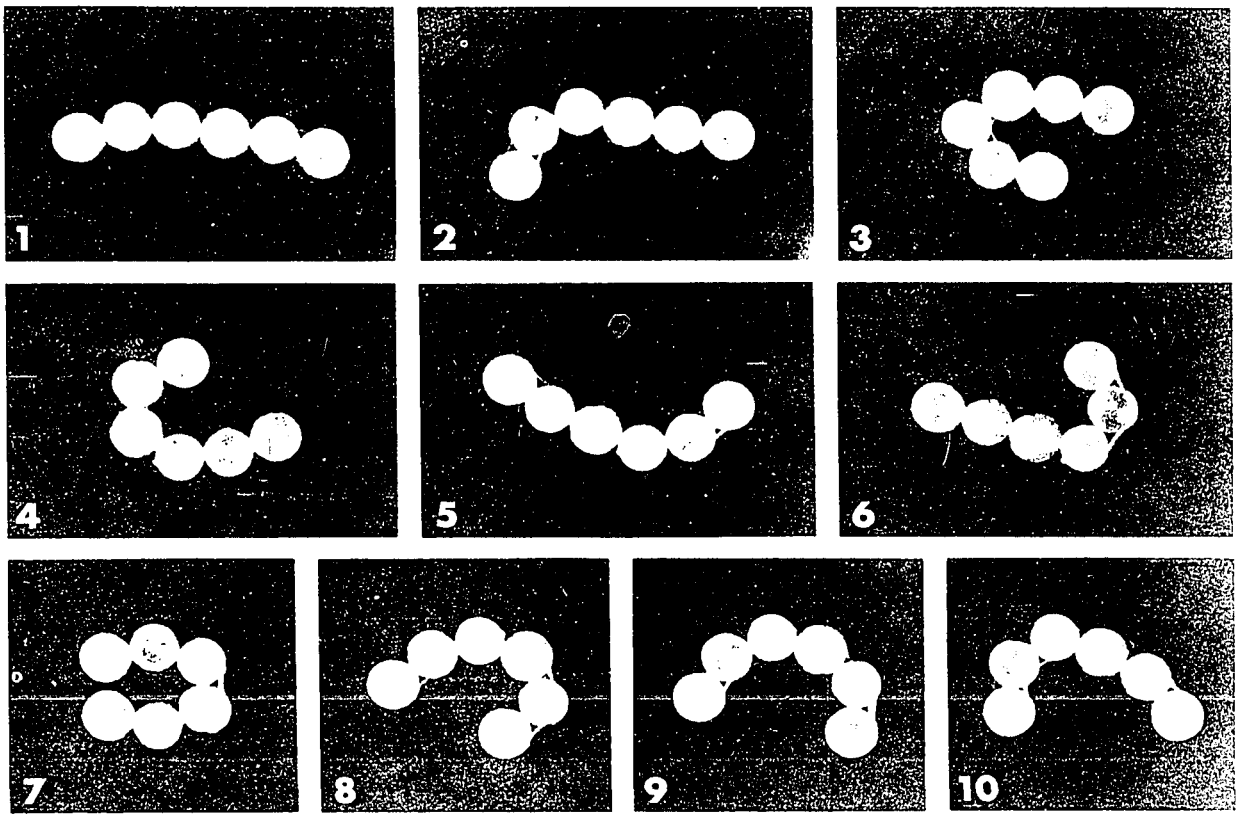

Figure 6 Rotation of a long flexible chain of spheres bridged by aqueous menisci which can be seen in the photograph. The capability of independent movement by the two ends of the chain is characteristic of the snake turn[6]. $n = 6$, $\gamma = 0.0936\ \mathrm{sec}^{-1}$.

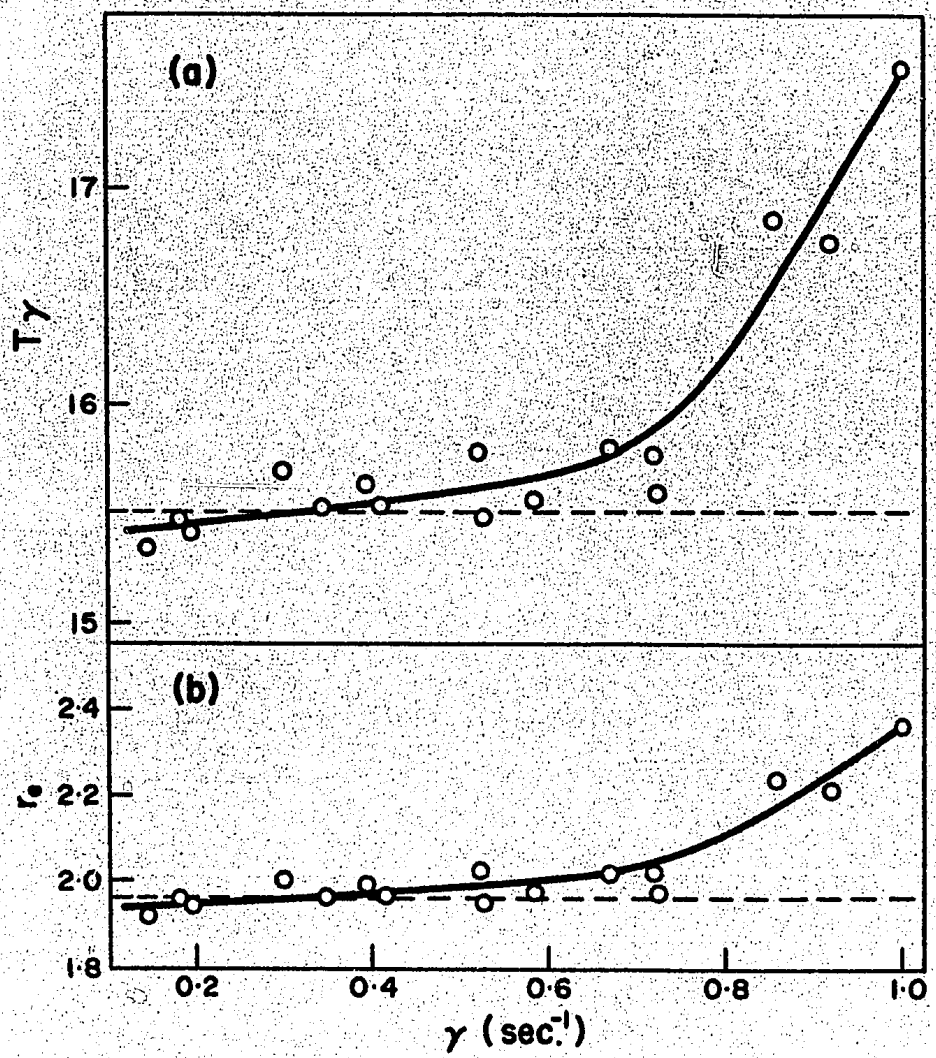

Figure 7 The variation of (a) $T\Upsilon$ and (b) r_e with Υ for a flexible chain consisting of 2 spheres bridged by a meniscus. The dashed lines represent the average values of $T\Upsilon$ and r_e for rigid chains of 2 spheres.

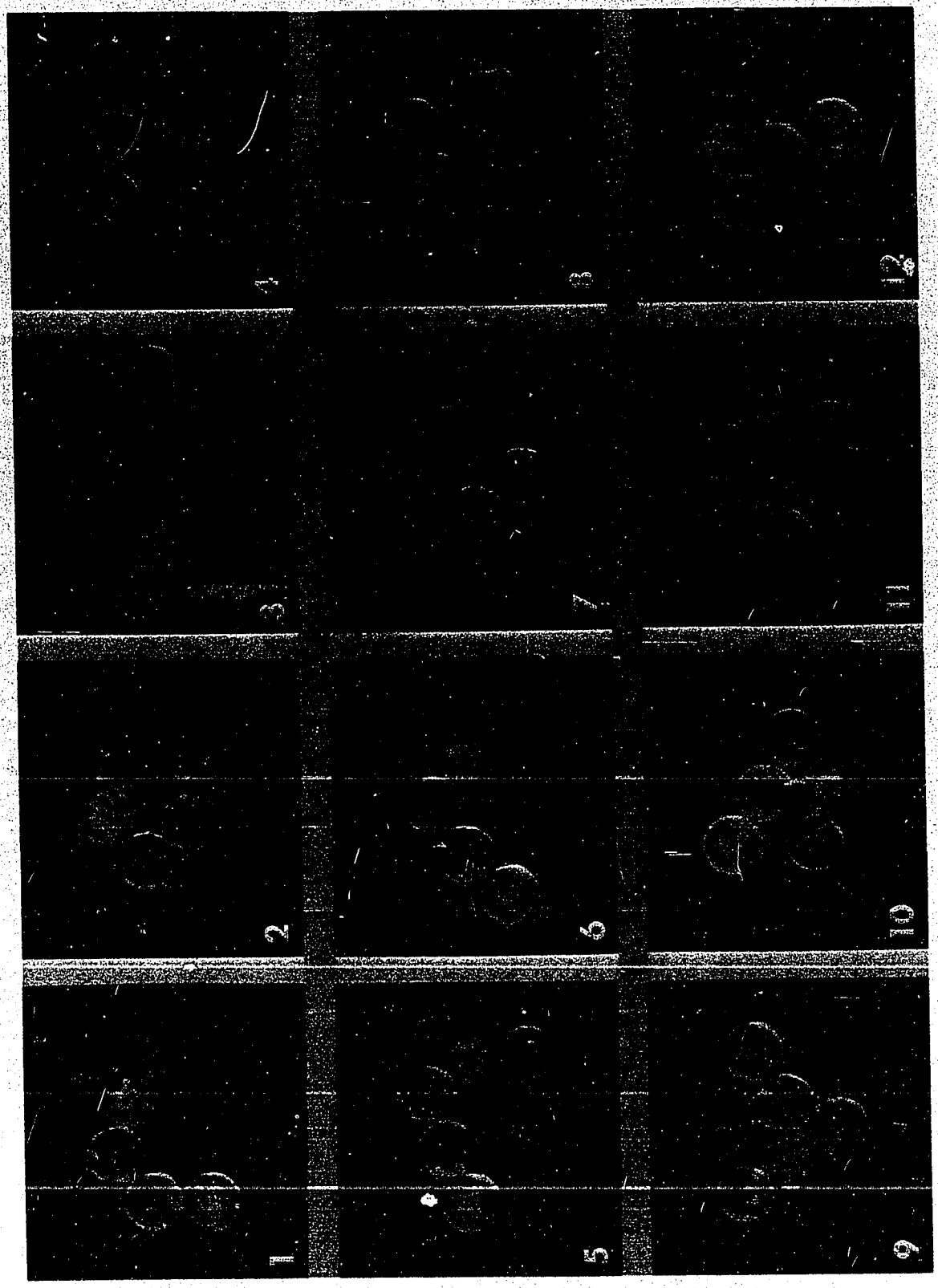

Figure 8 Formation of a non-linear aggregate by a chain of spheres bridged by menisci. $n = 5$, $\gamma = 0.170\ sec^{-1}$.

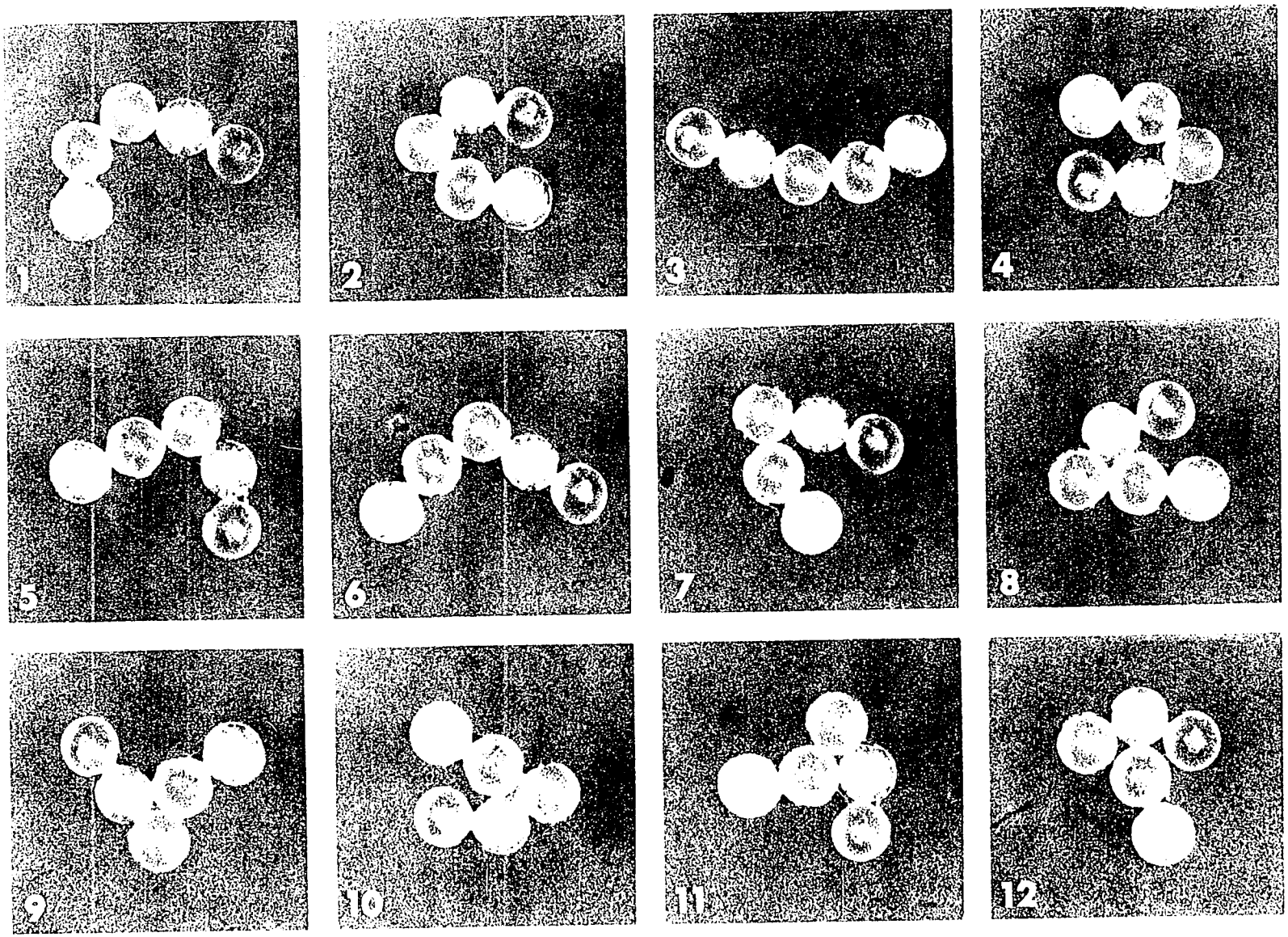

Figure 8 Formation of a non-linear aggregate by a chain of spheres bridged by menisci. $n = 5$, $\gamma = 0.170$ sec^{-1}.

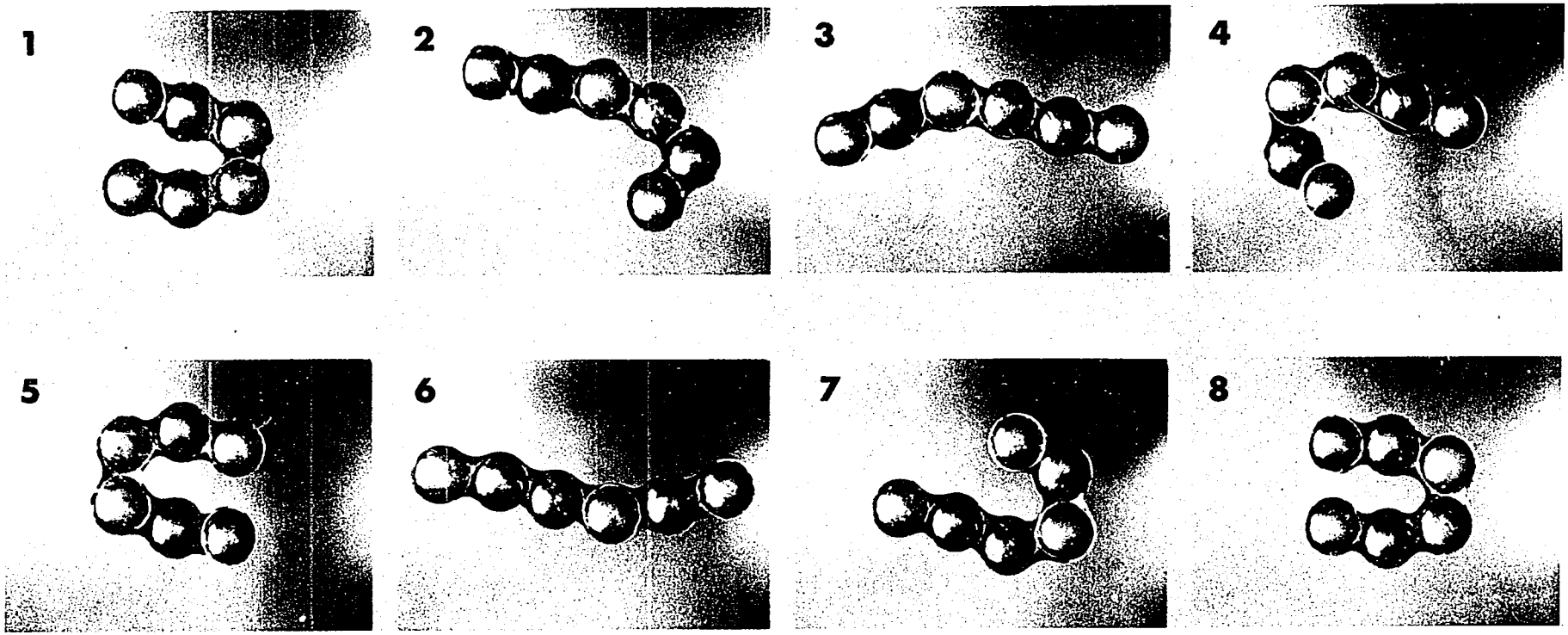

Figure 9 Rotation of a flexible chain of spheres in a combined shear and electric field. $n = 6$, $\Upsilon = 0.129$ sec.$^{-1}$, $T = 311.2$ sec. and $\Delta E = 0.5$ kv/cm.

viscous fluids, however, showed a much stronger tendency than water to unite non-neighbouring spheres and form non-linear aggregates.

Chain bending was not reversible; even when the flow was reversed before the formation of non-linear aggregates, the chains did not resume their initial shape (Figure 10).

As the three above liquids are much more viscous than water, it became extremely difficult to keep the amount of the liquid to the bare minimum just enough to hold the chain together. It was observed that when there was too much fluid the chains bent and formed aggregates even at $\Upsilon = 0$. Thus, the excess liquid present between the spheres might be expected to increase the flexibility of the chains and so offers some explanation for the unexpectedly high flexibility observed experimentally.

(c) Non-Linear Aggregates of Spheres

Tetrahedral and some planar triangular and hexagonal aggregates of spheres held together by aqueous Aerosol AY solution were briefly studied. They all rotated in Couette flow with almost constant angular velocity (Figure 2b) behaving like rigid spheres or discs at $C = \infty$. At high Υ, however, they were distorted and became disordered.

(d) Aggregates of Discs (Rouleaux)

Rouleaux consisting of from 8 to 14 discs were studied; their original rod-like shape was constantly distorted by the shear flow and they exhibited a definite tendency to leave the horizontal X_2X_3 plane. Thus, no analysis of the dependence of rouleau length on $\emptyset$ was made.

When a rouleau was only slightly distorted from linearity, it rotated in a manner quite similar to that for a rod (Figures 2c and 11).

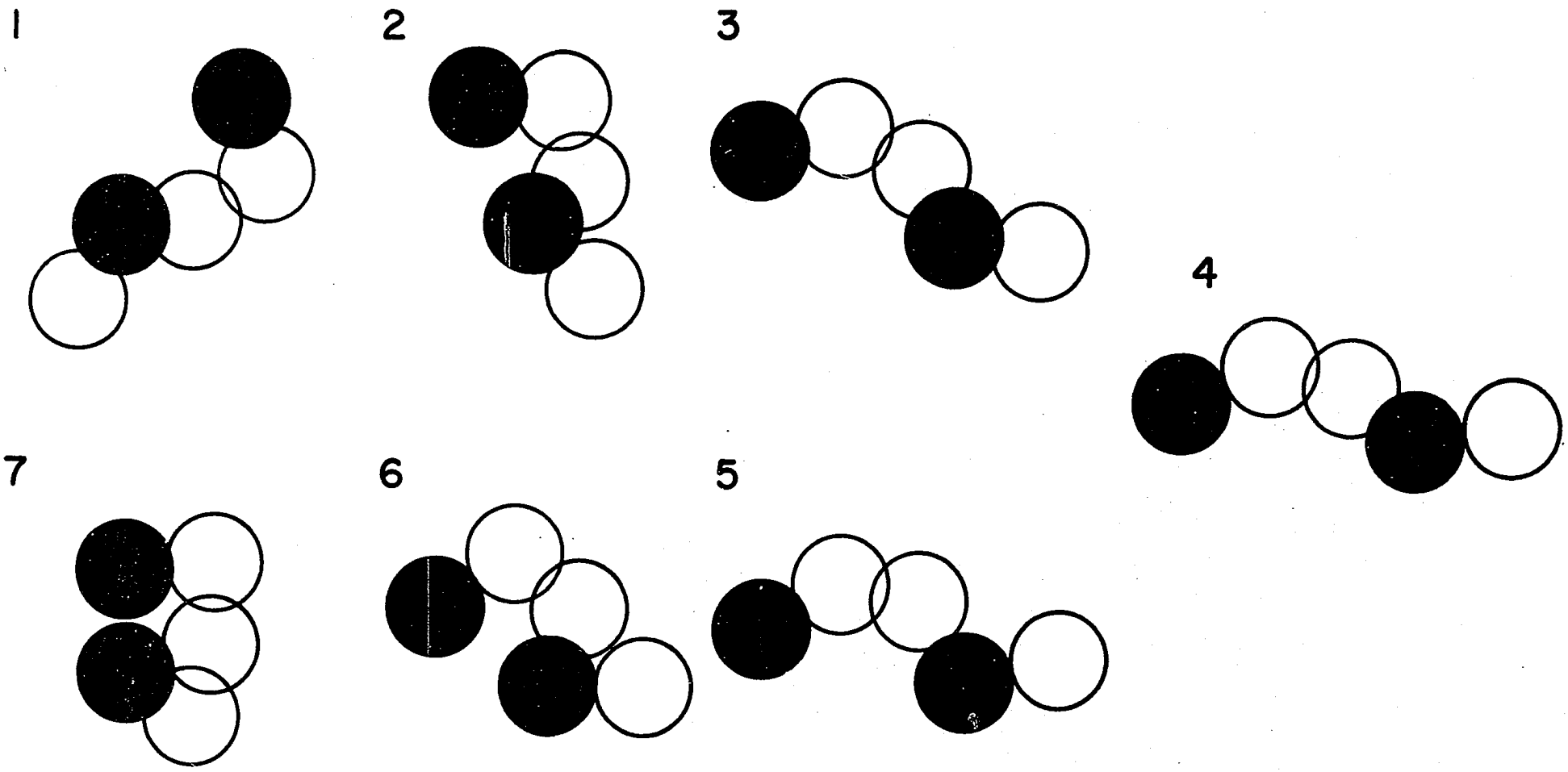

Figure 10 Irreversible rotation of a chain of 5 spheres held together by Ucon 50HB260. Flow reversed at (4); (1)-(4) counterclockwise and (4)-(7) clockwise rotation. $\gamma = 0.0733$ sec^{-1}. These drawings are tracings of ciné pictures at intervals of 20 sec.

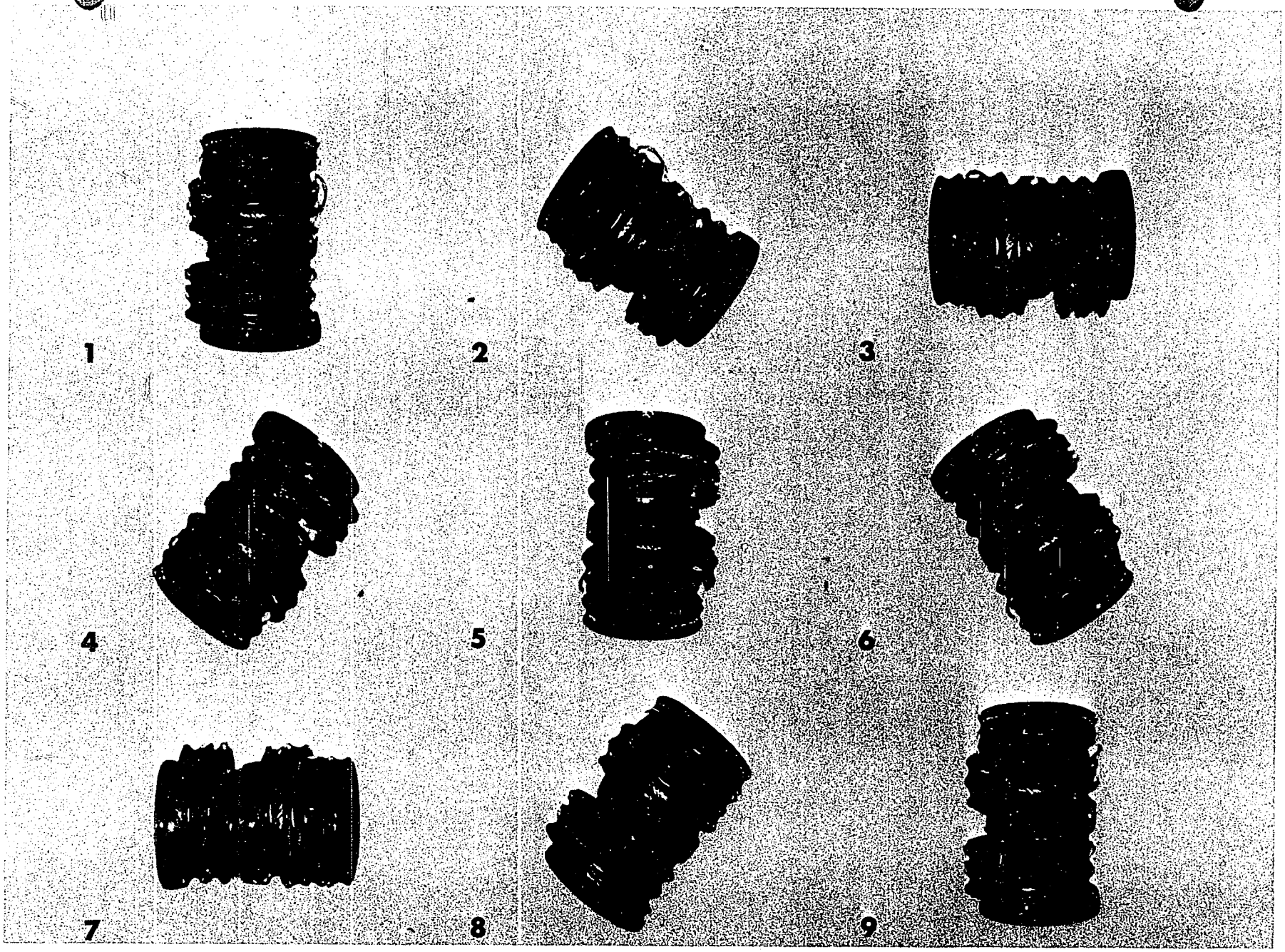

Figure 11 Rotation of a rouleau in Couette flow. $n = 9$, $\gamma = 0.0251\ sec^{-1}$, $T = 526.2$ sec, $r_e = 1.38$.

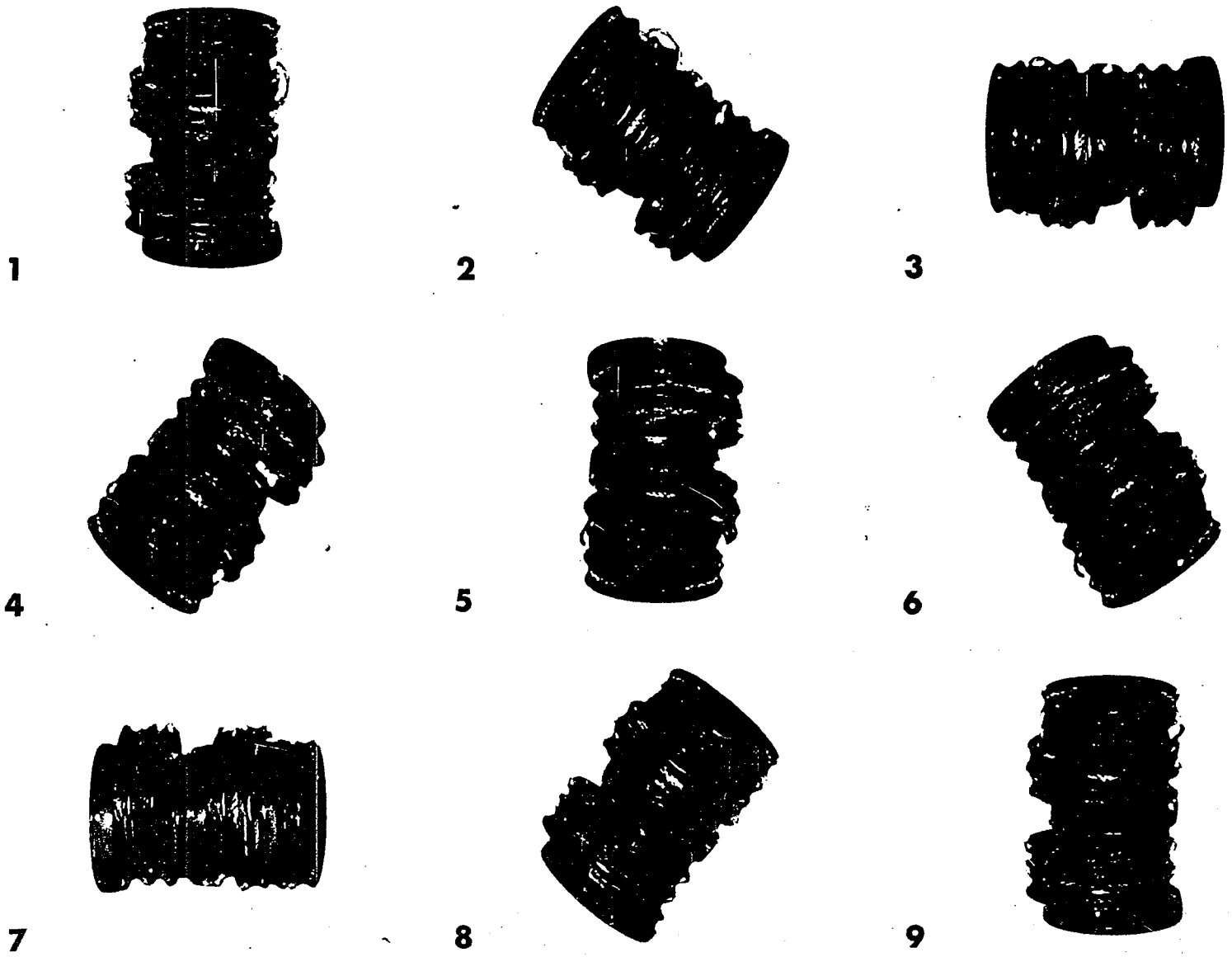

Figure 11 Rotation of a rouleau in Couette flow. $n = 9$, $\gamma = 0.0251\ sec^{-1}$, $T = 526.2$ sec, $r_e = 1.38$.

After prolonged shearing, however, a rouleau could be broken at Υ as low as 0.03 sec.$^{-1}$ and the higher the Υ, the sooner it broke. It might therefore be conjectured that this type of break-up, preceded by gradual sliding of the discs over one another, is explainable on the basis solely of the creeping motion equations and hence is of an entirely different nature to the breakage of a chain of spheres. A rouleau appeared to be bent when there was relative sliding between all neighbouring discs (Figure 12), but this was rarely observed experimentally. It was far more common for two or more segments (each consisting of a few discs) to slide against each other and finally break apart.

Because of the constant distortion and the ease with which rouleaux broke, experiments were limited to a narrow range of Υ and thus the variation of $T\Upsilon$ with Υ could not be used effectively as a measure of flexibility, although the limited experimental data (Table III) did show a general trend of increasing $T\Upsilon$ with increasing Υ.

(e) Aggregates of Rods

For the sake of completeness, aggregates of rods were also briefly studied. Two kinds of aggregates were possible: end-to-end or side-by-side, the former being very easily broken (Figure 13a) and attempts to measure its period of rotation failed. The side-by-side aggregates were less easily broken; they rotated in Couette flow like rigid rods (Figure 13b), plots similar to Figure 2 being obtained.

Aggregates consisting of 3 or more rods were formed but they were easily broken and no detailed study was carried out.

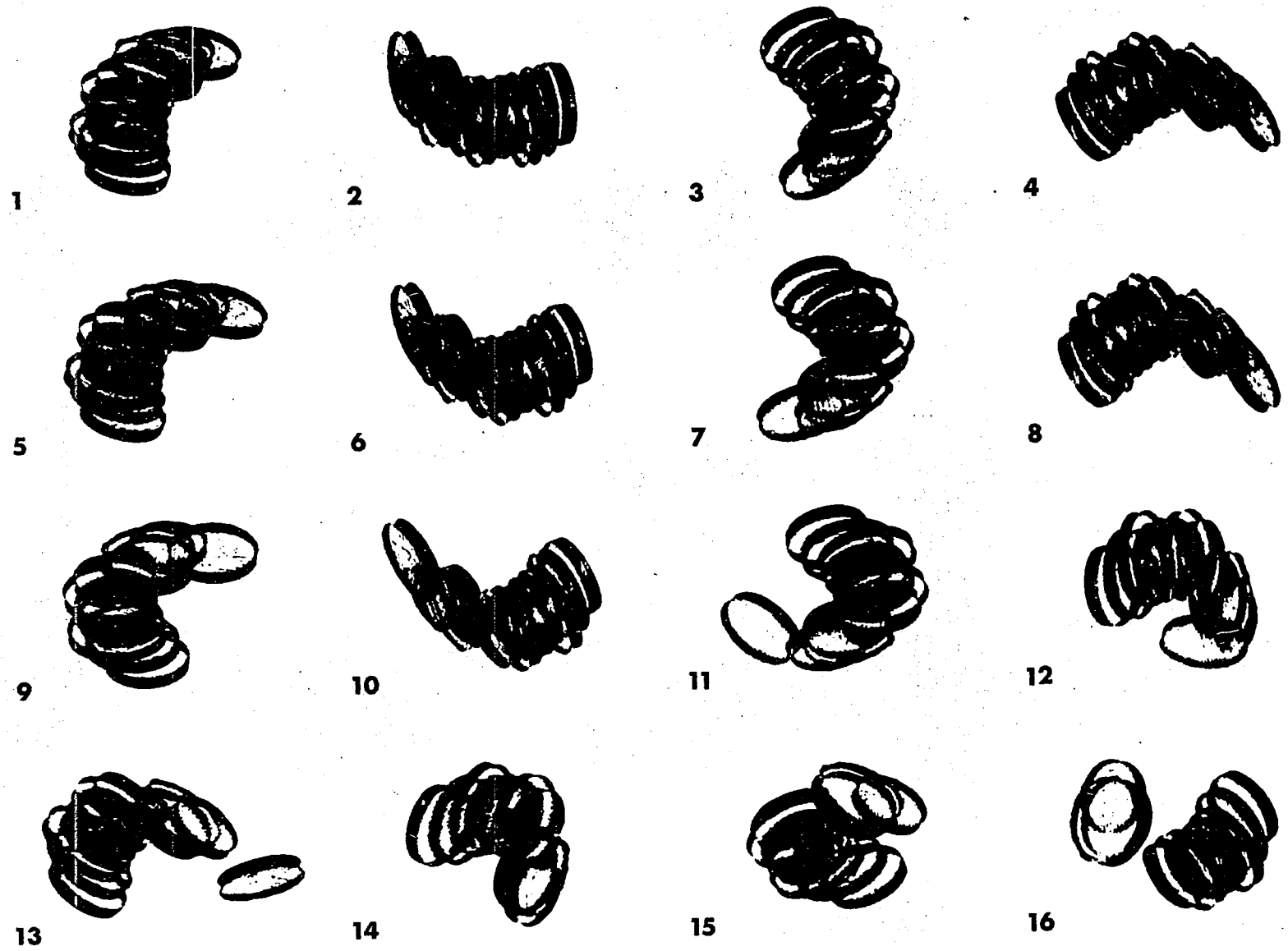

Figure 12 Bending and breaking-up of a rouleau in Couette flow. $n = 11$, $\gamma = 0.0567 - 0.172\ sec^{-1}$.

TABLE III

Aggretates of discs

disc dimension: diameter 0.79 mm., thickness 0.13 mm.

n	r_p*	range of γ $sec.^{-1}$	range of $T\gamma$	range of r_e/r_p
8	1.32	0.026 - 0.067	12.8 - 14.1	0.92 - 1.23
9	1.48	0.025 - 0.160	12.7 - 14.6	0.78 - 1.19
10	1.65	0.024 - 0.096	13.5 - 15.3	0.89 - 1.16
11	1.81	0.025 - 0.081	13.7 - 15.5	0.84 - 1.08
12	1.97	0.028 - 0.128	13.7 - 16.4	0.77 - 1.09
13	2.14	0.022 - 0.038	14.0 - 15.3	0.75 - 0.89
14	2.31	0.022 - 0.230	15.7 - 16.8	0.87 - 0.97

*r_p: n x (thickness)/(diameter)

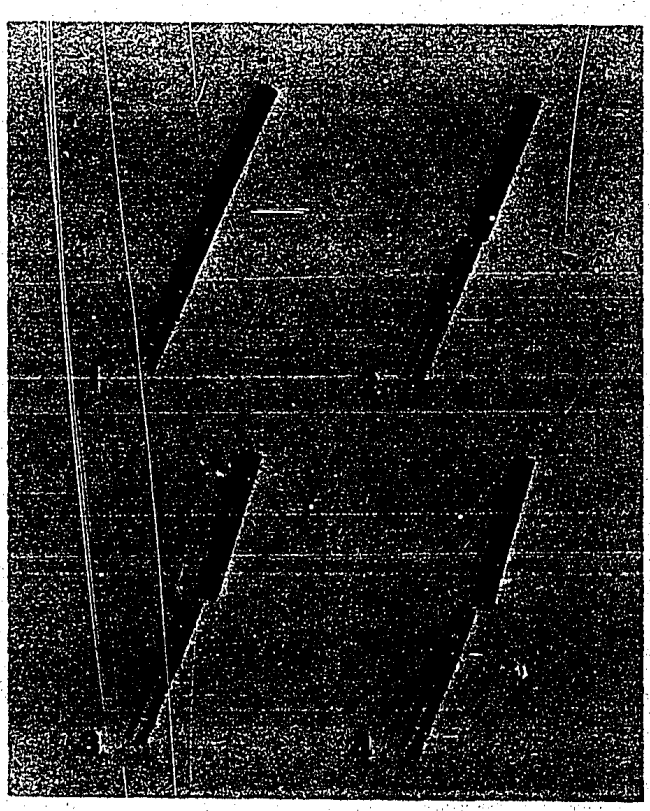

Figure 13 (a) Breaking-up of end-to-end aggregate of rods. $n = 2$, $\gamma = 0.0237$ sec.$^{-1}$.

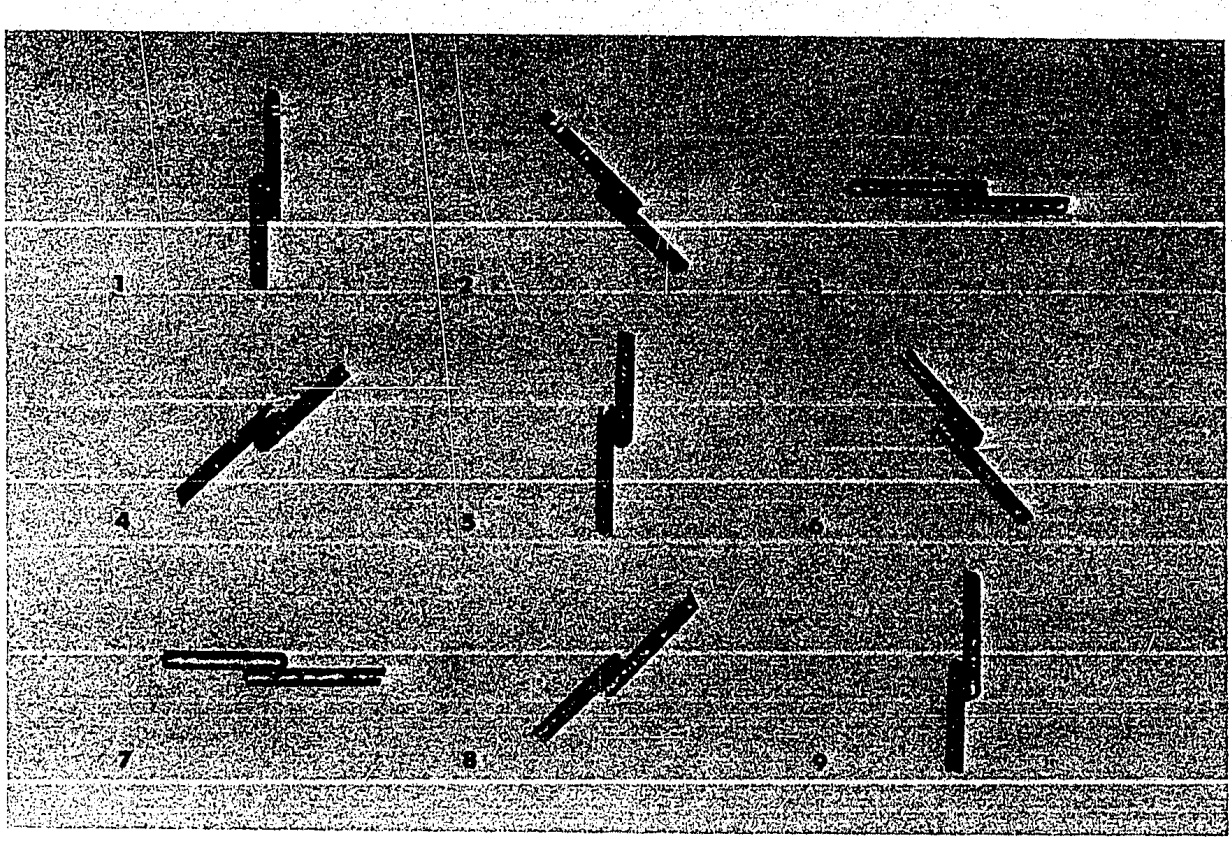

Figure 13 (b) Rotation of side-by-side aggregate of rods. $n = 2$, $\gamma = 0.185$ sec.$^{-1}$, $T = 226.8$ sec., $r_e = 6.54$.

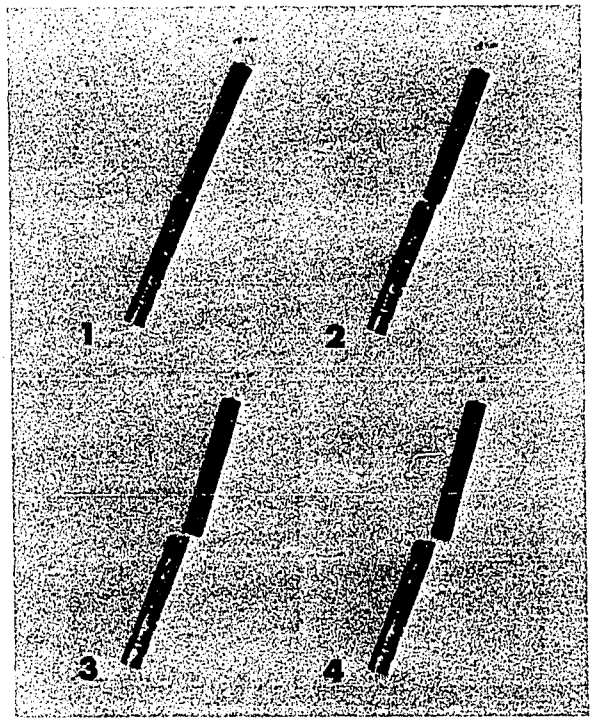

Figure 13 (a) Breaking-up of end-to-end aggregate of rods. $n = 2$, $\gamma = 0.0237$ sec.$^{-1}$.

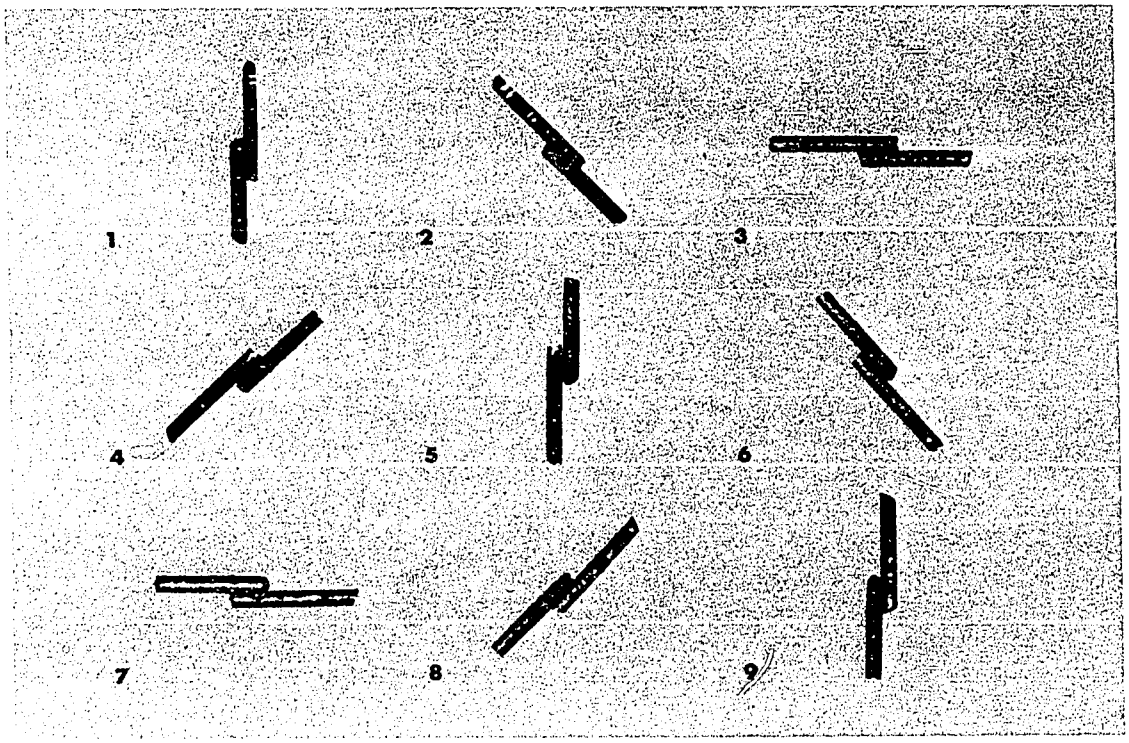

Figure 13 (b) Rotation of side-by-side aggregate of rods. $n = 2$, $\gamma = 0.185$ sec.$^{-1}$, $T = 226.8$ sec., $r_e = 6.54$.

4. CONCLUDING REMARKS

The chains of spheres formed in an electric field behaved like rigid rods, there being good agreement between the experimental results and the theoretical equations of motions. However, such a rigid chain differed from the single rigid rod by (1) the drift of C toward zero, (2) the periodic variation of the chain length with ϕ and (3) the breakage at higher Υ. It was observed that since the chain only broke at high Υ and since the motion after breaking was not reversible, the breakage cannot be explained purely on the basis of the linear creeping motion equations. The chain breakage might be due to one or more of the following effects: (1) surface roughness of the spheres; (2) non-Newtonian behaviour of the fluid due to the very large velocity gradient experienced in the gaps; (3) cavitation and fluid compressibility due to the very large negative and positive pressures existing in the gaps; (4) fluid inertia; (5) the molecular nature of the fluid within the very narrow gaps; and (6) other surface effects.

It has been shown[1] that for small gap widths the relative motion between neighbouring spheres causes in the gaps large positive and negative pressures, whose order of magnitude is given by

$$p_n \sim \frac{\eta_o \gamma_b^{3/2}}{h_o^{3/2} \ln(h_o/b)} .$$

Thus, we may expect cavitation of the fluid when this pressure becomes equal to the atmospheric pressure (minus fluid vapour pressure). Under our experimental conditions this would occur at $h_o \sim 10^{-5}$ cm., a value of sphere separation which could quite reasonably have occurred, so that rupture by cavitation is feasible.

The chains of spheres held together by a liquid behaved like flexible threads; although an improved mathematical treatment to take into account the effect of the interfacial tension would be very complicated, such aggregates provide useful physical models of flexible threads[7] and rouleaux of red blood cells[12] which it is proposed to study further.

REFERENCES

1. This Thesis, Part II.
2. Trevelyan, B.J. and Mason, S.G., J. Colloid Sci., 6, 354 (1951).
3. Bartok, W. and Mason, S.G., J. Colloid Sci., 12, 243 (1957).
4. Jeffery, G.B., Proc. Roy. Soc., A102, 161 (1922).
5. Arlov, A.P., Forgacs, C.L. and Mason, S.G., Svensk Papperstidn., 61(3), 61 (1958).
6. Forgacs, O.L. and Mason, S.G., Tappi, 41, 695 (1958).
7. Forgacs, O.L. and Mason, S.G., J. Colloid Sci., 14, 473 (1959).
8. Goldsmith, H.L. and Mason, S.G., J. Fluid Mech., 12, 88 (1962).
9. Goldsmith, H.L. and Mason, S.G., "Rheology: Theory and Application", Vol. IV. Edited by F.R. Eirich. Academic Press, New York (In Press 1966).
10. Darabaner, C.L., Raasch, J.K. and Mason, S.G., To be published.
11. Allan, R.S. and Mason, S.G., Proc. Roy. Soc., A267, 62 (1962).
12. Goldsmith, H.L., Science (In Press 1966).

PART IV

CONCLUSION

1. GENERAL DISCUSSION

Since various specific aspects of this research have already been discussed in Parts II and III, only some general similarities between chains of particles and flexible threads, macromolecules and rouleaux of red blood cells remain to be discussed.

Direct comparison has already been made between chains of spheres held together by liquid menisci[1] and flexible threads[2-4]; they are similar except for chain stretching and formation of three-dimensional aggregates by the flexible chains. With increasing velocity gradient and the number of spheres in a chain, the flexible chains of spheres become more flexible, and spend an increasingly larger portion of the period of rotation in a position aligned near the direction of flow.

It has been known for some time that the viscosity of a polymer solution can be reduced by high speed stirring as a result of mechanical breakage of long-chain molecules. In their study of mechanical degradation of polymers (polystyrene and DNA (deoxyribose nucleic acid) in various solvents) by controlled hydrodynamic shear, Harrington and Zimm[5] showed that the important quantity in the degradation process is not viscosity alone but the product of shear rate and viscosity. This is to be expected on the basis of the force equations developed in Part II. Furthermore, Harrington[6] also indicated on the basis of the hydrodynamic theory of laminar boundary layers that polymer chains breaking in a hydrodynamic shear field are virtually completely extended along the streamlines of flow. This is in qualitative

agreement with the studies of flexible threads in Couette flow by Forgacs and Mason[3,4]. Although the degradation of polymers is further complicated by non-Newtonian behaviour of the polymer solution and the coil-like molecular structure, experiments on the breakage of chains of particles in Couette flow may provide further insights into the mechanism of breakup of polymer molecules.

The aggregates of rigid discs can be considered as physical models of rouleaux formed by red blood cells (Figure 1). Human red blood cells are flexible biconcave discs having a diameter of 8.5 ± 0.41 microns[7] and of maximum and minimum thickness of 2.4 ± 0.13 microns and 1.0 ± 0.08 microns. It is of interest to note that Goldsmith[8] has recently found that the undeformed rouleaux of red blood cells rotated in orbits predicted for rigid spheroids by Jeffery's theory[9] with $r_e < 1$ for $n < 4$, $r_e \approx 1$ for $n = 4$ and $r_e > 1$ for $n > 4$, n being the number of cells in the rouleau. These findings are in qualitative agreement with the study of aggregates of rigid discs described in Part III.

Goldsmith[8] also observed bending of rouleaux of red blood cells, especially at higher velocity gradients and for rouleaux consisting of a large number of cells; they bend under the compressive force and then straighten out under the tensile force in the succeeding quadrant. The striking similarity in the bending of rouleaux and of flexible fibres is illustrated in Figure 2. Goldsmith's results[8] indicate that bending for a rouleau can occur at a velocity gradient 10^{-7} times that for a dacron filament of the same diameter, indicating a bending modulus 10^{-7} that of dacron.

2. SUGGESTIONS FOR FURTHER RESEARCH

1. To study more extensively bending and breaking of chain of spheres, especially under conditions of prolonged shearing at constant velocity

Figure 1 Photomicrographs of rouleaux of human red blood cells showing two separate aggregates (upper) and networks of rouleaux (lower). Courtesy of Dr. H.L. Goldsmith. See also Figures 11 and 12, Part III for comparison with aggregates of rigid discs.

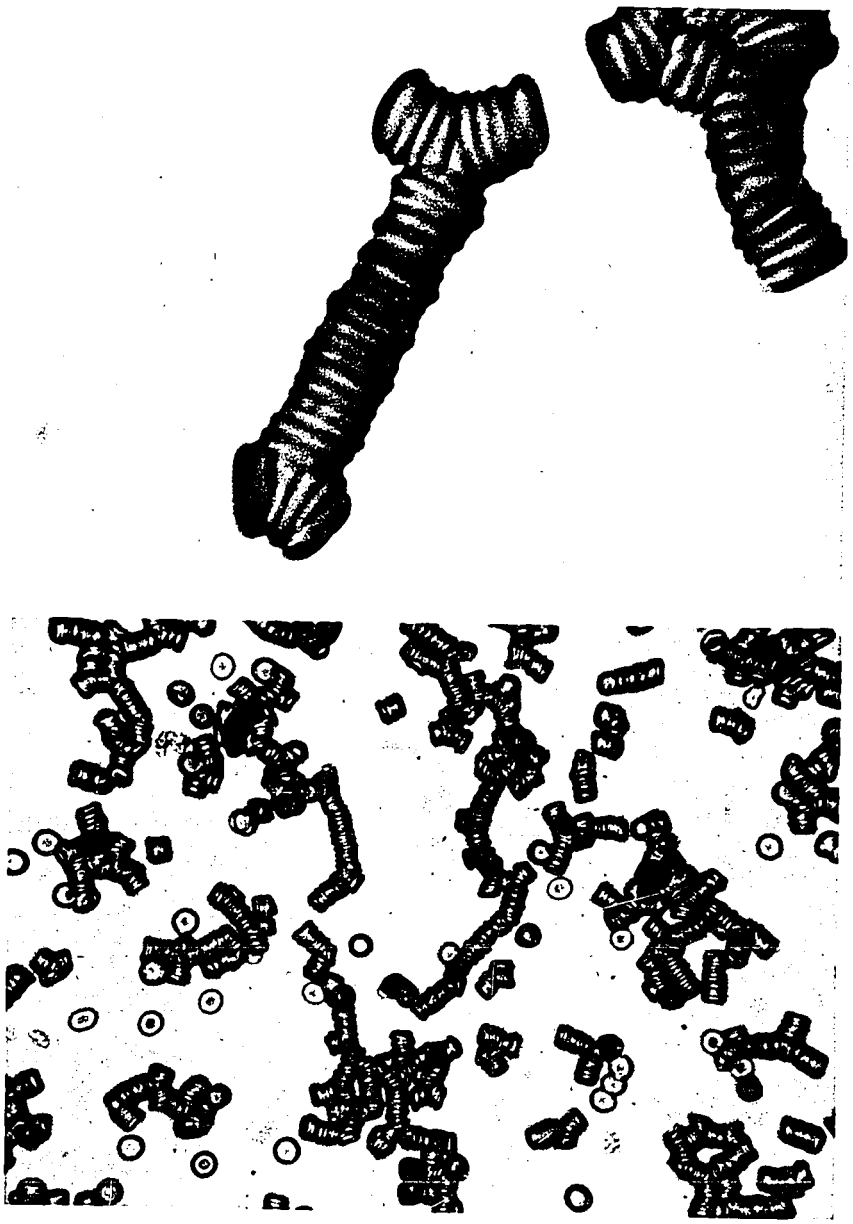

Figure 1 Photomicrographs of rouleaux of human red blood cells showing two separate aggregates (upper) and networks of rouleaux (lower). Courtesy of Dr. H.L. Goldsmith. See also Figures 11 and 12, Part III for comparison with aggregates of rigid discs.

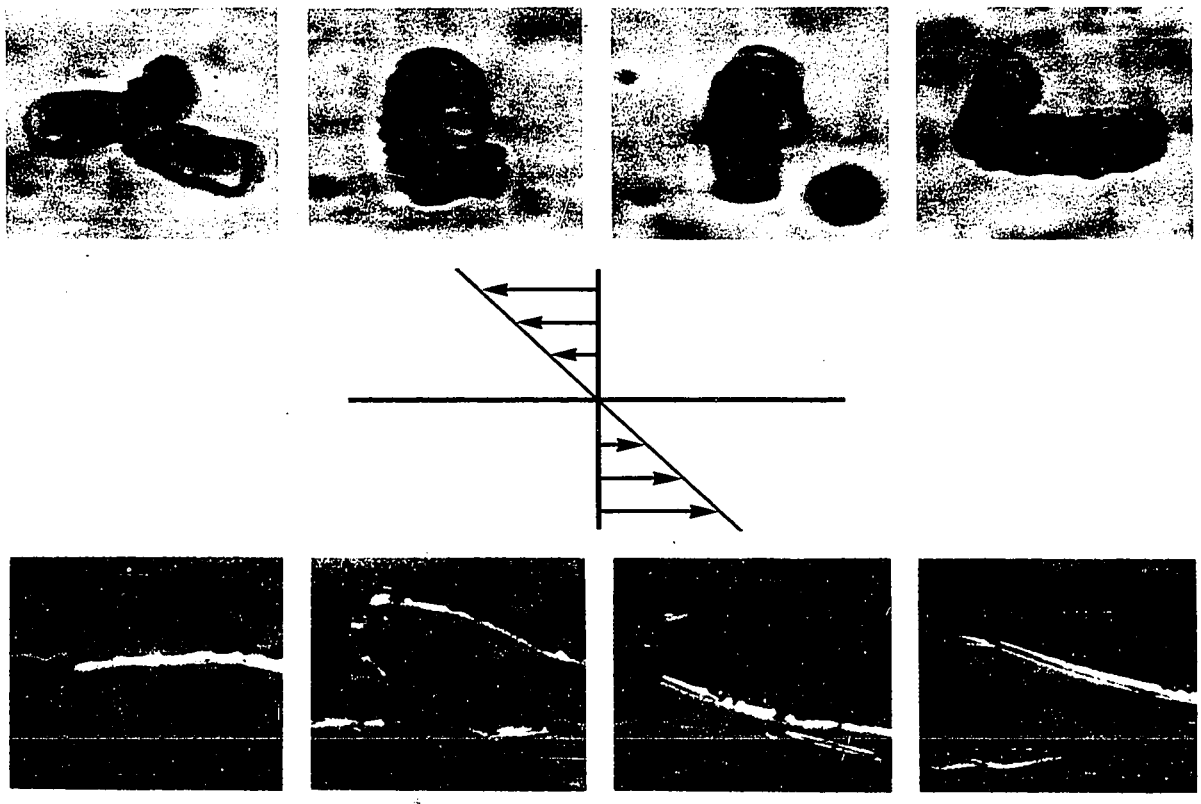

Figure 2 Striking similarity in the bending of flexible fibre and of rouleau of human red blood cells in shear flow. Courtesy of Drs. O.L. Forgacs and H.L. Goldsmith.

gradient and for chain consisting of non-uniform spheres.

2. To study various other kinds of chains of particles such as (a) chains of liquid drops, (b) chains of liquid drops held together by meniscus of a third liquid phase, (c) chains of rigid spheres held together by flexible threads, (d) stacks of discs held together by liquid bridges and (e) linear aggregates of rods held end-to-end by menisci.

3. To study the behaviour of linear aggregates of particles in combined shear and electric fields.

4. To study the interaction and collision of linear aggregates.

3. CLAIMS TO ORIGINAL RESEARCH

1. On the basis of the creeping motion and lubrication equations a theory for the behaviour of a straight chain of spheres in shear flow was developed. The equations of motion for a chain of spheres in contact with one another were experimentally verified.

2. A variety of ordered aggregates of rigid particles simulating fibres of zero stiffness, linear polymer molecules and rouleaux of red blood cells were formed and their behaviour in Couette flow studied.

3. A centrifugal bubble cell was designed and built for the study of deformation of a monolayer of bubbles. Theoretical equations for small deformations were derived and solved numerically and confirmed experimentally.

4. A method of measuring interfacial tension from the shape of a rotating drop was developed. Vonnegut's approximate solutions were extended to lower speeds of rotation by numerical solutions of exact equations and a rotating drop apparatus was designed and constructed.

REFERENCES

1. This Thesis, Part III.
2. Arlov, A.P., Forgacs, O.L. and Mason, S.G., Svensk Papperstidn., 61(3), 61 (1958).
3. Forgacs, O.L. and Mason, S.G., J. Colloid Sci., 14, 457 (1959).
4. Forgacs, O.L. and Mason, S.G., J. Colloid Sci., 14, 473 (1959).
5. Harrington, R.E. and Zimm, B.H., J. Phys. Chem., 69, 161 (1965).
6. Harrington, R.E., J. Polymer Sci., Part A-1, 4, 489 (1966).
7. Ponder, "Hemolysis and Related Phenomena", Grune and Stratton, New York, 1948.
8. Goldsmith, H.L., Science (In Press 1966).
9. Jeffery, G.B., Proc. Roy. Soc., A102, 161 (1922).

APPENDIX I

THEORY OF CHAINS OF SPHERES: MATHEMATICAL DETAILS

(See Part II)

(1) Derivation of (7) and (8).

It can be shown from the linearity of the creeping motion equations that the force and couple about the x_i-axis for a section of the chain from the first to the ith spheres inclusive are given by

$$f_i^i = \eta_o b^2 (C_{ijk}^i a_{jk} + L_{ij}^i \omega_j) \qquad (I - 1)$$

and

$$g_i^i = \eta_o b^3 (D_{ijk}^i a_{jk} + M_{ij}^i \omega_j) \ , \qquad (I - 2)$$

where

ω_j = angular velocity of the chain about x_j-axis,

a_{jk} = the second order tensor A_{jk} (see (3)) taken relative to x_1, x_2, x_3 coordinate system,

C_{ijk}^i = a third-order true tensor,

D_{ijk}^i = a third-order pseudotensor,

L_{ij}^i = a second-order pseudotensor,

M_{ij}^i = a second-order true tensor,

and C_{ijk}^i, D_{ijk}^i, L_{ij}^i and M_{ij}^i depend on the chain geometry only. By symmetry of the body shape it may be shown that for $i \leqslant (n-1)$:

(i) $C_{ijk}^i = 0$, except

$$C_{111}^i, \ C_{122}^i = C_{133}^i, \ C_{212}^i = C_{313}^i \text{ and } C_{221}^i = C_{331}^i; \qquad (I - 3)$$

(ii) $D^i_{ijk} = 0$, except

$$D^i_{123} = -D^i_{132},\ D^i_{231} = -D^i_{321} \text{ and } D^i_{312} = -D^i_{213}; \qquad (I-4)$$

(iii) $L^i_{ij} = 0$, except $L^i_{23} = -L^i_{32}$; (I - 5)

(iv) $M^i_{ij} = 0$, except M^i_{11} and $M^i_{22} = M^i_{33}$; (I - 6)

and for i = n:

(i) $C^n_{ijk} = 0$; (I - 7)

(ii) $D^n_{ijk} = 0$, except

$$D^n_{123} = -D^n_{132},\ D^n_{231} = -D^n_{321} \text{ and } D^n_{312} = -D^n_{213}; \qquad (I-8)$$

(iii) $L^n_{ij} = 0$; (I - 9)

(iv) $M^n_{ij} = 0$, except M^n_{11} and $M^n_{22} = M^n_{33}$. (I - 10)

Making use of the tensor transformation formula

$$a_{ij} = \alpha_{pi}\alpha_{qj}A_{pq}$$

and substituting (4) for Couette flow into (I - 1) and (I - 2) give

$$f^i_1 = \eta_o b^2(\gamma C^i_{ijk}\alpha_{3j}\alpha_{2k} + L^i_{ij}\omega_j) \qquad (I-11)$$

and

$$g^i_1 = \eta_o b^3(\gamma D^i_{ijk}\alpha_{3j}\alpha_{2k} + M^i_{ij}\omega_j)\ , \qquad (I-12)$$

which with the aid of (I - 3) - (I - 6) can be rewritten as (7) and (8).

(2) Derivation of (12) and (13) and the quantities A^i.

Substituting (10) and (6) into (7) and (8) leads to

$$f^i_1 = \eta_o \gamma b^2(C^i_{111} - C^i_{122})\sin^2\theta\sin\phi\cos\phi$$

$$f_2^i = \eta_o \gamma_b^2 \left[\left(C_{212}^i - \frac{L_{23}^i D_{312}^n}{M_{22}^n} \right) \sin\theta\sin\phi(-\sin\phi\sin\psi + \cos\theta\cos\phi\cos\psi) \right.$$

$$\left. + \left(C_{221}^i + \frac{L_{23}^i D_{231}^n}{M_{22}^n} \right) \sin\theta\cos\phi(\cos\phi\sin\psi + \cos\theta\sin\phi\sin\psi) \right] \qquad (I - 13)$$

$$f_3^i = \eta_o \gamma_b^2 \left[\left(C_{212}^i - \frac{L_{23}^i D_{312}^n}{M_{22}^n} \right) \sin\theta\sin\phi(-\sin\phi\cos\psi - \cos\theta\cos\phi\sin\psi) \right.$$

$$\left. + \left(C_{221}^i + \frac{L_{23}^i D_{231}^n}{M_{22}^n} \right) \sin\theta\cos\phi(\cos\phi\cos\psi - \cos\theta\sin\phi\sin\psi) \right]$$

and

$$g_1^i = \eta_o \gamma_b^3 \left(\frac{M_{11}^i D_{123}^n}{M_{11}^n} - D_{123}^i \right) \cos\theta$$

$$g_2^i = \eta_o \gamma_b^3 \left[\left(D_{231}^i - \frac{M_{22}^i D_{231}^n}{M_{22}^n} \right) \sin\theta\cos\phi(\cos\phi\cos\psi - \cos\theta\sin\phi\sin\psi) \right.$$

$$\left. + \left(D_{312}^i - \frac{M_{22}^i D_{312}^n}{M_{22}^n} \right) \sin\theta\sin\phi(\sin\phi\cos\psi + \cos\theta\cos\phi\sin\psi) \right] \qquad (I - 14)$$

$$g_3^i = \eta_o \gamma_b^3 \left[\left(D_{231}^i - \frac{M_{22}^i D_{231}^n}{M_{22}^n} \right) \sin\theta\cos\phi(-\cos\phi\sin\psi - \cos\theta\sin\phi\cos\psi) \right.$$

$$\left. + \left(D_{312}^i - \frac{M_{22}^i D_{312}^n}{M_{22}^n} \right) \sin\theta\sin\phi(-\sin\phi\sin\psi + \cos\theta\cos\phi\cos\psi) \right],$$

which can be simplified to (12) and (13) by changing from x_1, x_2, x_3 to X_1^o, X_2^o, X_3^o coordinates defined by (11). The quantities A^i are then given by

$$
\begin{aligned}
A_1^i &= C_{111}^i - C_{122}^i \,, \\
A_2^i &= (C_{212}^i + C_{221}^i) - \frac{L_{23}^i}{M_{22}^n}(D_{312}^n - D_{231}^n) \,, \\
A_3^i &= \frac{L_{23}^i D_{312}^n}{M_{22}^n} - C_{212}^i \,, \\
A_4^i &= \frac{L_{23}^i D_{231}^n}{M_{22}^n} + C_{221}^i \,, \\
A_5^i &= \frac{M_{11}^i D_{123}^n}{M_{11}^n} - D_{123}^i \,, \\
A_6^i &= D_{312}^i - \frac{M_{22}^i D_{312}^n}{M_{22}^n} \,, \\
A_7^i &= D_{231}^i - \frac{M_{22}^i D_{231}^n}{M_{22}^n} \,, \\
A_8^i &= \frac{M_{22}^i}{M_{22}^n}(D_{231}^n - D_{312}^n) + (D_{312}^i - D_{231}^i) \,.
\end{aligned}
\qquad (I - 15)
$$

(3) Derivation of (16).

It has been shown[1] that

$$
\frac{d(\alpha_{ip})}{dt} = \varepsilon_{ijk}\alpha_{kp}\alpha_{j\ell}\omega_\ell \,, \qquad (I - 16)
$$

where

ω_ℓ = angular velocity of the chain about x_ℓ- axis, and

$$
\varepsilon_{ijk} = \begin{cases} +1, \text{ if } (i\ j\ k) \text{ is an even permutation of } (1\ 2\ 3) \\ -1, \text{ if } (i\ j\ k) \text{ is an odd permutation of } (1\ 2\ 3) \\ 0, \text{ otherwise.} \end{cases}
$$

It follows then that

$$\frac{d(\alpha_{11})}{dt} = (\alpha_{31}\alpha_{22} - \alpha_{21}\alpha_{32})\omega_2 + (\alpha_{31}\alpha_{23} - \alpha_{21}\alpha_{33})\omega_3 ,$$

which becomes

$$\frac{d(\alpha_{11})}{dt} = \frac{\gamma(D^n_{231} - D^n_{312})}{M^n_{22}}(\alpha_{21}\alpha_{31})(\alpha_{23}\alpha_{32} - \alpha_{22}\alpha_{33}) \qquad (I - 17)$$

when ω_2 and ω_3 are eliminated with the aid of (10).

Differentiating (6) yields

$$\frac{d(\alpha_{11})}{dt} = - \sin\theta \frac{d\theta}{dt} , \qquad (I - 18)$$

which can then be combined with (I - 17) to give (16a).

Similarly one can obtain

$$\frac{d(\alpha_{21})}{dt} = \frac{\gamma}{M^n_{22}}\Big[D^n_{231}(\alpha_{21}\alpha_{31})(\alpha_{12}\alpha_{33} - \alpha_{13}\alpha_{32}) + D^n_{312}(\alpha_{31}\alpha_{11})(\alpha_{23}\alpha_{32} - \alpha_{22}\alpha_{33}) + D^n_{312}\alpha^2_{31}(\alpha_{13}\alpha_{22} - \alpha_{12}\alpha_{23})\Big] \qquad (I - 19)$$

and

$$\frac{d(\alpha_{12})}{dt} = \gamma(\alpha_{22}\alpha_{33} - \alpha_{32}\alpha_{23})\Big[\frac{D^n_{123}}{M^n_{11}}(\alpha_{32}\alpha_{21} - \alpha_{22}\alpha_{31}) + \frac{1}{M^n_{22}}(D^n_{312}\alpha_{31}\alpha_{22} - D^n_{231}\alpha_{32}\alpha_{21})\Big] , \qquad (I - 20)$$

which finally lead to (16b) and (16c).

(4) Derivation of (18c).

At $\theta = 0$, the chain rotates with an angular velocity $\omega_1 = \gamma/2$. Thus from (17)

$$\frac{D^n_{123}}{M^n_{11}} = \frac{1}{2} \qquad \text{(I - 21)}$$

and

$$\omega_1 = \frac{\gamma}{2}\cos\theta$$

for all θ.

(5) Derivation of (21).

It follows from the definition of the quantities D^n_{213}, D^n_{231} and M^n_{22} that

$$M^n_{22} = D^n_{231} - D^n_{213} \qquad \text{(I - 22)}$$

and hence from (19)

$$B_2 + B_3 = 1 \qquad \text{and} \qquad B_1 = B_3 - B_2 . \qquad \text{(I - 23)}$$

If one lets

$$\frac{B_3}{B_2} = r_e^2 , \qquad (20)$$

then by solving (I - 23) and (20) simultaneously one obtains (21), i.e.,

$$B_1 = \frac{r_e^2 - 1}{r_e^2 + 1}, \qquad B_2 = \frac{1}{r_e^2 + 1}, \qquad B_3 = \frac{r_e^2}{r_e^2 + 1} .$$

(6) Derivation of (26).

Substituting (12a) and (23a) into (22) and combining the resulting equation with (25) give

$$\gamma A^i_1 \sin^2\theta\sin\phi\cos\phi = \frac{3}{2}\pi\frac{1}{h_i}\frac{dh_i}{dt} . \qquad \text{(I - 24)}$$

With the help of (18), Θ and ϕ can be eliminated from (I - 24) which then integrates to yield

$$h_i = (h_o)_i\left[\frac{(C^2B_3 + B_2)\sin^2\sqrt{B_2B_3}\,\gamma t + (C^2+1)B_2\cos^2\sqrt{B_2B_3}\,\gamma t}{B_2(C^2+1)}\right]^{\frac{A_1^i}{3\pi B_1}} . \quad \text{(I - 25)}$$

When h_i is expressed in terms of ϕ, (I - 25) becomes (26).

(7) Derivation of (31) and (32).

The quantities $(V_2^i - V_2^{i+1})$ and $(V_3^i - V_3^{i+1})$ can be expressed in terms of $d(X_j^o)^i/dt$ and $d\psi/dt$ by the relations

$$\begin{aligned} \frac{d(X_2^o)^i}{dt} &= -(X_3^o)^i\frac{d\psi}{dt} + V_2^i \\ \frac{d(X_3^o)^i}{dt} &= +(X_2^o)^i\frac{d\psi}{dt} + V_3^i \ . \end{aligned} \quad \text{(I - 26)}$$

Thus, upon using (I - 26) and substituting (12b) (12c) (23b) and (23c) into (22) one obtains

$$\begin{aligned} \pi l n h_i\left[\frac{d(\Delta X_2^o)^i}{dt} + (\Delta X_3^o)^i\frac{d\psi}{dt} - b(\Omega_3^i + \Omega_3^{i+1})\right] \\ = -\gamma b A_2^i \sin\theta\cos\theta\sin\phi\cos\phi \\ \pi l n h_i\left[-\frac{d(\Delta X_3^o)^i}{dt} + (\Delta X_2^o)^i\frac{d\psi}{dt} - b(\Omega_2^i + \Omega_2^{i+1})\right] \\ = \gamma b\sin\theta(A_3^i\sin^2\phi + A_4^i\cos^2\phi) \ , \end{aligned} \quad \text{(I - 27)}$$

while similarly from (13) and (24)

$$\begin{aligned} \frac{3}{5}\pi l n h_i(\Omega_2^{i+1} - \Omega_2^i) &= \gamma\sin\theta(A_6^i\sin^2\phi + A_7^i\cos^2\phi) \\ \frac{3}{5}\pi l n h_i(\Omega_3^{i+1} - \Omega_3^i) &= \gamma A_8^i\sin\theta\cos\theta\sin\phi\cos\phi \ , \end{aligned} \quad \text{(I - 28)}$$

where

$$(\Delta X_2^o)^i = (X_2^o)^i - (X_2^o)^{i+1}$$
$$(\Delta X_3^o)^i = (X_3^o)^i - (X_3^o)^{i+1} \quad . \qquad \text{(I - 29)}$$

If there is fore-aft symmetry with regard to the gap widths and the chain contains n = 2m spheres, then in (I - 27) and (I - 28) there are 4m independent variables: $(\Delta X_2^o)^i$, $(\Delta X_3^o)^i$, Ω_2^i and Ω_3^i for $1 \leqslant i \leqslant m$. Since (I - 28) is trivial for i = m, there are only (4m - 2) independent equations in (I - 27) and (I - 28). The extra two equations necessary for the determination of the 4m variables are

$$(\Delta X_2^o)^m = (\Delta X_3^o)^m = 0 \ , \qquad \text{(I - 30)}$$

which also serve to define the straight line joining the centers of the mth and (m+1)th spheres as the X_1^o-axis for a bent chain.

From fore-aft symmetry

$$\Omega_2^m = \Omega_2^{m+1} \quad \text{and} \quad \Omega_3^m = \Omega_3^{m+1}$$

and from (I - 27), (I - 28) and (I - 30) one can obtain the following solutions for Ω_2^i and Ω_3^i:

$$\Omega_2^i = - \sum_{j=1}^{m} \frac{\gamma \sin\theta}{\ln h_j} (T_{ij}^* \sin^2\phi + U_{ij}^* \cos^2\phi)$$

(I - 31)

and

$$\Omega_3^i = \sum_{j=1}^{m} \frac{\gamma S_{ij}^*}{\ln h_j} \sin\theta\cos\theta\sin\phi\cos\phi \ ,$$

where T_{ij}^*, U_{ij}^* and S_{ij}^* are (m x m) matrices.

Substituting (I - 31) back into (I - 27) and (I - 28) leads to

$$-\frac{d(\Delta X_2^o)^i}{dt} - (\Delta X_3^o)^i \frac{d\psi}{dt} = \sum_{j=1}^{m} \frac{b\gamma}{\ln h_j}(S_{ij}\sin\theta\cos\theta\sin\phi\cos\phi)$$

$$\frac{d(\Delta X_3^o)^i}{dt} - (\Delta X_2^o)^i \frac{d\psi}{dt} = \sum_{j=1}^{m} \frac{b\gamma\sin\theta}{\ln h_j}(T_{ij}\sin^2\phi + U_{ij}\cos^2\phi) \quad , \qquad \text{(I - 32)}$$

which can be rewritten with the aid of (16), (18), (21) and (26) as

$$-\frac{d(\Delta X_2^o)^i}{dt} - (\Delta X_3^o)^i \left\{ \frac{1 - 2(B_2\sin^2\phi + B_3\cos^2\phi)}{2\left[(C^2B_3 + B_2\sin^2\phi + B_3\cos^2\phi)(B_2\sin^2\phi + B_3\cos^2\phi)\right]^{1/2}} \right\}$$

$$= \sum_{j=1}^{m} \left\{ \frac{1}{(B_2\sin^2\phi + B_3\cos^2\phi)^{1/2}(C^2B_3 + B_2\sin^2\phi + B_3\cos^2\phi)} \right.$$

$$\left. \cdot \frac{bC\sqrt{B_3}\, S_{ij}\sin\phi\cos\phi}{\ln(h_o)_j + \frac{A_1^j}{3\pi B_1}\ln\left[\frac{1}{C^2+1} + \frac{C^2B_3}{(C^2+1)(B_3\cos^2\phi + B_2\sin^2\phi)}\right]} \right\}$$

and (I - 33)

$$\frac{d(\Delta X_3^o)^i}{dt} - (\Delta X_2^o)^i \left\{ \frac{1 - 2(B_2\sin^2\phi + B_3\cos^2\phi)}{2\left[(C^2B_3 + B_2\sin^2\phi + B_3\cos^2\phi)(B_2\sin^2\phi + B_3\cos^2\phi)\right]^{1/2}} \right\}$$

$$= \sum_{j=1}^{m} \left\{ \frac{1}{(B_2\sin^2\phi + B_3\cos^2\phi)(C^2B_3 + B_2\sin^2\phi + B_3\cos^2\phi)^{1/2}} \right.$$

$$\left. \cdot \frac{bC\sqrt{B_3}(T_{ij}\sin^2\phi + U_{ij}\cos^2\phi)}{\ln(h_o)_j + \frac{A_1^j}{3\pi B_1}\ln\left[\frac{1}{C^2+1} + \frac{C^2B_3}{(C^2+1)(B_3\cos^2\phi + B_2\sin^2\phi)}\right]} \right\} ,$$

S_{ij}, T_{ij} and U_{ij} being (m x m) matrices.

By imposing the restrictions (30), (I - 33) reduces to (31) and (32). Integration of (32) then gives (33) with

$$p^i = \sum_{j=1}^{m} \frac{B_3 T_{ij} - B_2 U_{ij}}{B_1 \sqrt{B_2 B_3}\, \ln(h_o)_j} \qquad (I - 34)$$

and

$$Q^i = \sum_{j=1}^{m} \frac{-T_{ij} + U_{ij}}{B_1 \ln(h_o)_j}$$

REFERENCE

1. Cox, R.G., Ph.D. Thesis, Cambridge University, 1964.

APPENDIX II

DETAILS OF EXPERIMENTS WITH CHAINS OF PARTICLES

1. COUETTE APPARATUS

The Couette Mark 2 apparatus consisting of two counter-rotating cylinders has been described previously[1,2], but for the sake of completeness a brief description is given here.

It can be shown that the transverse velocity V of the fluid in the annular gap between the cylinders is given by

$$V = \left(\frac{\Omega_1 R_1^2 + \Omega_2 R_2^2}{R_2^2 - R_1^2}\right) R - \frac{(\Omega_1 + \Omega_2) R_1^2 R_2^2}{R_2^2 - R_1^2} \cdot \frac{1}{R}, \qquad (1)$$

where R_1 and R_2 are the radii and Ω_1 and Ω_2 the angular velocities of the inner and outer cylinders respectively (Figure 1). Thus at the stationary layer for which $V = 0$, the local velocity field may be shown to be equivalent to a simple plane shear of value γ given by

$$\gamma = \frac{2(\Omega_1 R_1^2 + \Omega_2 R_2^2)}{R_2^2 - R_1^2}. \qquad (2)$$

Hence if a particle, small compared with the annular gap width, is placed at the stationary layer, it will experience a fluid motion which is a plane shear of value γ given by (2). Since cylinders of $R_1 = 13.344$ cm. and $R_2 = 15.222$ cm. were used in most experiments (2) can be written as

$$\gamma = 0.6950 N_1 + 0.9044 N_2 \text{ sec.}^{-1}, \qquad (3)$$

where N_1 and N_2 are the RPM of the inner and outer cylinders. As the two cylinders are driven by two separate and continuously variable motors, Ω_1 and Ω_2 can be changed at will to make the stationary layer coincide with the centre of a particle aggregate for prolonged study.

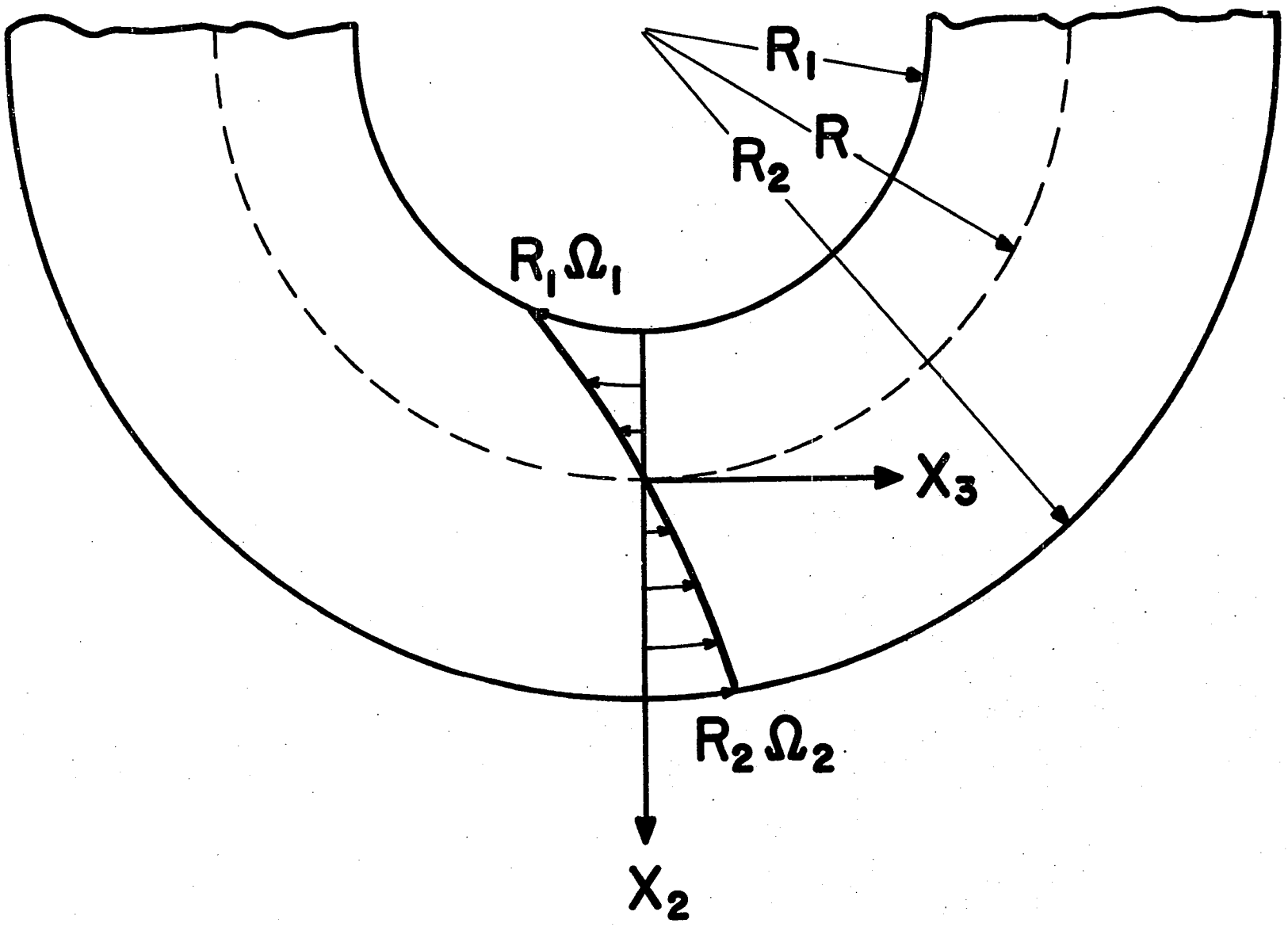

Figure 1 Principle of the Couette apparatus. (After Trevelyan and Mason[3])

A photograph of the Couette apparatus is shown in Figure 2. In the centre are the two cylinders and the adjustable common support for the microscope and camera above and the microscope illuminator below the cylinders. The outer cylinder has a sealed glass plate bottom to permit illumination of the field from below. The motors and gear boxes are at either side of the Couette device. By means of three sets of reduction worm gears a wide range of velocity gradients (0 to 40 sec.$^{-1}$) can be obtained. The speed controls and the tachometers are mounted on the right hand panel, while the variable a.c. and d.c. voltage supplies and a chopper device for timing are on the left hand panel.

Though similar to Mark 2 Couette apparatus in principle, the Mark 4 device is more versatile and precise. Different sizes of transparent (lucite or epoxy resin) cylinders or discs can be mounted on two accurately machined concentric counter-rotating vertical spindles to allow observation along both X_1 and X_2 directions. The cylinders or discs can be machined *in situ* with a built-in lathe and the radial position of the microscope mounted on a frame assembly can be determined accurately with a dial gauge. In the experiments discussed in the text, the chains of spheres were suspended in the annulus between two concentric lucite cylinders. Two copper strips — one inside the inner cylinder and another outside the outer cylinder — acted as the electrodes.

2. PROCEDURES

(a) Formation of the Aggregates

Chains of spheres formed in electric field

Aluminum coated polystyrene spheres were introduced into the Couette apparatus and manipulated with a needle probe to be as close together as possible along the X_2-axis. They were then aligned in an

Figure 2 Photograph of Couette Mark 2 apparatus.

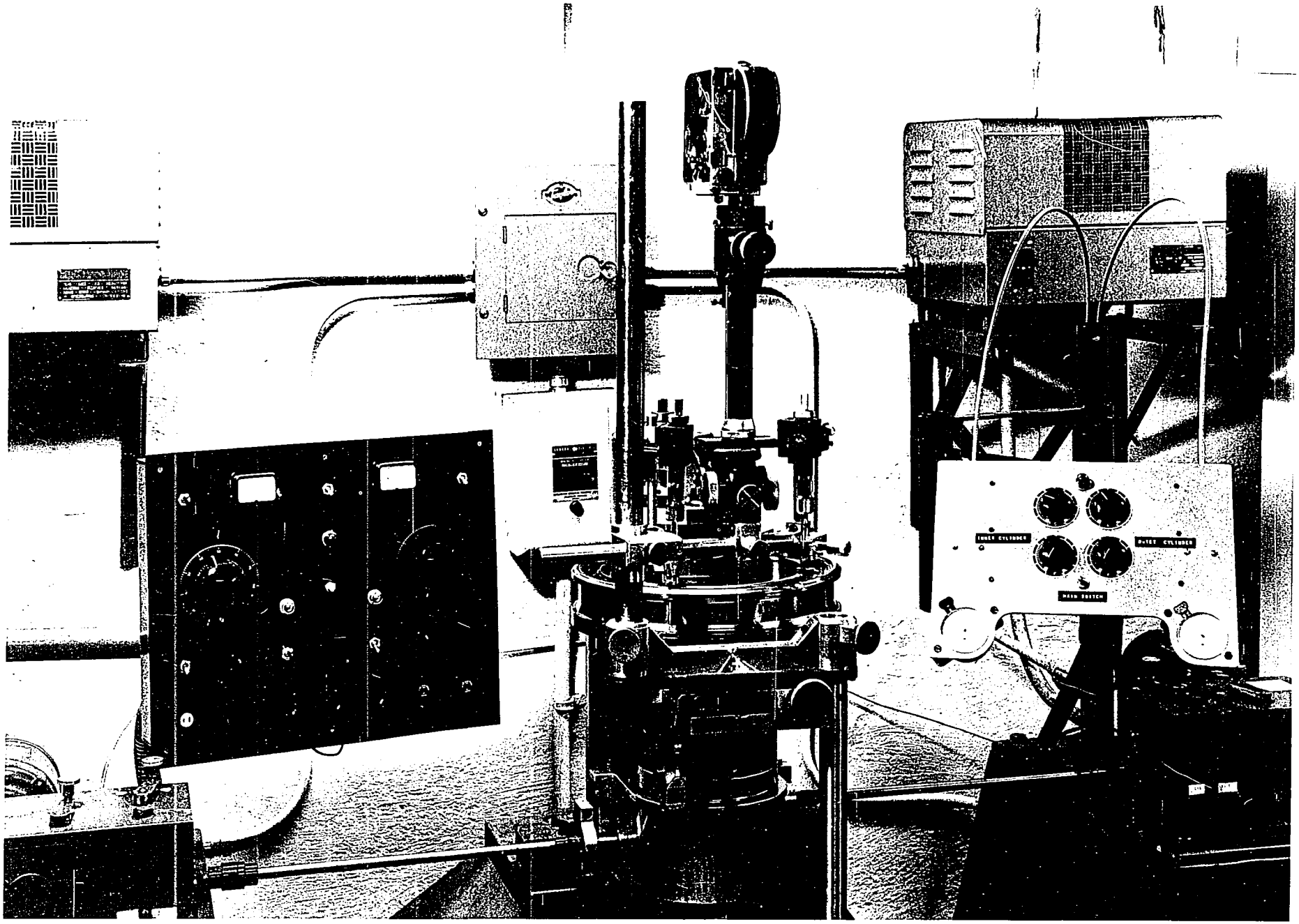
INNER CYLINDER
OUTER CYLINDER
MAIN SWITCH

electric field created by a potential difference of up to 7 kv. between the gap with a 60 cycle a.c. power supply. When necessary the manipulation and electric alignment were repeated until a satisfactorily straight chain of spheres was formed. For fore-aft symmetrical chains of unequal sized spheres, they must be arranged in the proper order before alignment by electric field.

Chains of spheres held together by a fluid

Polystyrene spheres were completely wetted with a fluid and then arrayed with a needle probe into a chain at the edge of a microscope slide. Care was taken to ensure that there was just enough fluid between the spheres since too much fluid often resulted in the formation of non-linear three-dimensional aggregate while too little fluid made the chain easily broken. The chain of spheres was then transferred into the Couette apparatus by gently dipping the slide into and raising it out of the suspending medium.

Non-linear aggregates of spheres

Tetrahedral and some planar triangular and hexagonal aggregates of spheres were formed by arranging a suitable number of spheres, all enclosed in a drop of 0.1% Aerosol AY solution, into the desirable order on a microscope slide with a needle probe. Evaporation was allowed to proceed until only a trace of water was left between the spheres and then the aggregate was slowly and carefully shuffled into the Couette apparatus from the slide.

Aggregates of discs

The discs were wetted with the suspending medium and then piled up one by one on a microscope slide with a needle probe. Extreme care was taken to keep the rouleau as straight as possible. The rouleau was then stuck to a needle probe sideways and dipped nearly horizontally into the

suspending medium. Upon raising the probe with some light jerking the rouleau was left in the Couette apparatus.

Aggregates of rods

Aluminum coated rods were introduced into the Couette apparatus and drawn together end-to-end with a needle probe. They were then aligned in an electric field as described earlier for forming a chain with metal coated spheres. Side-by-side aggregates of rods were more easily formed.

(b) Measurements of ϕ, θ and t

The orientation of an aggregate is defined by its reference line which for chains of spheres formed in an electric field is the chain axis. For a flexible aggregate this reference line is an imaginary straight line joining the centres of the two particles at both ends and for all the non-linear aggregates studied it is any straight line passing through the centres of 2 or 3 spheres. The camera was aligned with one of its frames parallel to the X_2-axis so that the angle ϕ could readily be measured from the photograph.

Since the camera looks down along the X_1-axis, the photographs show the projection of an aggregate on the X_2X_3 plane. Then, for a rigid aggregate it follows by definition that

$$\sin\theta = \frac{\ell_{23}}{\ell_o} \quad ,$$

where ℓ_o is the true aggregate length and ℓ_{23} the length of the projection of the aggregate on the X_2X_3 plane.

An electronic timing device called a chopper cuts off the light path and registers on the movie film as dark frames at a suitable and constant time interval and thereby provides a time scale.

REFERENCES

1. Bartok, W. and Mason, S.G., J. Colloid Sci., 12, 243 (1957).

2. Bartok, W., Ph.D. Thesis, McGill University, 1957.

3. Trevelyan, B.J. and Mason, S.G., J. Colloid Sci., 6, 354 (1951).

APPENDIX III

ROTATING BUBBLE RAFTS

ABSTRACT

A cell was designed and constructed in which a hexagonally packed horizontal monolayer (or raft) of uniform bubbles could be rapidly generated and then compressed by centripetal force. The deformation of individual bubbles and of the entire bubble raft was studied experimentally and fairly good agreement was obtained with a theory derived and solved numerically for small deformations.

1. INTRODUCTION

The stability of suspensions is of considerable academic and practical interest. In this laboratory this problem has been approached by a series of investigations[1-10] on the coalescence of pairs of fluid (gas or liquid) drops suspended in a liquid in gravity, electric and shear fields and combinations thereof. The present work is an extension of the studies of drop coalescence phenomena from systems consisting of two particles to multiparticle systems particularly under conditions of high particle crowding. In order to simplify the systems, experiments were conducted with the drops in a monolayer. In this connection the studies of bubble rafts as models of crystal behaviour first suggested by Marshall[11] and later extended by Bragg and others[12-18] were very helpful.

Five cells were designed and built in numerous attempts to bring about coalescence of bubbles by compression. However, the experiments performed with them all proved to be abortive because of multilayer formation or leakage of bubbles from the cells; finally a centrifugal bubble cell was

designed and constructed which made it possible to generate and then compress by centripetal force a hexagonally packed monolayer (or raft) of uniform bubbles. Two solid surfaces confined the bubbles into a single layer while compression of bubbles by centripetal force instead of a piston eliminated bubble leakage. Although liquid/liquid systems can also be studied by replacing the gas with the lighter liquid, this work was hindered by the difficulty in finding a suitable system which neither wets nor chemically attacks lucite of which the cell was made. Consequently only works on gas/liquid system are described here.

Although bubbles could be made to coalesce simply by increasing the speed of cell rotation, the study of coalescence was unsuccessful. It is known[2-4] that the rest time of a fluid drop at a flat interface between two immiscible fluids follows a roughly Gaussian distribution even for a single given system. For a bubble raft, however, in addition to the distribution of "rest time", there is also a distribution of the origin of coalescence. Another complexity arises from the fact that once coalescence occurred, it spread out rapidly and drastically altered the experimental conditions for further coalescence. A brief qualitative description of the work done on coalescence was, however, given in Appendix IV.

The cell nevertheless has a number of interesting features and was used to study the deformation of bubbles and bubble rafts and its use for this application is discussed in detail here and in Appendix IV.

It was found that bubble deformation increased with increasing speed of rotation ω, bubble radius R_o, bubble raft radius ℓ_o, the distance between the piston and the cover h, but with decreasing radius of rotation r; and that ω predominated all the other factors. By assuming that slightly deformed bubbles were mainly spherical, theoretical equations were derived

and solved numerically. Fairly good agreement between the theory and the experiments was obtained for low deformation (at $\omega < 10$ RPM).

2. EXPERIMENTAL PART

The centrifugal bubble cell is a disc-like cylinder mainly made of lucite (Figures 1 and 2). After the cell was filled up with the continuous phase liquid, as many as 15,000 bubbles with radius of 1 mm. could be generated from a series of hypodermic needles within 100 seconds by pumping air into and sucking liquid out of the cell simultaneously at the same constant rate with an infusion/withdrawal pump (Harvard Apparatus Co., Dover, Mass.). To confine the bubbles in a monolayer, the piston was raised; the distance between the cover and the piston h was measured with a built-in micrometer. In the rotating cell, the bubbles were compressed as they moved radially inward and the continuous liquid phase radially outward because of the density difference. Photographs of bubbles under compression were made through the transparent cover for detailed analysis; two electronic flashes with flash duration less than 10^{-4} second were used to arrest the motion. Further detailed description of the cell is given in Appendix IV.

As the continuous phase the very stable foaming solution used by Bragg[13] was prepared (composition: oleic acid, triethanolamine, glycerine and distilled water); its surface tension γ was 25.9 and 25.7 dynes/cm. measured at 25°C by a du Nuoy tensiometer and by the pendant drop method, respectively and its density ρ was 1.027 g/ml.

The bubble diameter was measured from the average distance between the centres of two neighbouring bubbles along the three axes of symmetry; the assumption that film thickness was negligible in comparison to bubble diameter was proved experimentally. The size of the bubble raft could be

Figure 1 Photograph of centrifugal bubble cell.

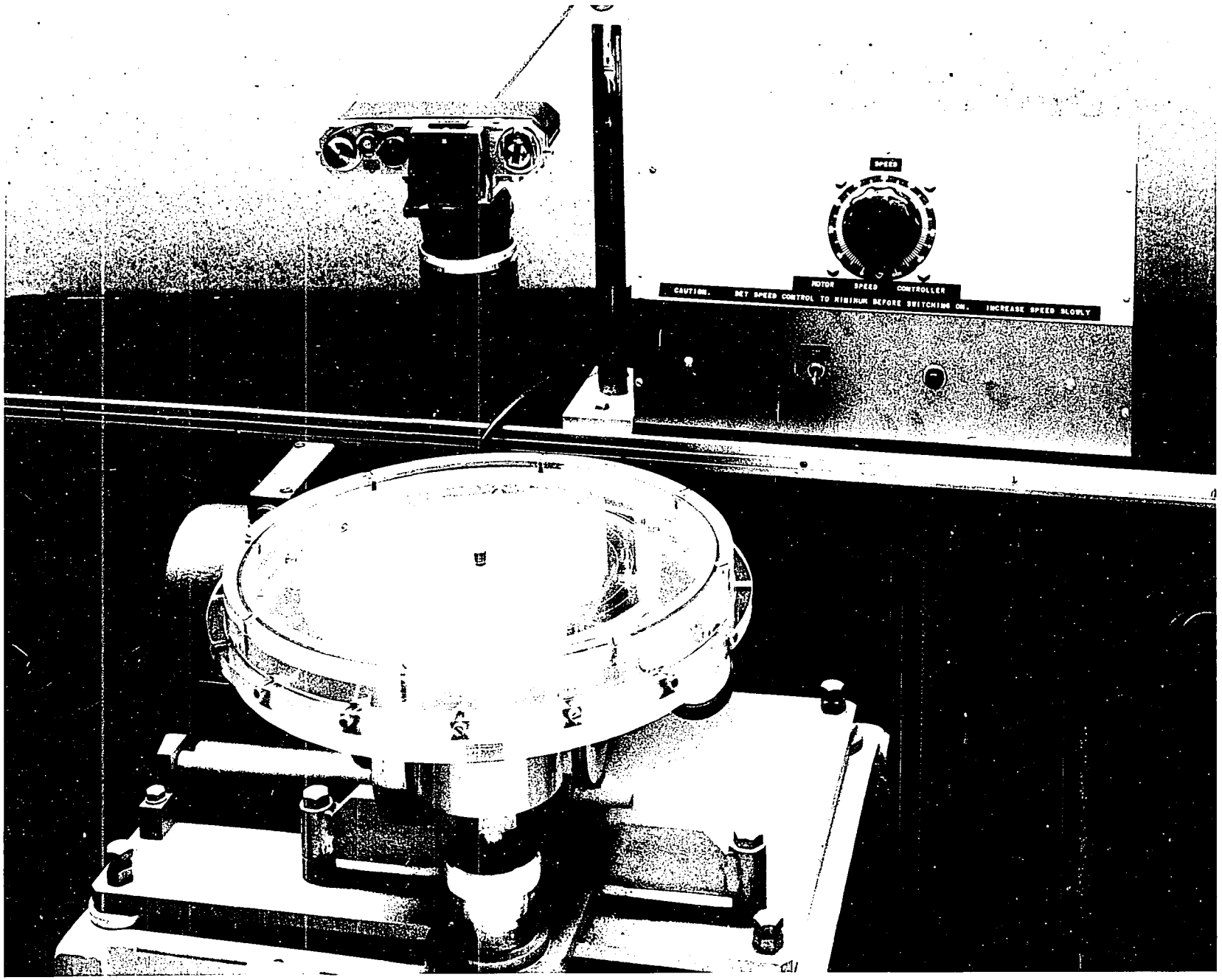
SPEED
MOTOR SPEED CONTROLLER
CAUTION. SET SPEED CONTROL TO MINIMUM BEFORE SWITCHING ON. INCREASE SPEED SLOWLY

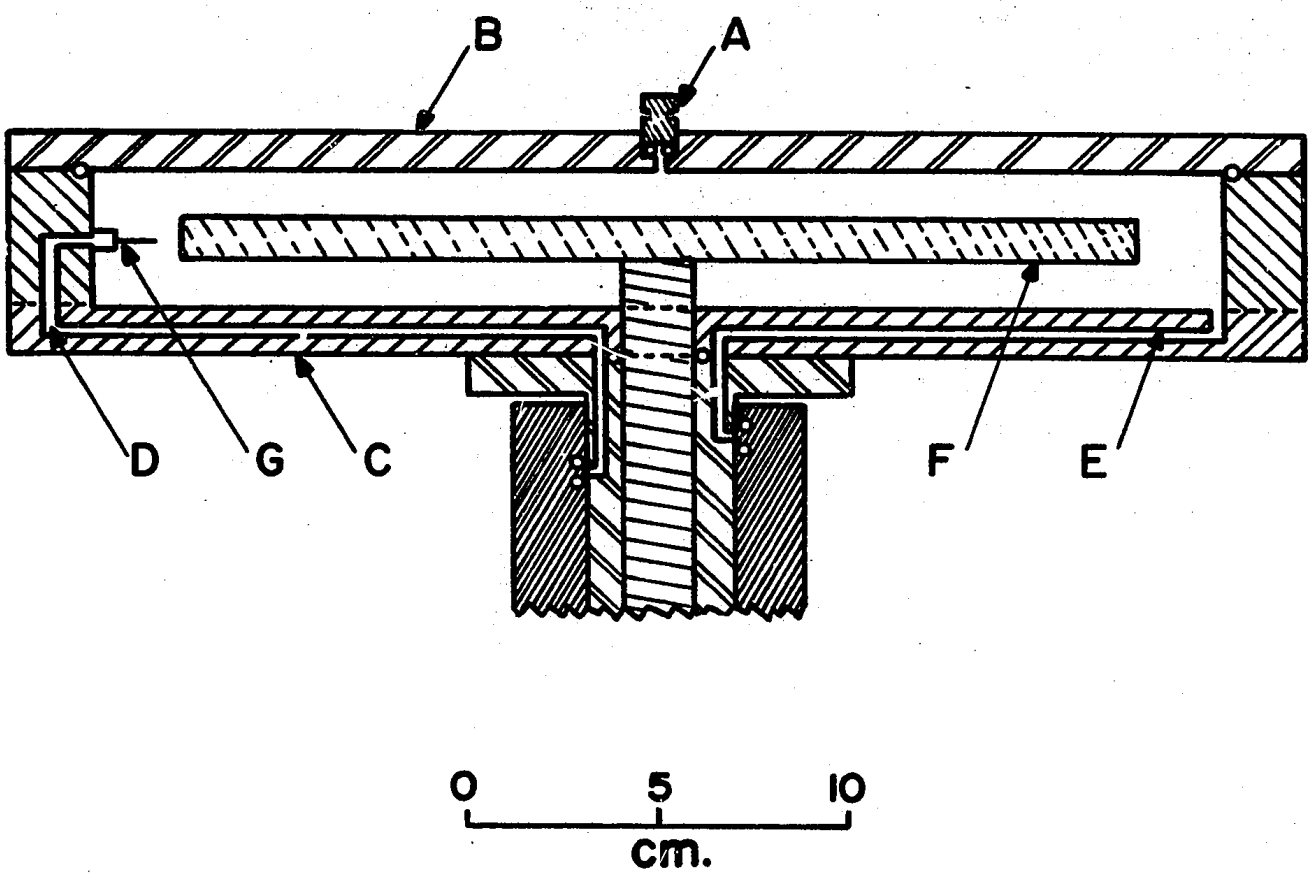

Figure 2 Centrifugal bubble cell (schematic).
A: gas escape B: cover C: cylinder
D: gas channel E: liquid channel F: piston
G: hypodermic needle

measured in terms of the total volume V and number N of the bubbles and the radius of the bubble raft ℓ. Since air is compressible, V was measured from the volume of the liquid sucked out; ℓ was simply measured from the photographs of the circular bubble raft.

It was found experimentally that ℓ decreased with increasing speed of rotation ω, but at constant ω, ℓ reached a constant value very rapidly (Figure 3). It is evident that there could be no relative motion between the liquid and the bubbles under equilibrium conditions. Henceforth the radius of the bubble raft is taken to be the equilibrium value.

As ω increased from zero, the decrease in ℓ was initially very rapid, then slowed down gradually and then increased (Figure 4). Photographic evidence showed that coalescence occurred at and after the point where ℓ dropped suddenly. If ω was kept below the critical speed, there was no coalescence and the compression of the bubble raft was reversible, as illustrated by Figure 5.

On the basis of these preliminary experiments, deformation as a function of the variables involved was studied. When possible, only one variable was changed at a time.

3. RESULTS

At $\omega = 0$, the bubbles can be considered as spherical, each being surrounded by six others in a hexagonal array. When $\omega > 0$, however, the bubbles are compressed horizontally by the centripetal force and as a consequence they expand vertically allowing ℓ to decrease. Each deformed bubble has six flat circles of contact which grow with increasing ω until finally a limiting deformation is reached where a bubble becomes a cylinder with hexagonal cross section and of height h. Although the exact shape of

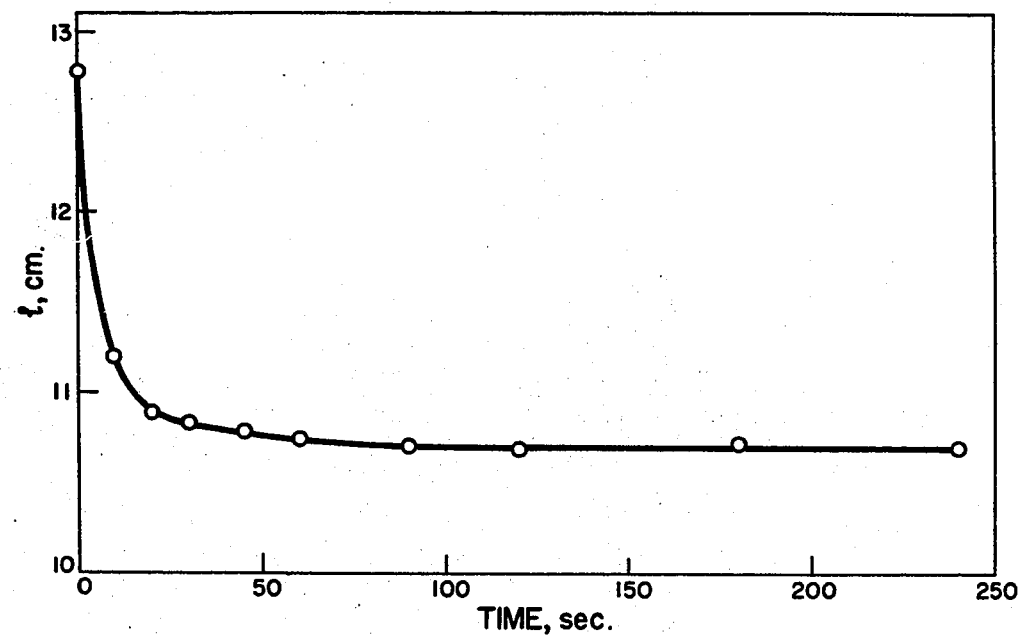

Figure 3 Change of radius of bubble raft with time. Initially ℓ = 12.78 cm. at ω = 8.76 RPM when ω was suddenly increased to 52.59 RPM. Zero time is the moment when ω was suddenly changed.

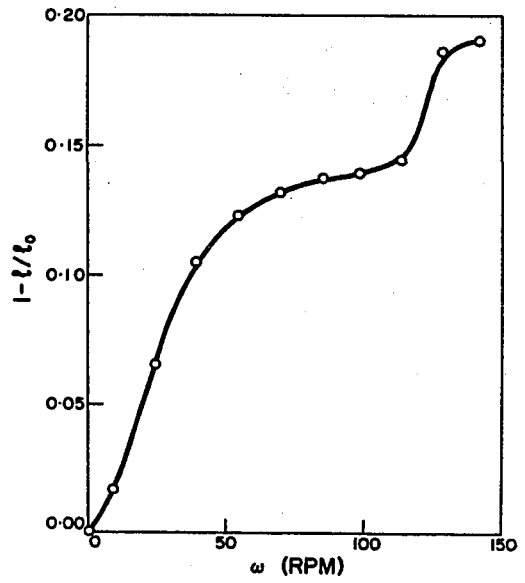

Figure 4 The variation of bubble raft size with ω.

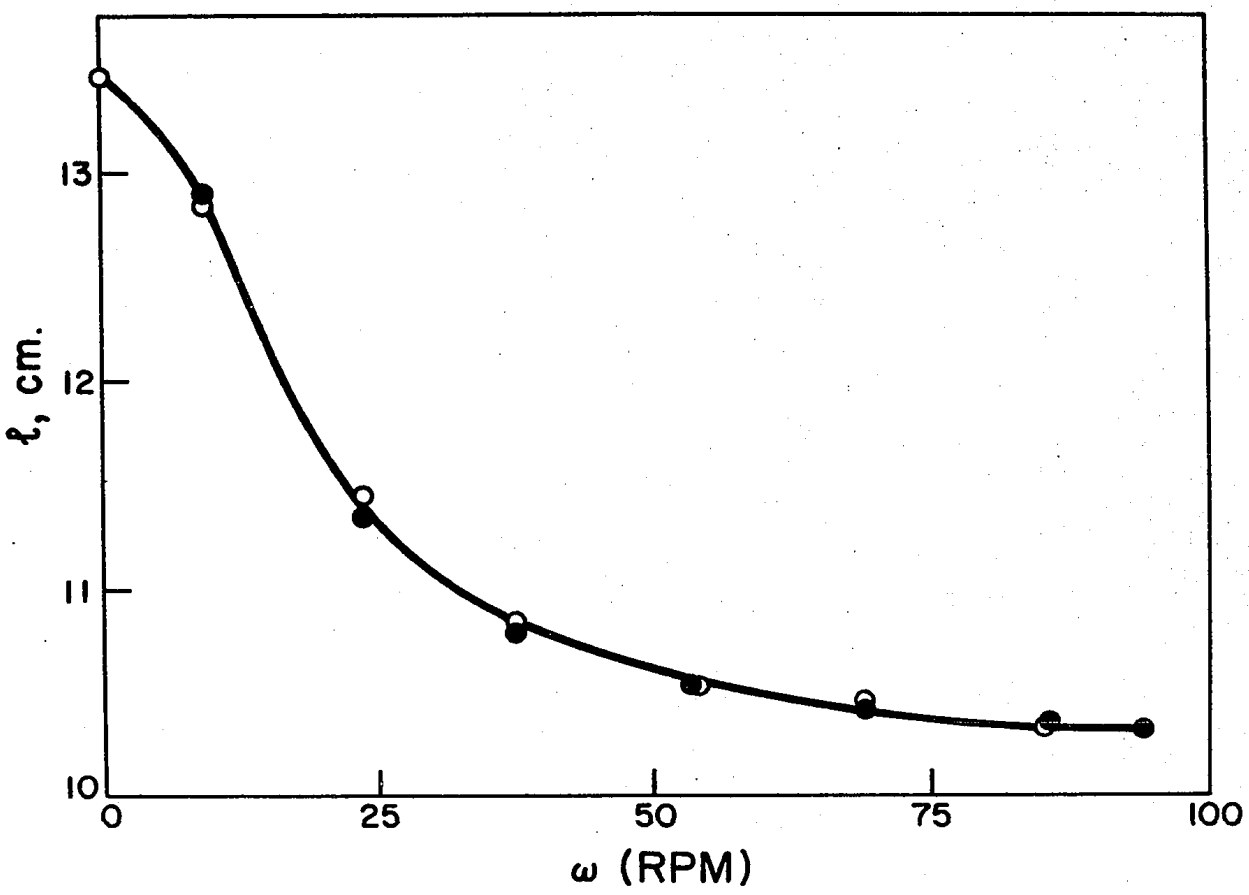

Figure 5 The reversibility of compression of the bubble raft. Closed and open circles for increasing and decreasing ω, respectively.

a deformed bubble is difficult to determine, a simplified model based on the experimental observations is shown in Figure 6.

The most readily measurable quantities which reflect the deformation are ℓ and the distance between the centres of two neighbouring bubbles $2DR_o$ (Figure 7); their variation with ω is given in Table I. It is, however, more convenient to use $(1 - \ell/\ell_o)$ and $(1 - D)$ in displaying the results, since both increase with increasing deformation.

The deformation increased with increasing ω, R_o, ℓ_o and h, but with decreasing radius of rotation r (Figure 8). The rate of increase of deformation, however, decreased with increasing ω and finally approaches zero at high ω. The effects of r and ℓ_o were most pronounced at medium ω, while the effects of R_o and h were always enhanced by increasing ω.

These results can be readily explained. Increasing ω, ℓ_o and decreasing r increased the force acting on the bubbles and therefore the bubbles suffered more deformation. Deformation increased with increasing R_o, because big bubbles are more easily deformed than small ones. It should be pointed out that in studying the effect of R_o, h was also changed. Thus, these two effects were superimposed. Increasing h allowed the bubbles to expand vertically more freely so that they moved closer together, resulting in greater deformation.

The speed of rotation is, however, the predominating factor. At low ω, all other variables had little effect on deformation since the bubbles were only slightly deformed. At medium ω, these effects became more pronounced since a wide range of deformation became possible. The effects of r and ℓ_o were masked at high ω, since there could be no further deformation after the bubbles assumed the limiting shape of hexagonal cylinder. On the other hand, the effects of R_o and h were always enhanced by increasing ω,

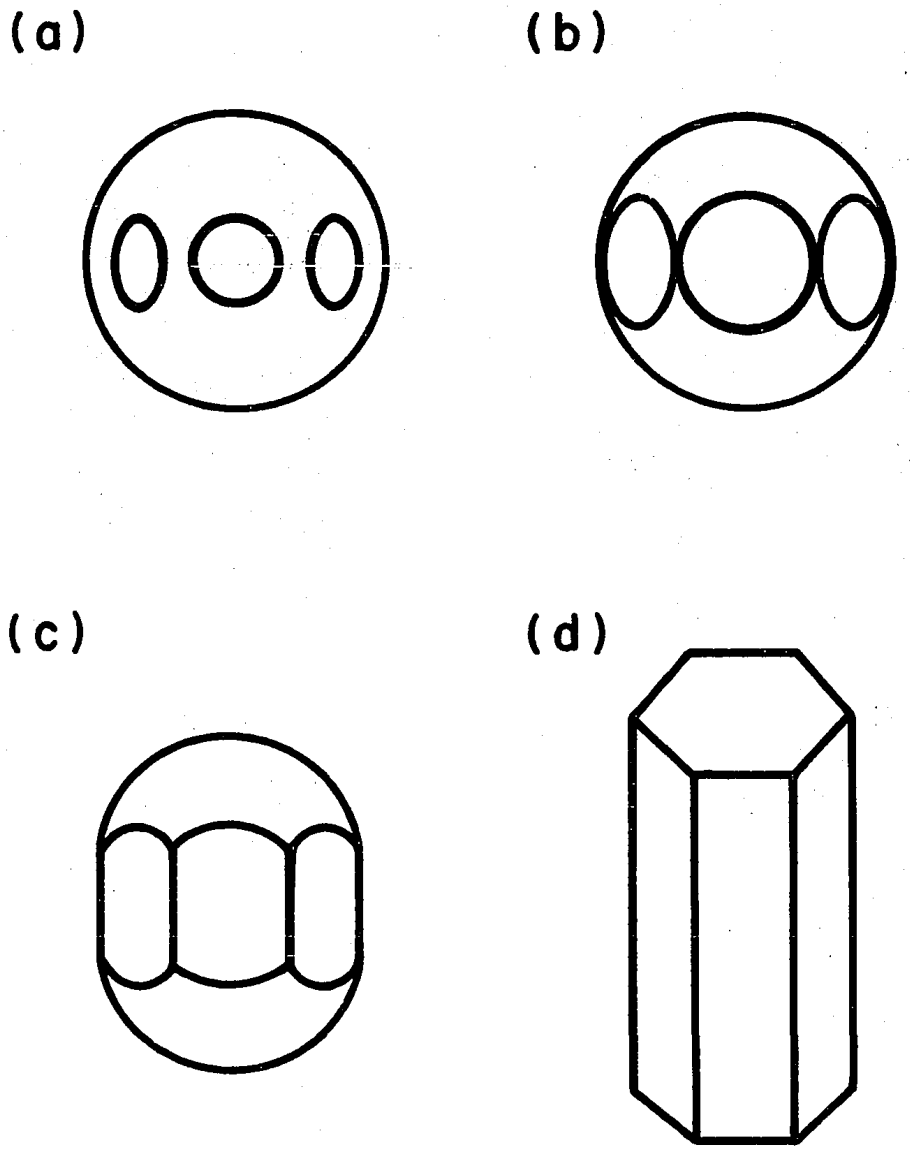

Figure 6 Shape of a bubble at various stages of deformation.
(a) Each bubble has six circles of contact which grow with increasing ω. The bubble is still mainly spherical with radius RR_o ($R > 1$). The distance between the centres of two neighbouring bubbles is $2DR_o$ ($D < 1$), R_o being the original bubble radius (bubble volume $v = 4\pi R_o^3/3$).
(b) The six circles of contact just touch one another. The two parameters R and D are related by $R = D/\cos 30°$.
(c) The bubble, having a hexagonal section in the middle, can no longer be considered as a sphere.
(d) An extremely compressed bubble has the shape of a cylinder with hexagonal cross section and of height h.

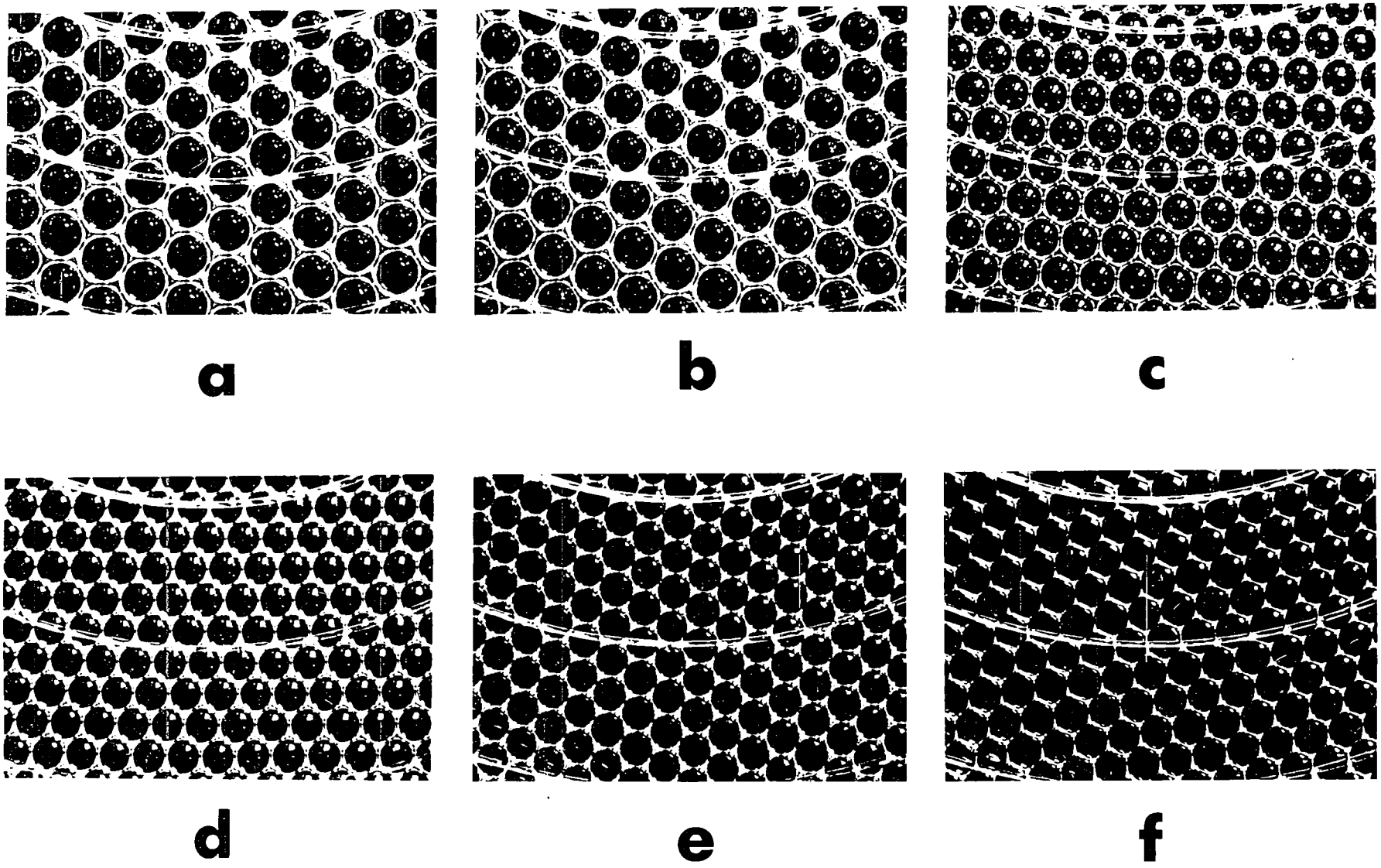

Figure 7 Photographs of bubbles undergoing various deformations. ω(RPM) = 0 (a), 8.75 (b), 22.20 (c), 35.72 (d), 49.42 (e) and 63.81 (f); $R_o = 0.184$ cm. Increasing deformation causes the bubbles to move closer together. (a) - (c) correspond roughly to Figure 6a-6b, (d) and (e) to Figure 6c and (f) nearly approaches Figure 6d.

TABLE I

Measurement of deformation

ω	Radius of bubble raft	Distance between the centres of two neighbouring bubbles	$\frac{\ell}{\ell_0}$	D	$1 - \frac{\ell}{\ell_0}$	1 - D	
0	ℓ_0	$2R_0$	1	1	0	0	No deformation
> 0	ℓ	$2DR_0$	< 1	< 1	> 0	> 0	deformation
Increases	Decreases	Decreases	Decreases	Decreases	Increases	Increases	More deformation

Figure 8 Deformation of individual bubbles and of bubble raft.

(a) Effect of R_o on the deformation of individual bubbles.

	R_o(cm.)	ℓ_o(cm.)	h(cm.)	$2R_o/h$
○	0.111	10.7	0.250	0.855
△	0.120	10.5	0.300	0.800
●	0.163	10.6	0.400	0.815

All at r = 3.75 cm.

(b) Effect of r on the deformation of individual bubbles.
R_o = 0.158 cm., ℓ_o = 7.22 cm., h = 0.40 cm.
ω(RPM): ○ 8.71, △ 21.64, ● 34.40, ▲ 48.55, X 61.41.

(c) Effect of ℓ_o on the deformation of individual bubbles.
R_o = 0.162 cm., h = 0.40 cm., r = 2.75 cm.
ℓ_o(cm.): ○ 6.50, △ 8.61, ● 11.30.

(d) Effect of ℓ_o on the deformation of the bubble raft.
R_o = 0.161 cm., h = 0.40 cm.
ℓ_o(cm.): ○ 6.80, △ 8.76, ● 11.30.

(e) Effect of h on the deformation of individual bubbles.
R_o = 0.157 cm., ℓ_o = 10.30 cm., r = 3.75 cm.
h(cm.): ● 0.30, △ 0.34, ○ 0.38, ▲ 0.42.

(f) Effect of h on deformation of the bubble raft.
R_o = 0.108 cm., ℓ_o = 11.3 cm.
h(cm.): ● 0.200, △ 0.225, ○ 0.250.

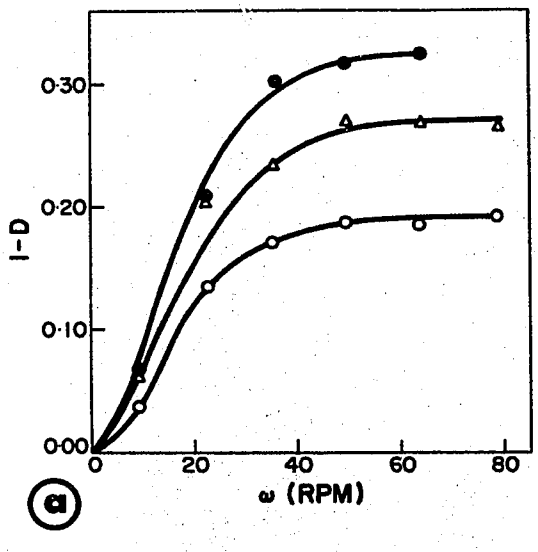
0·30
0·20
0·10
0·00
I-D
0
20
40
60
80
ω (RPM)
a

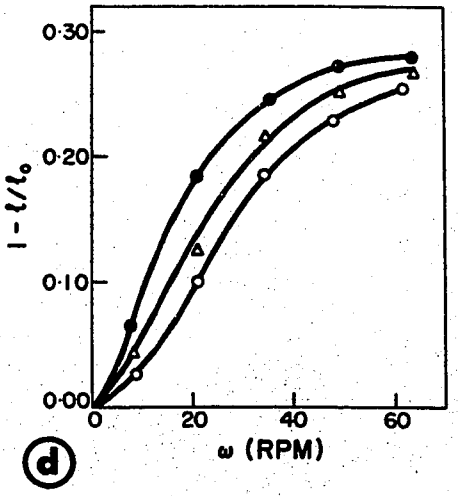
0·30
0·20
0·10
0·00
1 - t/t₀
0
20
40
60
ω (RPM)
d

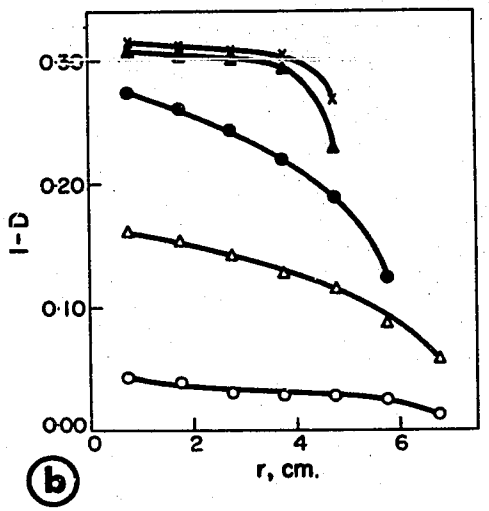
0·30
0·20
0·10
0·00
I-D
0
2
4
6
r, cm.
b

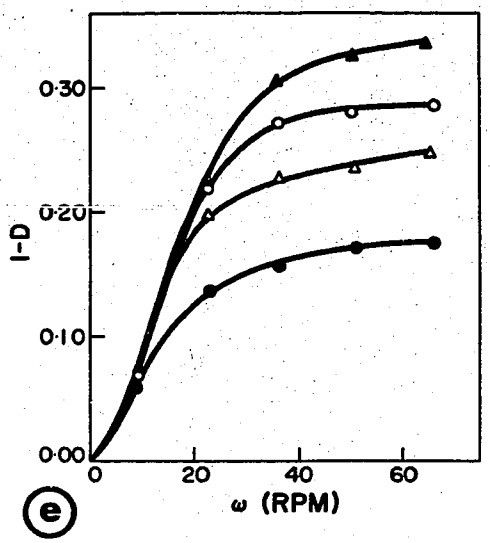
0·30
0·20
0·10
0·00
I-D
0
20
40
60
ω (RPM)
e

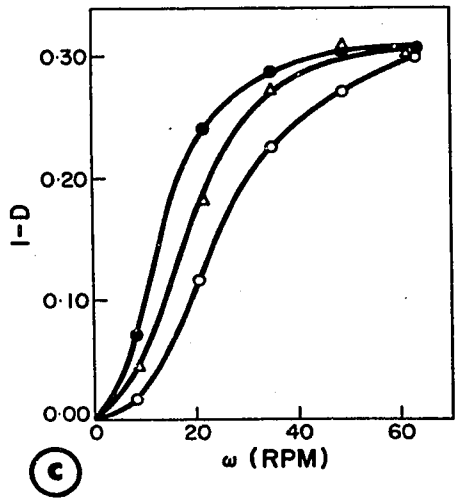
0·30
0·20
0·10
0·00
I-D
0
20
40
60
ω (RPM)
c

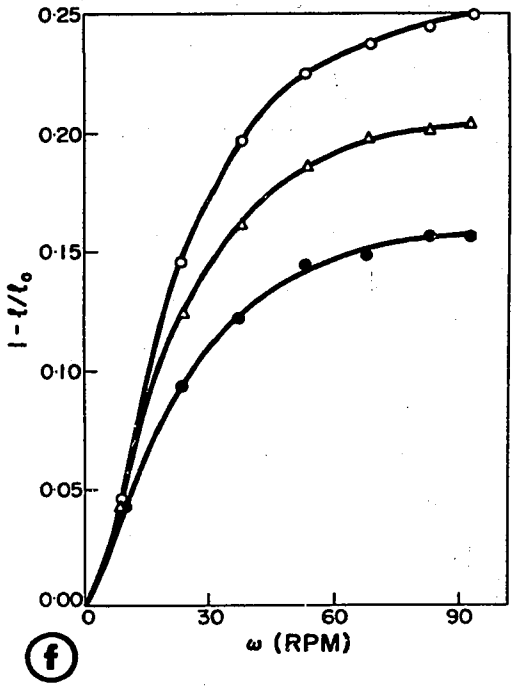
0·25
0·20
0·15
0·10
0·05
0·00
1 - t/t₀
0
30
60
90
ω (RPM)
f

because the limiting shape of the extremely deformed bubble itself varied with R_o and h.

In conclusion it may be said that small bubbles are more rigid, that a small bubble raft is less deformable and that bubbles near the centre are more deformed than those close to the edge of the bubble raft.

4. DISCUSSION

The relative radial movement between the bubbles and the foaming solution in the centrifugal field caused (1) compression and deformation of the individual bubbles and (2) thinning of the film separating the bubbles. Although both processes contributed to the experimentally measured deformation, it can be shown[19] that the effect of film thinning is negligible by comparison.

A knowledge of the shape of the deformed bubble is essential for theoretical analysis of the deformation process. In the simplified model illustrated by Figure 6, the bubble at low deformation ((a) and (b)) is approximated by a sphere with six identical segments cut off at 60°-angle interval and at high deformation ((c) and (d)) the bubble becomes more like a cylinder than a sphere. For small deformations, the shape of the deformed bubble can be calculated.

It can be shown[19] from (1) the constancy of bubble volume before and during deformation (since the pressure in the liquid generated by centrifugation and the excess pressure in the bubble are negligible in comparison to the atmospheric pressure), (2) the balance of the forces acting on a single flat circle of contact under equilibrium conditions and (3) the constancy of the total number of bubbles in the raft (when there is no coalescence) that

$$4R^3 - 9R^2D + 3D^3 + 2 = 0 \,, \tag{1}$$

$$\int_r^{\ell} \frac{r^2 dr}{D^2} = \frac{9\gamma r(R^2 - D^2)}{\sqrt{3}\, R_o \Delta\rho\omega^2 DR} \,, \tag{2}$$

$$\frac{\ell_o^2}{2} = \int_o^{\ell} \frac{r dr}{D^2} \,, \tag{3}$$

where RR_o is the radius of the deformed bubble, $2DR_o$ the distance between the centres of two neighbouring deformed bubbles, $\Delta\rho$ the density difference between the bubble and the foaming solution and all other symbols have already been defined.

Though these equations cannot be solved exactly, because both D and R depend on r, they can be reduced, by making some approximations[19], to

$$\frac{\ell_o^2}{2} = \int_o^{\ell} (1 + 2\beta + 3\beta^2) r dr \,, \tag{4}$$

$$\beta = -\frac{1}{5} + \left\{ \frac{1}{25} + \frac{e^{-r^2/K}}{2.5Kr} \left[F(\ell) - F(r) \right] \right\}^{1/2} \,, \tag{5}$$

$$F(r) = \sum_{i=1}^{5} \frac{r^{2i+1}}{(2i+1)K^{i-1}(i-1)!} \,, \tag{6}$$

$$K = \frac{18\gamma}{\sqrt{3}\, R_o \Delta\rho\omega^2} \tag{7}$$

with

$$\beta = 1 - D \,, \qquad 0.110 \geqslant \beta \geqslant 0 \,; \tag{8}$$

$$\alpha = R - 1 \,, \qquad 0.027 \geqslant \alpha \geqslant 0 \,; \tag{9}$$

and

$$\alpha = \frac{3\beta^2}{2(1 - 3\beta)} \,. \tag{10}$$

Equations (8) and (9) define mathematically the region of small deformation where the theory is valid.

Equation (4) was solved numerically with the results plotted in Figure 9 to give a picture of the complicated relationships between the variables.

In Figure 10, ℓ/ℓ_o was plotted against ω in (a) and (b) for two bubble rafts. The agreement was good at low ω, but at higher ω the theory predicted less than experimentally measured deformation. The deformation of the individual bubble β was plotted against ω in (c) and (d) for two r's and against r in (e) for $\omega = 8.71$ RPM, all data being taken from a single experiment. It can be seen that $\beta_{theo.} > \beta_{exp.}$ at small r, but $\beta_{theo.} < \beta_{exp.}$ at large r.

Although the theory is not in perfect agreement with the experimental results, it does give correct qualitative relationships between the variables (Figure 9). It may be noted that h does not appear in the theoretical equations, as there is very little vertical expansion in the stage of low deformation (from $2R_o$ to $2.054R_o$, since $1.027 \geq R \geq 1$) and the experimental conditions were such ($h > 2.25R_o$) that there was always enough room for free vertical expansion.

REFERENCES

1. Bartok, W. and Mason, S.G., J. Colloid Sci., 14, 13 (1959).
2. Charles, G.E. and Mason, S.G., J. Colloid Sci., 15, 105 (1960).
3. Charles, G.E. and Mason, S.G., J. Colloid Sci., 15, 236 (1960).
4. Allan, R.S., Charles, G.E. and Mason, S.G., J. Colloid Sci., 16, 150 (1961).
5. Allan, R.S. and Mason, S.G., Trans. Faraday Soc., 57, No. 467, Part II, 2027 (1961).

Figure 9 Numerical evaluations of Equation (4) for $\gamma = 25.8$ dynes/cm. and $\Delta\rho = 1.027$ g/ml.
(a) Effect of ℓ_o on the deformation of individual bubbles.
$R_o = 0.150$ cm., $r = 3.75$ cm.
ℓ_o (cm.): (1) 5.00, (2) 7.50, (3) 10.00.
(b) Effect of ℓ_o on the deformation of the bubble raft.
$R_o = 0.150$ cm.
ℓ_o (cm.): (1) 5.00, (2) 7.50, (3) 10.00.
(c) Effect of r. $\omega = 7.50$ RPM, $R_o = 0.150$ cm.
ℓ_o (cm.): (1) 5.00, (2) 7.50, (3) 10.00.
(d) Effect of r. $\omega = 10.00$ RPM, $\ell_o = 7.50$ cm.
R_o (cm.): (1) 0.100, (2) 0.150, (3) 0.200.
(e) Effect of R_o on the deformation of individual bubbles.
$\ell_o = 7.50$ cm., $r = 2.75$ cm.
R_o (cm.): (1) 0.100, (2) 0.150, (3) 0.200.
(f) Effect of R_o on the deformation of the bubble raft.
$\ell_o = 7.50$ cm.
R_o (cm.): (1) 0.100, (2) 0.150, (3) 0.200.

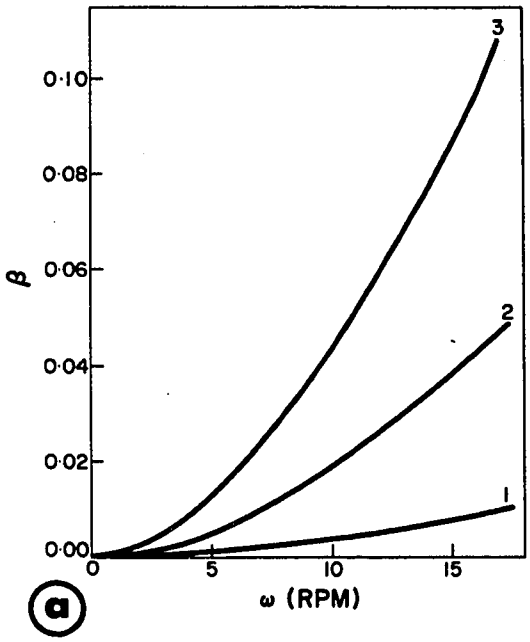
0·10
0·08
0·06
0·04
0·02
0·00
β
3
2
1
0
5
10
15
ω (RPM)

(a)

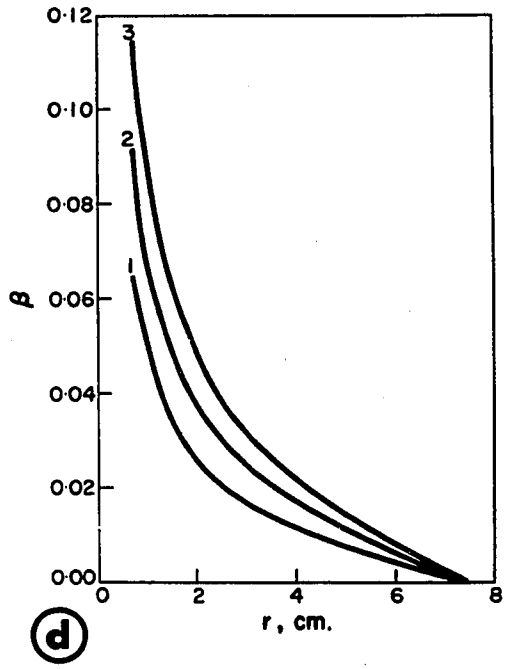
0·12
0·10
0·08
0·06
0·04
0·02
0·00
β
3
2
1
0
2
4
6
8
r, cm.

(d)

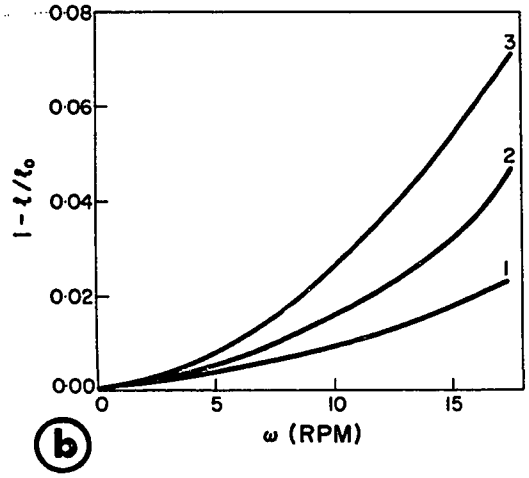
0·08
0·06
0·04
0·02
0·00
1 - t/t₀
3
2
1
0
5
10
15
ω (RPM)

(b)

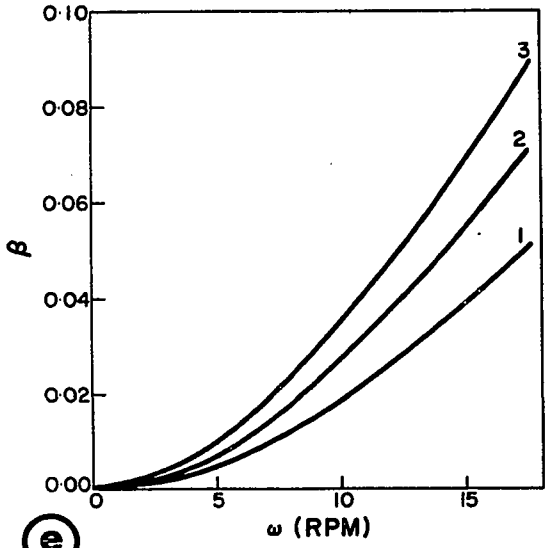
0·10
0·08
0·06
0·04
0·02
0·00
β
3
2
1
0
5
10
15
ω (RPM)

(e)

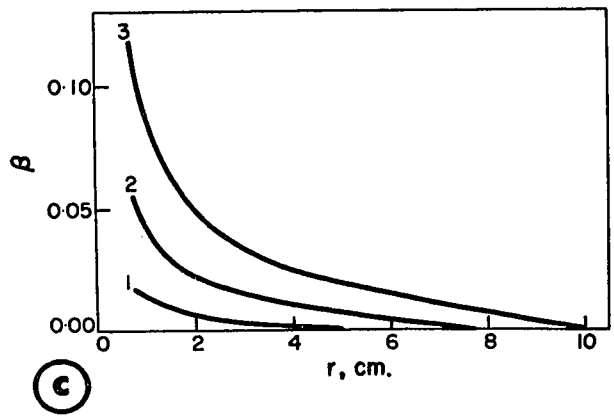
0·10
0·05
0·00
β
3
2
1
0
2
4
6
8
10
r, cm.

(c)

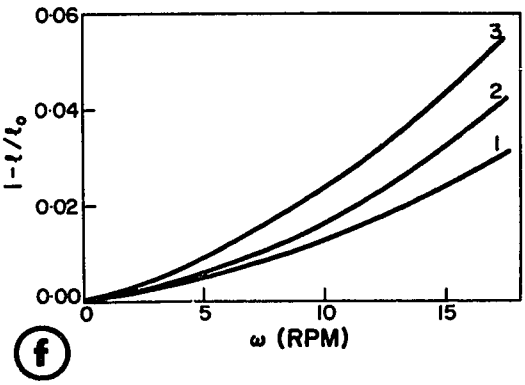
0·06
0·04
0·02
0·00
1 - t/t₀
3
2
1
0
5
10
15
ω (RPM)

(f)

Figure 10 Comparison between theory (curves) and experiment (points).
Deformation of bubble raft: (a) $R_o = 0.163$ cm., $\ell_o = 8.61$ cm.; (b) $R_o = 0.157$ cm., $\ell_o = 11.30$ cm.
Deformation of individual bubbles: $R_o = 0.158$ cm., $\ell_o = 8.08$ cm.
Effect of ω for $r = 0.75$ cm. (c) and $r = 2.75$ cm. (d).
Effect of r for $\omega = 8.71$ RPM (e).
It should be pointed out that the theory is valid only for small deformation ($\beta \leq 0.110$) and consequently there were very few experimental points available for comparison in this region.

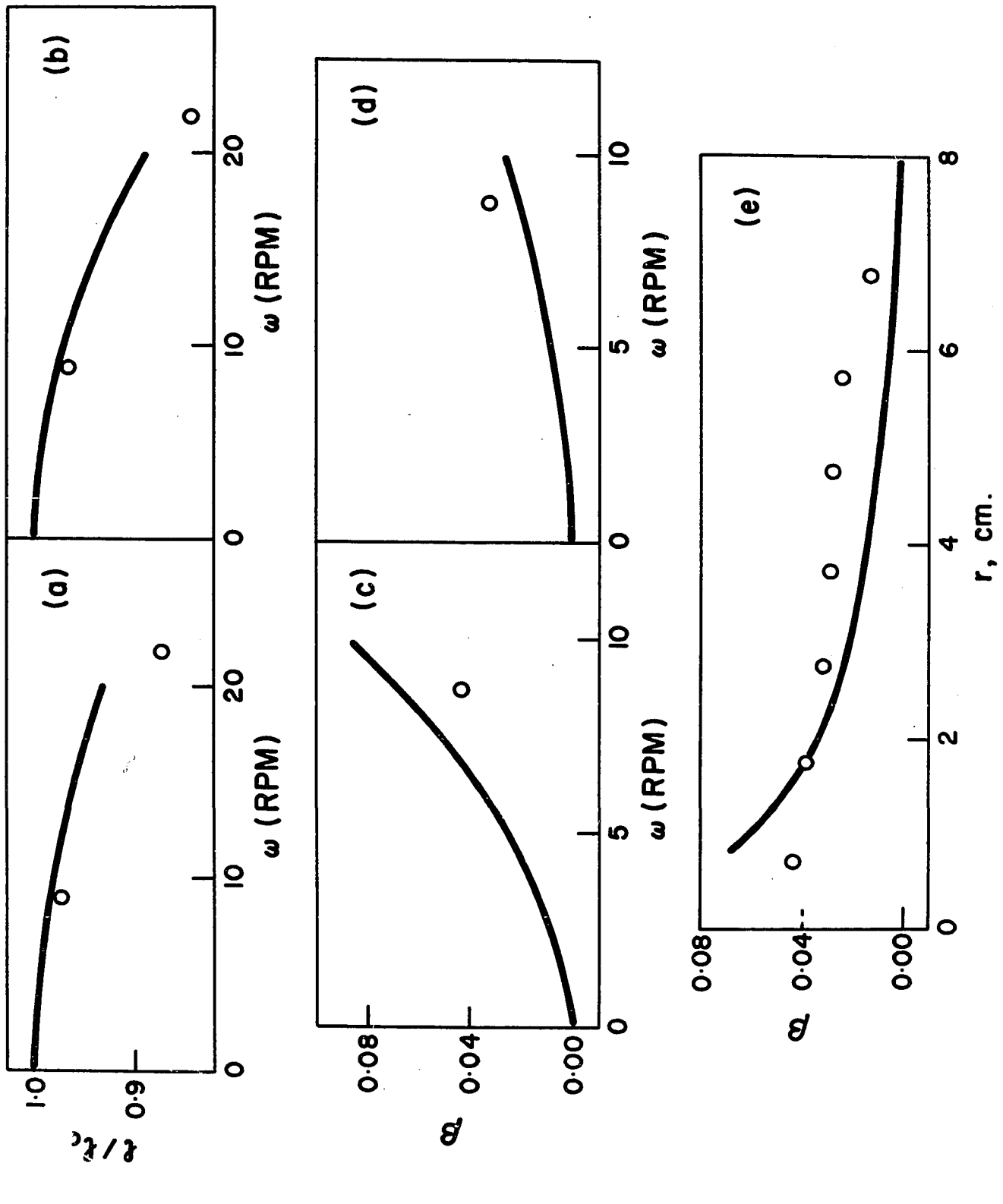
(a)
(b)
(c)
(d)
(e)
ω (RPM)
ω (RPM)
ω (RPM)
ω (RPM)
r, cm.
ℓ / ℓc
β
β
1·0
0·9
0·08
0·04
0·00
0·08
0·04
0·00
0
10
20
0
5
10
0
2
4
6
8

6. Allan, R.S. and Mason, S.G., J. Colloid Sci., 17, 383 (1962).

7. MacKay, G.D.M. and Mason, S.G., Nature, 191, 488 (1961).

8. MacKay, G.D.M. and Mason, S.G., Can. J. Chem. Engr., 41, 203 (1963).

9. MacKay, G.D.M. and Mason, S.G., J. Colloid Sci., 18, 674 (1963).

10. MacKay, G.D.M. and Mason, S.G., Kolloidzeitschrift und Zeitschrift für Polymere, 195, 138 (1964).

11. Marshall, M.J., J.A.C.S., 39, 2386 (1917).

12. Bragg, L., J. Sci. Instrum., 19, 148 (1942).

13. Bragg, L. and Nye, J.F., Proc. Roy. Soc., A190, 474 (1947).

14. Bragg, L. and Lomer, W.M., Proc. Roy. Soc., A196, 171 (1949).

15. Lomer, W.M., Proc. Camb. Phil. Soc., 45, 660 (1949).

16. Lomer, W.M., Proc. Roy. Soc., A196, 182 (1949).

17. Nicolson, M.M., Proc. Camb. Phil. Soc., 45, 288 (1949).

18. Lomer, W.M. and Nye, J.F., Proc. Roy. Soc., A212, 576 (1952).

19. This Thesis, Appendix IV.

APPENDIX IV

DETAILS OF APPENDIX III

1. CENTRIFUGAL BUBBLE CELL

The cell (Appendix III, Figures 1 and 2) has an inner diameter of 30 cm. and a depth of 3 cm. On the bottom surface of the transparent lucite cover a series of concentric circles 1 cm. apart was engraved to facilitate the measurement of r. While an O-ring between the cover and the cylinder renders the cell air tight, a gas escape in the centre of the cover provides an exit for air and the undesirable foam generated in filling the cell.

Two interchangeable pistons with diameter of 24 cm. are available; one made of lucite to allow transmitted illumination and another made of carbon black epoxy resin to provide a background of high contrast for incident illumination. The cylinder, the piston and the cover all rotate as a unit so that there is no shear stress between them. The position of the piston is adjusted by turning the micrometer thimble and h can be read off directly from the micrometer to 0.05 mm. A key mechanism allows the piston to be moved up or down even during cell rotation.

Two separate channels were tunnelled through the cell from two stationary inlets to the movable inner part of the cell. The 16 nozzles, connected to the gas channel and evenly distributed around the cylinder, can be fitted with different sizes of hypodermic needles for the generation of gas bubbles of desirable sizes. By means of rotary seal the two channels remain open even when the cell is rotating.

The centrifugal aggregation cell is driven by a Bepco variable speed d.c. motor with a speed range of 300 - 3,000 RPM and maximum output

of 1/4 HP. The speed of the motor is regulated by a controller, the scale reading of which is linearly proportional to the motor speed throughout the entire speed range. Through two different combinations of flywheels two ranges of cell speed of rotation are available, one from 0 to 150 RPM and another from 0 to 300 RPM. The tachometer is connected to a reduction pulley so that ω can be measured to 0.03 RPM.

To carry out an experiment, the cell is first cleaned thoroughly and then filled up with the foaming solution. The bubbles are generated by pumping air into and sucking liquid out of the cell simultaneously at the same constant rate. When enough bubbles are generated, the piston is raised to a distance slightly greater than $2R_o$ below the cover. The bubbles are then compressed by rotating the cell. Photographs of the bubbles are taken at various stages of compression for detailed analysis.

2. THE RELATIVE IMPORTANCE OF BUBBLE DEFORMATION AND FILM THINNING

The packing of a monolayer of uniform bubbles confined between the piston and the cover is equivalent to that of the circles on a plane[1,2]. It can be shown that for hexagonal packing the number of circles per unit area is

$$n = \frac{\sqrt{3}}{6a^2}, \tag{1}$$

where a is the radius of the circles. If there are N bubbles of radius R_o in a bubble raft, then the total volume of the bubbles is

$$V = N \cdot \frac{4}{3}\pi R_o^3 \tag{2}$$

and the area necessary for hexagonal packing of all these bubbles is

$$A = \frac{N}{n} = \pi \ell_o^2 , \tag{3}$$

where ℓ_o is the radius of the stationary bubble raft. Combining (1), (2) and (3) leads to

$$\ell_o = \left(\frac{9V}{2\sqrt{3}\,\pi^2 R_o}\right)^{1/2} \tag{4}$$

and

$$\ell_o = \left(\frac{6NR_o^2}{\sqrt{3}\,\pi}\right)^{1/2} . \tag{5}$$

The radius of the bubble raft reaches minimum when the bubbles are extremely compressed and they can be considered as cylinders with hexagonal cross section and with the height equal to h. If the total volume of the bubbles is fixed, then

$$V = \pi \ell_{min}^2 h \tag{6}$$

and hence

$$\ell_{min} = \left(\frac{V}{\pi h}\right)^{1/2} . \tag{7}$$

Dividing (7) by (4) gives

$$\frac{\ell_{min}}{\ell_o} = \left(\frac{2\sqrt{3}\,\pi R_o}{9h}\right)^{1/2} = 0.778\left(\frac{2R_o}{h}\right)^{1/2} . \tag{8}$$

In the special case when $h = 2R_o$ (8) becomes

$$\frac{\ell_{min}}{\ell_o} = 0.778 . \tag{9}$$

Thus, when $h = 2R_o$, ℓ_{min} is about 78% of ℓ_o and if $h > 2R_o$, ℓ_{min} can be reduced still further.

If the distance between the centres of two neighbouring bubbles in a stationary bubble raft is

$$R'_o = (1 + \delta)R_o , \tag{10}$$

where δR_o is the film thickness at zero speed, then the bubble raft can be

considered as a raft of N circles with radius R'_o at the stationary state and R_o at the extreme state of film thinning. It follows from (5) and (10) that

$$\frac{\ell_{min}}{\ell_o} = (1 + \delta)^{-1} . \qquad (11)$$

It is clear from Table I that even when $\delta = 10^{-2}$, i.e., a film thickness in the order of 10^{-3}cm., since R_o in all experiments is in the order of 10^{-1}cm., the maximum possible decrease in ℓ due to film thinning alone is only 1%.

Thus the change in ℓ due to the deformation of the individual bubbles is obviously much more important in comparison with that due to film thinning. In fact, the effect of film thinning is negligible.

3. DERIVATION AND APPROXIMATE SOLUTIONS OF THE BUBBLE RAFT DEFORMATION EQUATIONS

(a) Derivation

Under our experimental conditions the pressure in the liquid generated by centrifugation (max. 5600 dynes/cm.^{2}) and the excess pressure in the bubble (max. 520 dynes/cm.^{2}) are negligible in comparison with the atmospheric pressure. Furthermore the temperature fluctuation during an experiment was less than 1°C. Thus, the volume of the bubble remains constant during deformation.

According to our simplified model of a deformed bubble (Figure 1) the volume of the deformed bubble is given by

$$v = \frac{4}{3}\pi(RR_o)^3 - 6v' , \qquad (12)$$

where

$$v' = \frac{\pi R_o^3}{3}(R - D)^2(2R + D) . \qquad (13)$$

TABLE I

Effect of film thinning

δ	0	10^{-4}	10^{-3}	10^{-2}	10^{-1}
$1 + \delta$	1	1.0001	1.001	1.010	1.100
$(1 + \delta)^{-1}$	1	0.9999	0.999	0.990	0.909

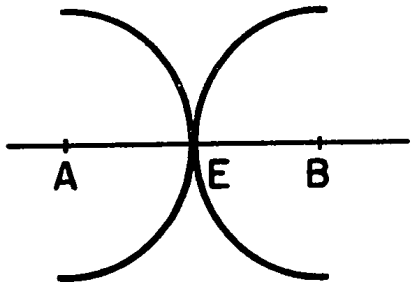

(a) NON-DEFORMED BUBBLE

$AE = EB = R_0$

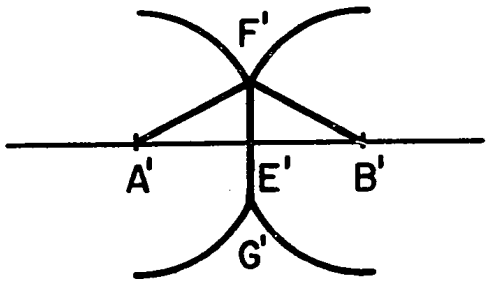

(b) DEFORMED BUBBLE

$A'F' = F'B' = RR_0$, $R \geqslant 1$

$A'E' = E'B' = DR_0$, $D \leqslant 1$

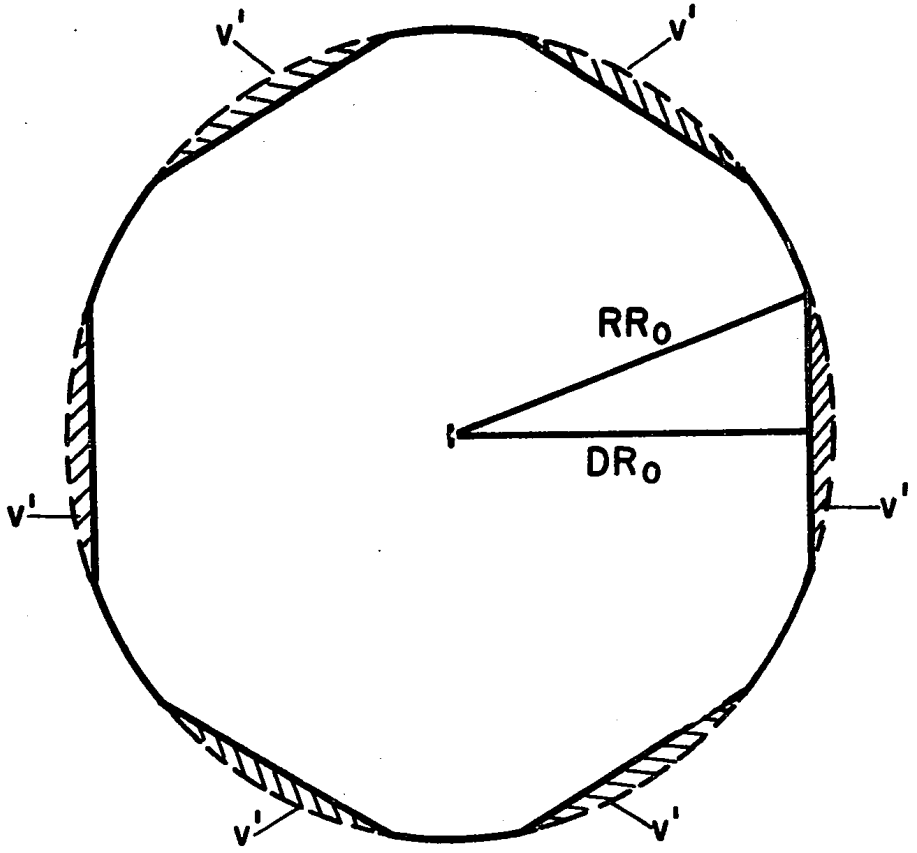

(c) VOLUME CONSTANCY

$$\frac{4}{3}\pi R_0^3 = \frac{4}{3}\pi (RR_0)^3 - 6v'$$

$$v' = \frac{\pi R_0^3}{3}(R-D)^2(2R+D)$$

Figure 1 Definition of dimensionless parameters D and R and constancy of bubble volume.

Equating (12) with $v = 4\pi R_o^3/3$ and simplifying the resulting equation give (III - 1)

$$4R^3 - 9R^2D + 3D^3 + 2 = 0 \ . \qquad \text{(III - 1)}$$

It must be pointed out that (III - 1) is valid only when the six circles of contact of the same bubble are isolated from one another. The limiting state of deformation is reached when the circles of contact just touch one another (Figure 6b, Appendix III), i.e., when

$$R = \frac{D}{\cos 30^\circ} = \frac{2D}{\sqrt{3}} \ . \qquad (14)$$

By solving (III - 1) and (14) simultaneously one obtains the following limiting values of D and R:

$$D = 0.8896 \quad \text{and} \quad R = 1.027 \ . \qquad (15)$$

Thus, the range of low deformation can be exactly defined by

$$1 \geqslant D \geqslant 0.8896 \quad \text{or} \quad 1.027 \geqslant R \geqslant 1 \ . \qquad (16)$$

If a ring with radius r and width dr is considered as an element of the bubble raft, then the number of bubbles in it is $2\pi rndr$. Since the centripetal force acting on a bubble radially inward is $4\pi R_o^3 \Delta\rho\omega^2 r/3$, the force acting on the periphery of the ring element is

$$dF = \frac{8}{3}\pi^2 R_o^3 \, \Delta\rho\omega^2 nr^2 dr \ . \qquad (17)$$

Since the ring is also being pushed by the bubbles outside of it, the total force acting on its periphery is

$$F = \frac{8}{3}\pi^2 R_o^3 \, \Delta\rho\omega^2 \int_r^\ell nr^2 dr \ . \qquad (18)$$

The force acting on a single bubble at a distance r from the centre of the cell is

$$f = F \cdot \frac{2DR_o}{2\pi r} = \frac{8}{3}\pi R_o^4 \, \Delta\rho\omega^2 \, \frac{D}{r} \int_r^\ell nr^2 dr \ . \qquad (19)$$

The error introduced by this approximating factor $2DR_o/2\pi r$ is less than one per cent when $r \geqslant 5R_o$, and less than one-tenth of a per cent when $r \geqslant 10R_o$.

In a rotating bubble raft, one can consider the deformed bubbles as circles of variable sizes, only the distance between the two neighbouring bubbles $2DR_o$ becomes the diameter of the circle. The number of bubbles per unit area is therefore given by

$$n = \frac{\sqrt{3}}{6D^2R_o^2} . \tag{20}$$

Substituting (20) into (19) finally yields

$$f = \frac{4\sqrt{3}}{9} \pi R_o^2 \Delta\rho\omega^2 \frac{D}{r} \int_r^{\ell} \frac{r^2 dr}{D^2} . \tag{21}$$

Since the excess pressure in the bubble is given by $\Delta\rho = 2\gamma/RR_o$ and the area of the flat circle of contact is $\pi R_o^2(R^2 - D^2)$ (Figure 1), the force acting on a single flat circle of contact from inside the bubble is therefore $2\pi\gamma R_o(R^2 - D^2)/R$.

Since there is no shear and $(R_o/\ell_o) \ll 1$, the force is isotropic and consequently the six circles of contact of the same bubble are equal in area. Furthermore, (21) indicates that in a rotating bubble raft the bubbles at equal distance away from the centre of the raft experience centripetal force of equal magnitude. Thus, it is permissible to consider a bubble lying on one of the axes of symmetry instead of any arbitrary one lying on the circumference. This greatly simplifies the geometry involved.

For a bubble lying on one of the three axes of symmetry, the radial direction from bubble centre to raft centre is perpendicular to one of the flat circle of contact. The force acting on a single bubble f and

that on a single flat circle of contact F_f is then related by the following equation

$$f = F_f + 2F_f\cos 60^\circ = 2F_f \ . \tag{22}$$

In the equilibrium state, the force acting on a single flat circle of contact must be balanced. Hence from (21) and (22),

$$\int_r^{\ell} \frac{r^2 dr}{D^2} = \frac{9\gamma r(R^2 - D^2)}{\sqrt{3}\, R_o \Delta\rho\omega^2 DR} \ . \tag{III - 2}$$

For a stationary bubble raft with radius ℓ_o, the total number of bubbles is

$$N = \int_o^{\ell_o} 2\pi rn dr = \frac{\pi\sqrt{3}\,\ell_o^2}{6R_o^2} \ , \tag{23}$$

since $n = \sqrt{3}/6R_o^2$ is independent of r. For a rotating bubble raft, the number of bubbles per unit area is given by (20) and therefore

$$N = \frac{\sqrt{3}\,\pi}{3R_o^2} \int_o^{\ell} \frac{rdr}{D^2} \ . \tag{24}$$

However, as long as there is no coalescence, N is a constant. Equations (23) and (24) can therefore be equated to give

$$\frac{\ell_o^2}{2} = \int_o^{\ell} \frac{rdr}{D^2} \ . \tag{III - 3}$$

The remaining problem is to solve equations (III 1-3) simultaneously for the three unknowns R, D and ℓ. The main difficulty lies in the integrations appearing in (III - 2) and (III - 3), since both R and D are functions of r.

(b) Approximate Solutions

If we let

$$\alpha = R - 1 \qquad \text{(III - 9)}$$

and

$$\beta = 1 - D \,, \qquad \text{(III - 8)}$$

then according to (16) the range of low deformation is defined exactly by

$$0.027 \geqslant \alpha > 0 \qquad \text{and} \qquad 0.110 \geqslant \beta \geqslant 0 \,. \qquad (25)$$

Making use of the following approximations

$$R^2 = 1 + 2\alpha \,, \qquad (26)$$

$$R^3 = 1 + 3\alpha \,, \qquad (27)$$

$$D^2 = 1 - 2\beta + \beta^2 \,, \qquad (28)$$

$$D^3 = 1 - 3\beta + 3\beta^2 \,, \qquad (29)$$

and

$$D^{-2} = 1 + 2\beta + 3\beta^2 \,, \qquad (30)$$

(III - 1) can be rewritten as a linear equation of α:

$$2\alpha(1 - 3\beta) - 3\beta^2 = 0 \,. \qquad (31)$$

The solution of (31):

$$\alpha = \frac{3\beta^2}{2(1 - 3\beta)} \,, \qquad \text{(III - 10)}$$

directly relates the two parameters; consequently it is now sufficient to use β only. After replacing R and D with β, (III - 3) and (III - 2) become

$$\frac{\ell_o^2}{2} = \int_0^{\ell} (1 + 2\beta + 3\beta^2) r \, dr \qquad \text{(III - 4)}$$

and

$$\int_r^{\ell} (1 + 2\beta + 3\beta^2) r^2 dr = \frac{18\gamma r(2\beta - 4\beta^2 + 3\beta^3)}{\sqrt{3}\, R_o \Delta\rho\omega^2 (2 - 8\beta + 9\beta^2)} \,, \qquad (32)$$

respectively. However, these two equations are much too complicated to be solved as integral equations[3-6]. In fact, even the differential equation obtained by differentiating (32) with respect to r is too complicated to be solved. Further simplification is therefore necessary.

Equation (32) can be rewritten as

$$\int_r^{\ell} (1 + 2\beta + 3\beta^2) r^2 dr = \frac{18\Upsilon r}{\sqrt{3}\, R_o \Delta\rho\omega^2} \left[f(\beta) \right] , \qquad (33)$$

where

$$f(\beta) = \beta \left[g(\beta) \right] \qquad (34)$$

and

$$g(\beta) = \frac{2 - 4\beta + 3\beta^2}{2 + 8\beta + 9\beta^2} . \qquad (35)$$

It can be shown that in the region $0.110 \geqslant \beta \geqslant 0$, $g(\beta)$ can be replaced by a linear function of β without introducing any significant error. When a plot of $g(\beta)$ vs. β is made, a straight line can be drawn to substitute for the real curve and the slope of the straight line is found to be 2.5. The plot is shown in Figure 2; the error introduced by this approximation is shown in Table II to be less than one per cent in most cases. Thus,

$$g(\beta) \doteq 1 + 2.5\beta , \qquad (36)$$

and (33) becomes

$$\int_r^{\ell} (1 + 2\beta + 3\beta^2) r^2 dr = \frac{18\Upsilon r}{\sqrt{3}\, R_o \Delta\rho\omega^2} \beta(1 + 2.5\beta) . \qquad (37)$$

Differentiating (37) with respect to r and letting

$$K = \frac{18\Upsilon}{\sqrt{3}\, R_o \Delta\rho\omega^2} \qquad (III - 7)$$

lead to

$$Kr(1 + 5\beta)d\beta + \left[K\beta(1 + 2.5\beta) + (1 + 2\beta + 3\beta^2) r^2 \right] dr = 0 . \qquad (38)$$

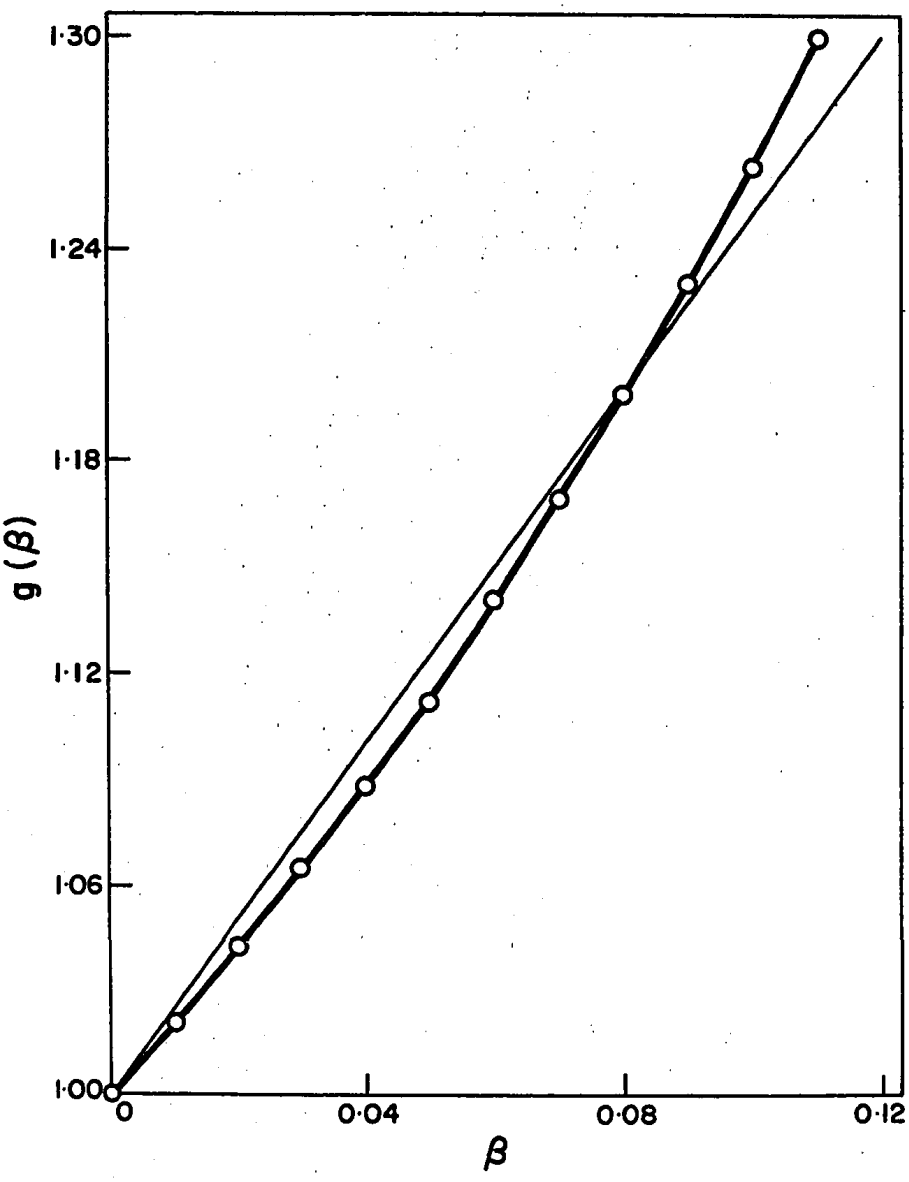

Figure 2 The approximation for g(β). The slope of the substituting straight line is 2.5.

TABLE II

The approximation $g(\beta) = 1 + 2.5\beta$

β	$g(\beta)$	$1 + 2.5\beta$	absolute error	relative error (%)
0.0000	1.0000	1.0000	0.0000	0.00
0.0100	1.0205	1.0250	0.0045	0.44
0.0200	1.0421	1.0500	0.0079	0.76
0.0300	1.0648	1.0750	0.0102	0.96
0.0400	1.0888	1.1000	0.0112	1.03
0.0500	1.1140	1.1250	0.0110	0.99
0.0600	1.1407	1.1500	0.0093	0.82
0.0700	1.1689	1.1750	0.0061	0.52
0.0800	1.1986	1.2000	0.0014	0.12
0.0900	1.2302	1.2250	- 0.0052	- 0.42
0.1000	1.2636	1.2500	- 0.0136	- 1.08
0.1100	1.2990	1.2750	- 0.0240	- 1.85

Though (38) cannot be solved analytically by the well known methods for differential equations of the first order and of the first degree[7,8], it can be reduced to an exact differential equation by introducing the approximation

$$1 + 2\beta + 3\beta^2 \doteq 1 + 2\beta + 5\beta^2 , \tag{39}$$

which is quite reasonable, since $0.110 \geqslant \beta \geqslant 0$. Then the solution of (38) becomes

$$\int r^2 e^{r^2/K} dr + K\beta r e^{r^2/K} + 2.5\beta^2 r e^{r^2/K} = \text{const.} \tag{40}$$

Substituting the boundary condition that

$$\beta = 0 \quad \text{when} \quad r = \ell , \tag{41}$$

into (40) and letting

$$\int r^2 e^{r^2/K} dr = F(r) \tag{42}$$

lead to

$$F(\ell) = \text{const.} \tag{43}$$

Substituting (43) into (40) and solving for β then yield

$$\beta = -\frac{1}{5} + \left\{ \frac{1}{25} + \frac{e^{-r^2/K}}{2.5Kr} \left[F(\ell) - F(r) \right] \right\}^{1/2} . \tag{III - 5}$$

The values of β at two special cases can be obtained from (III - 5) even though $F(r)$ is still unknown. (1) When $r = \ell$, $F(r) = F(\ell)$, $\beta = 0$; (2) when $\omega = 0$, $K \longrightarrow \infty$, $r^2/K \longrightarrow 0$, $e^{-r^2/K} = 1$, $1/K \longrightarrow 0$, $\beta = 0$. The first case is the boundary condition and the second case states that there is no deformation for stationary bubble raft.

After many unsuccessful attempts to integrate (42) by parts and by various transformations and after fruitless searches through the tables of integrations[9,10], integration by series was adopted. Thus,

$$e^{r^2/K} = 1 + \frac{r^2}{K} + \frac{r^4}{2!K^2} + \frac{r^6}{3!K^3} + \frac{r^8}{4!K^4} + \cdots \qquad (44)$$

and

$$F(r) = \int r^2 e^{r^2/K} dr = \sum_{i=1}^{\infty} \frac{r^{2i+1}}{(2i+1)K^{i-1}(i-1)!} . \qquad (45)$$

As can be proved with the ratio test[7], the series F(r) converges rapidly, especially at small r and large K. The approximation reached for F(r) when $r = r_{max}$ and $K = K_{min}$ is therefore adequate for all other possible values of r and K. Under our experimental conditions, $\gamma = 25.8$ dynes/cm., $\Delta\rho = 1.027$ g/ml, $r_{max} = 10.0$ cm., $(R_o)_{max} = 0.200$ cm. and $\omega_{max} = 20.0$ RPM = 2.09 rad/sec. According to (III - 7), $K = K_{min}$ when $R_o = (R_o)_{max}$ and $\omega = \omega_{max}$, thus

$$K_{min} = 300 \text{ cm.}^2 \quad \text{or} \quad K \geqslant 10^2 \text{cm.}^2 \qquad (46)$$

and (45) becomes

$$F(r) = \sum_{i=1}^{\infty} \frac{10^3}{(2i+1)(i-1)!} .$$

If the ith term is less than one per cent of the first term, then

$$\frac{1}{(2i+1)(i-1)!} < \frac{1}{100} \cdot \frac{1}{3} \quad \text{or} \quad (2i+1)(i-1)! > 300 .$$

It can be seen from Table III that only the first five terms need to be summed up and hence

$$F(r) = \sum_{i=1}^{5} \frac{r^{2i+1}}{(2i+1)K^{i-1}(i-1)!} . \qquad (III - 6)$$

The three equations derived earlier have been reduced to

$$\frac{\ell_o^2}{2} = \int_0^{\ell} (1 + 2\beta + 3\beta^2) r dr \qquad (III - 4)$$

TABLE III

The approximation sum of the series F(r)

i	2i+ 1	(i- 1)!	(2i+ 1)(i- 1)!	$\frac{10^3}{(2i+1)(i-1)!}$	$\sum_i \frac{10^3}{(2i+1)(i-1)!}$
1	3	1	3	333.3	333.3
2	5	1	5	200.0	533.3
3	7	2	14	71.43	604.73
4	9	6	54	18.52	623.25
5	11	24	264	3.788	627.038
6	13	120	1560	0.6410	627.679
7	15	720	10800	0.09259	627.772
8	17	5040	85680	0.01167	627.783

$$\beta = -\frac{1}{5} + \left\{\frac{1}{25} + \frac{e^{-r^2/K}}{2.5Kr}\left[F(\ell) - F(r)\right]\right\}^{1/2}, \qquad \text{(III - 5)}$$

where

$$F(r) = \sum_{i=1}^{5} \frac{r^{2i+1}}{(2i+1)K^{i-1}(i-1)!} \qquad \text{(III - 6)}$$

and

$$K = \frac{18\gamma}{\sqrt{3}\, R_o \Delta\rho\omega^2} . \qquad \text{(III - 7)}$$

Substituting (III - 5) and (III - 6) into (III - 4) and integrating the resulting equation give

$$f_1(\ell_o, \ell, K) = 0 , \qquad (47)$$

which can be solved for ℓ:

$$\ell = f_2(\ell_o, K) . \qquad (48)$$

By substituting (48) into (III - 5) the final solution for β can be obtained:

$$\beta = f_3(\ell_o, K, r) . \qquad (49)$$

For any given bubble raft, the quantities $\Delta\rho$, γ, R_o, and ℓ_o are known, then ℓ at any value of ω can be calculated from (48) and β at any values of ω and r from (49). However, the steps involved here such as the integration in (III - 4) and the solution of (47) are so complicated that only a numerical solution is possible.

The basic requirement in the computer programming was to find out for a given bubble raft at a given ω a suitable value of ℓ such that the relative difference between the left and the right hand sides of (III - 4) was less than one per cent. With this accepted value of ℓ, the values of β at different radii of rotation were then calculated from (III - 5). The entire programme was then repeated for other desirable values of ω.

4. COALESCENCE IN CENTRIFUGAL BUBBLE CELL

Two attempts to study coalescence in the centrifugal aggregation cell were made: 1) coalescence of air bubbles at air/liquid interface in the rotating cell and 2) coalescence of bubbles in rotating bubble raft. Although they have not been successful, a brief summary is given here.

(a) Coalescence of Air Bubbles at the Air/Liquid Interface

According to a theory which Chappelear[11] advanced for the approach of a fluid drop to a liquid/liquid interface, the rest time of the drop should increase when the force pushing them together is increased. This was tested in the centrifugal aggregation cell since the centrifugal acceleration can easily be changed by varying the speed of rotation and the radius of rotation.

Unfortunately the use of liquid/liquid systems was found to be impossible because one of the liquid pair caused the cell to leak. When air and aqueous Aerosol AY (American Cyanamide) solution were used as the two fluid phases, the rest time of air bubble at air/Aerosol AY solution interface could be measured under certain conditions.

Air bubbles were generated at a constant rate of n bubbles per second. They then travelled through the aqueous Aerosol AY solution because of the density difference and finally reached the air/liquid interface. When a steady state was reached, the number of bubbles reaching the interface was equal to the number of bubbles disappearing (by coalescence) at the interface and the net number of bubbles remaining at the interface N became a constant. Then one has the relation

$$\bar{\tau} = \frac{N}{n},$$

where $\bar{\tau}$ is the average rest time.

If the concentration of the Aerosol AY solutions, the speed of rotation of the cell and the rate of the generation of bubbles were properly chosen, the rest time of the air bubble could be measured. Otherwise, bubbles might coalesce with one another on their way to the interface or form layer thicker than one bubble at the interface. While only preliminary results were obtained from these steady state measurements because of the difficulty in the proper choice of experimental conditions, they indicate agreement with Chappelear's theory.

(b) Coalescence of Bubbles in Rotating Bubble Raft

A rotating camera technique was developed for the experimental study of coalescence of bubbles in rotating bubble raft. A 16 mm. Bolex movie camera with a special wide angle lens (angle of view $> 120°$) and a circular fluorescent lamp were mounted directly on the centrifugal aggregation cell (Figure 3) so that there was no relative motion between the bubble raft, the camera and the light source (Figure 4). Coalescence of bubbles in bubble raft was found to be very complicated.

The critical speed of rotation of the cell for coalescence, defined as the speed below which no coalescence of bubbles took place, was not sharp. It could be better described as a critical speed zone with latitude of about 5 RPM.

The first instance of coalescence could occur at different locations in the bubble raft and after different times of cell rotation, but the probability of coalescence was greater at smaller radii of rotation and with increasing duration of cell rotation. Once a large bubble was formed by coalescence, it was much more probable that further coalescence would occur between the large bubble and the neighbouring small bubbles than between two identical small bubbles elsewhere in the bubble raft. Thus, one instance

Figure 3 The arrangement for mounting the ciné camera and the circular fluorescent lamp directly on the centrifugal bubble cell.

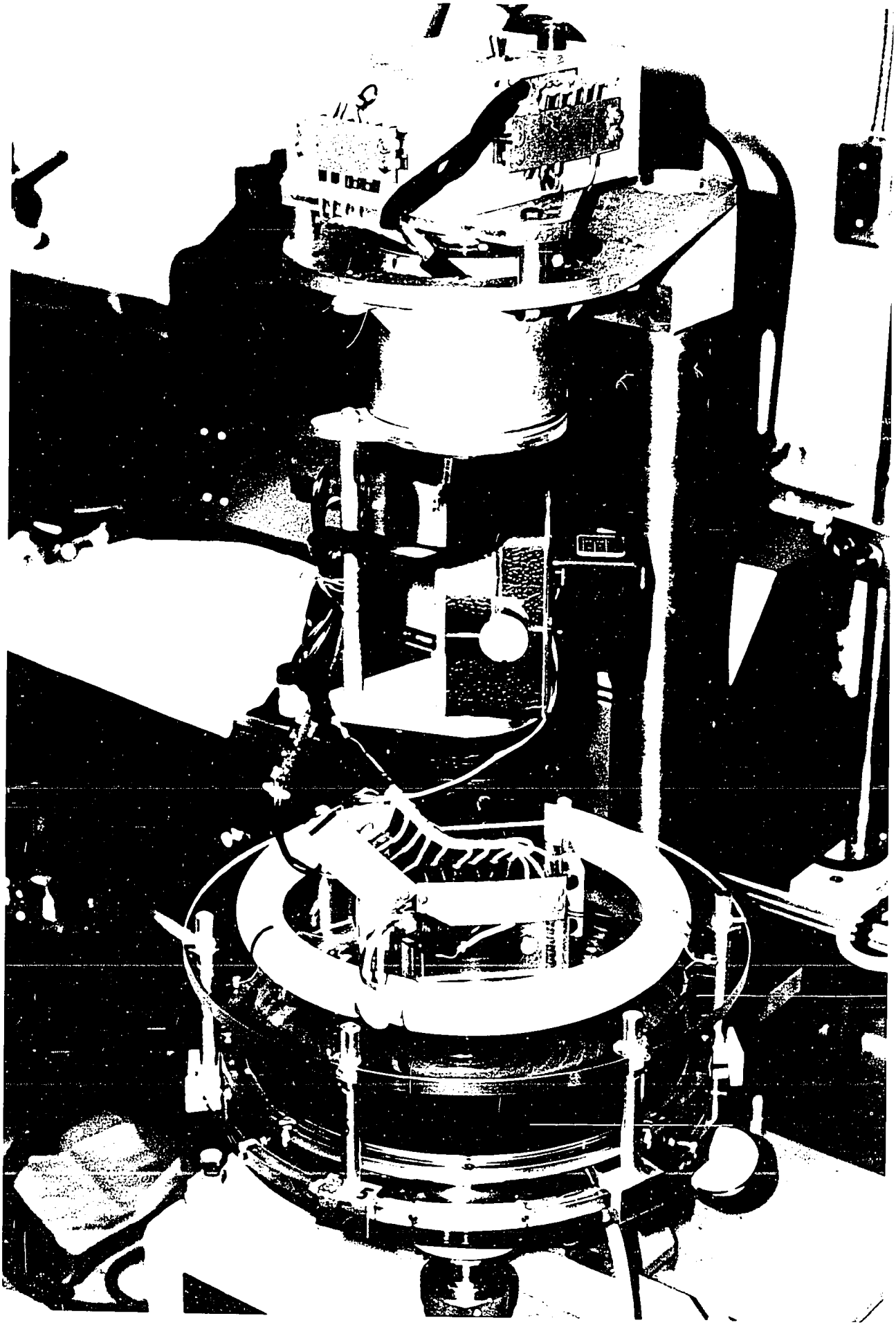

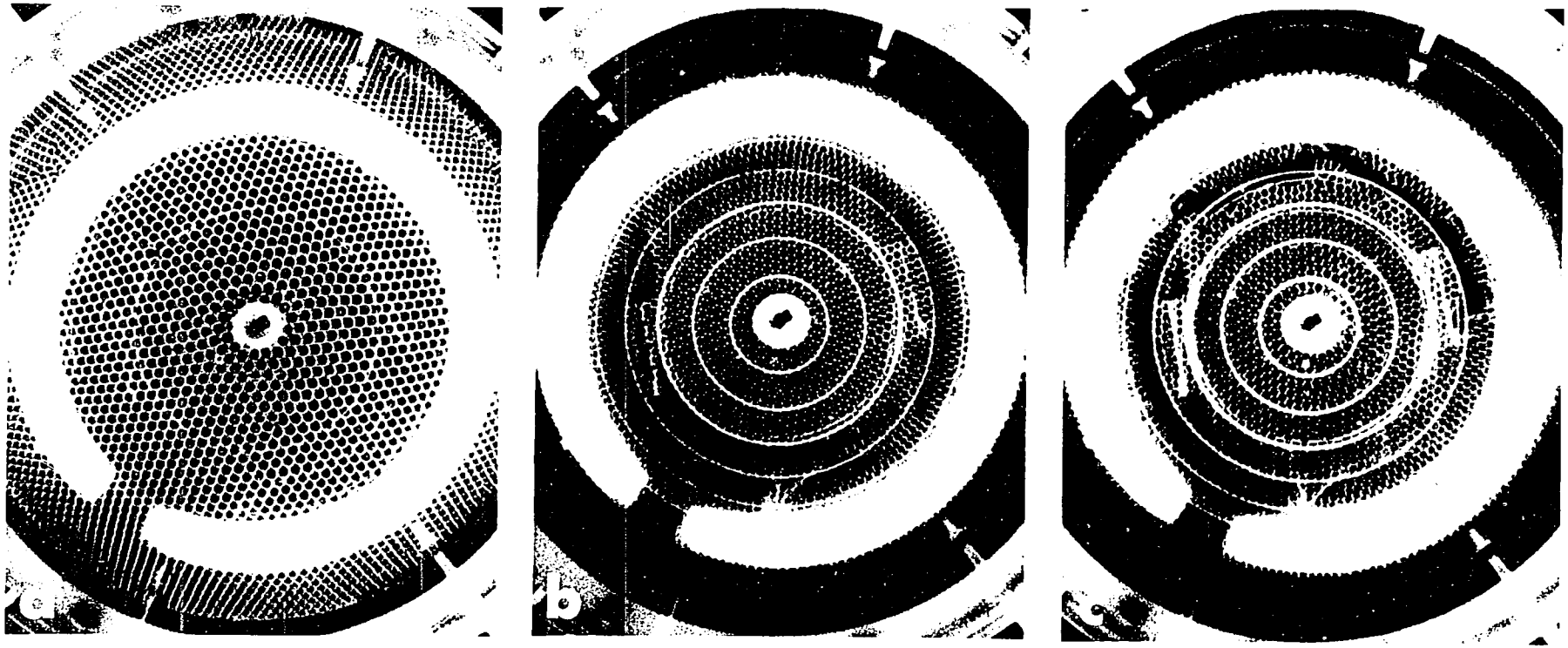

Figure 4 Photographs of a bubble raft in the centrifugal bubble cell taken with the rotating camera technique. As cell speed increases from 10 RPM (a) to 133 RPM (b), the bubble raft "shrinks" and finally coalescence takes place at about 3 minutes later (c). Distortion was caused by the wide angle lens; the series of concentric circles are actually all 1 cm. apart. The white circular belt is the reflection of the fluorescent illumination lamp.

of coalescence led to another and coalescence spread out from an origin. Although coalescence was occasionally observed to take place in isolation with little or no further coalescence in the surrounding area, it very often spread out immediately and very rapidly for a very short period of time from the original point of coalescence: a few thousand bubbles could coalesce within 10 seconds. The direction of spread could be either radially inward or outward, or along a circumference or a spiral. There could be more than one origin of coalescence.

In a bubble raft consisting of a few "crystals" of bubbles, the first instance of coalescence was most likely to take place at the boundaries between crystals. Once coalescence occurred, it spread readily along the boundaries of the crystals.

In summary it may be said that the probability of coalescence in a rotating bubble raft increased with increasing speed of rotation, duration of the cell rotation, bubble size and bubble raft size, but with decreasing radius of rotation.

REFERENCES

1. Round, G.F. and Newton, R., Nature, 198, No. 4882, 747 (1963).
2. McKean, Jr., Schreiber and Weiss, J. Math. Phys., 6, No. 3, 479 (1965).
3. Lovitt, W.V., "Linear Integral Equations", Dover, New York, 1950.
4. Smithies, F., "Integral Equations", Cambridge University Press, 1958.
5. Tricomi, F.G., "Integral Equations", Interscience, New York, 1957.
6. Yoshida, K., "Lectures on Differential and Integral Equations", Interscience, New York, 1960.
7. Kaplan, W., "Advanced Calculus", Addison-Wesley, Reading, Mass., 1952.

8. Wilson, E.B., "Advanced Calculus", Dover, 1958.

9. Dwight, H.B., "Tables of Integrals and other Mathematical Data", MacMillan, New York, Revised Edition, 1947.

10. Bois, P.G., "Tables of Indefinite Integrals", Dover, 1961.

11. Chappelear, D.C., J. Colloid Sci., 16, 186 (1961).

APPENDIX V

MEASUREMENT OF INTERFACIAL TENSION FROM THE SHAPE OF A ROTATING DROP

ABSTRACT

Vonnegut's approximate solution for the shape of a fluid drop in a horizontal rotating tube filled with a liquid of higher density has been extended and numerical solutions based on exact equations presented from which it is possible to calculate the interfacial tension from the length of the elongated drop along the axis of rotation when the drop volume, speed of rotation and density difference between the two phases are known. An experimental method is described and results given which show good agreement with other methods. The technique is considered to be especially useful for systems in which either phase is highly viscous or viscoelastic. The proposal by Vonnegut that the method be used to measure surface pressure-area curves of insoluble monolayers is shown on theoretical grounds to have limited applicability.

1. INTRODUCTION

When a fluid drop (phase 1) is placed in a liquid of higher density (phase 2) contained in a rotating horizontal tube it becomes elongated along the axis of rotation until the deformation forces due to the centrifugal field are balanced by the interfacial tension. Vonnegut[1] suggested that this principle be used to measure interfacial tension and developed an approximate theory in which the bubble is considered to be a cylinder with rounded ends. The theory is only strictly valid at high speeds of rotation, but Silberberg[2] improved it by calculating correction factors for low speeds. The method involved measuring the radius of the cylinder and thus required an optical correction factor which we have found to be a serious limitation. We have extended the theory by using exact equations for the bubble shape and have developed an experimental method based on measuring the bubble length without the need for optical correction.

Rosenthal[3] has recently presented similar calculations by a somewhat different method, but his results are less detailed and less suitable for the application considered in this paper.

2. THEORETICAL PART

It is assumed, as before[1-3], that the angular velocity of rotation ω is sufficiently high that buoyancy due to gravity is negligible and that the drop is aligned on the horizontal axis of rotation. Cylindrical coordinates x, y are chosen (Fig. 1) with origin at the left-hand end of the drop. The angle between the normal of the interface at (x, y) and the negative x-direction is Θ, and the semi-axes are x_o and y_o;

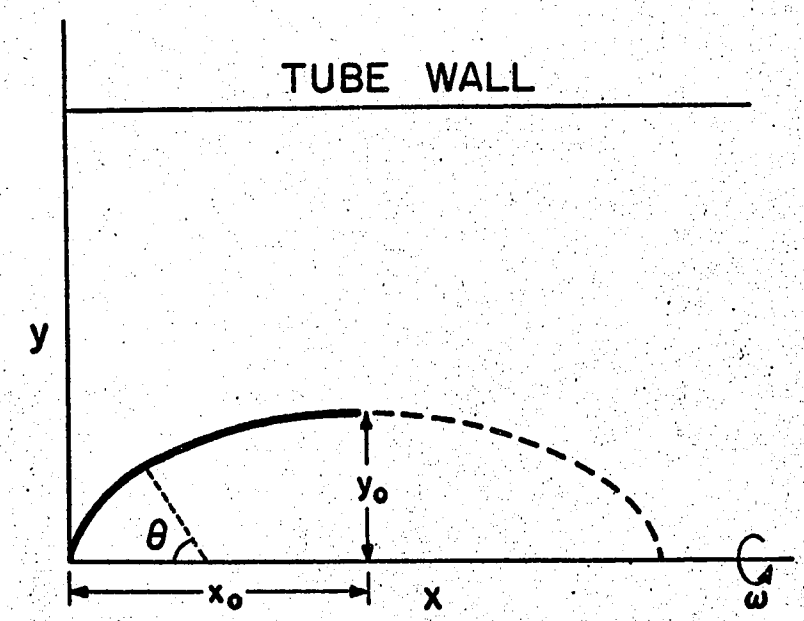

Figure 1 Coordinate system to describe the shape of a drop rotating about a horizontal axis.

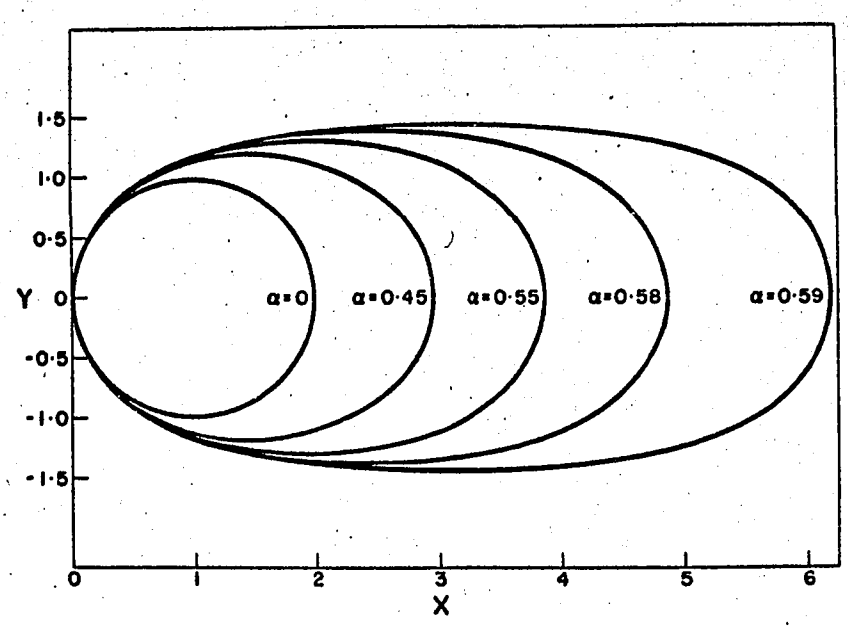

Figure 2 Shape of a rotating drop for various values of α. The radius of curvature at the drop end serves as the unit of length.

the densities of the drop and the outer phase are d_1 and d_2 ($d_2 > d_1$) and the interfacial tension is γ. Because of symmetry, it is sufficient to consider only the quarter drop between 0, 0 and x_o, y_o.

The pressure outside the drop is given by

$$p = p_o + \frac{d_2\omega^2 y^2}{2} , \tag{1}$$

and at $y = 0$ inside the drop by

$$p'_o = p_o + \frac{2\gamma}{a} , \tag{2}$$

where a is the radius of curvature of the drop surface at the origin. Thus, at y inside the drop

$$p' = p_o + \frac{2\gamma}{a} + \frac{d_1\omega^2 y^2}{2} , \tag{3}$$

so that at the surface

$$\Delta p = p' - p = \frac{2\gamma}{a} - \frac{\Delta d\omega^2 y^2}{2} , \tag{4}$$

where $\Delta d = d_2 - d_1$.

The pressure difference is balanced by the capillary pressure across the interface:

$$\Delta p = \gamma \left(\frac{1}{\rho_1} + \frac{1}{\rho_2}\right) , \tag{5}$$

where the principal curvatures are

$$\frac{1}{\rho_1} = \frac{d^2x/dy^2}{\left[1 + (dx/dy)^2\right]^{3/2}} = \frac{d\sin\theta}{dy} , \tag{6}$$

and

$$\frac{1}{\rho_2} = \frac{dx/dy}{y\left[1 + (dx/dy)^2\right]^{1/2}} = \frac{\sin\theta}{y} . \tag{7}$$

Equating (4) and (5) yields for the equation of interface

$$\frac{d\sin\theta}{dy} + \frac{\sin\theta}{y} = \frac{2}{a} - \frac{\Delta d\omega^2 y^2}{2\gamma} , \tag{8}$$

which can be written in the dimensionless form

$$\frac{d\sin\theta}{dY} + \frac{\sin\theta}{Y} = 2 - \alpha Y^2 , \tag{9}$$

where $Y = y/a$, and

$$\alpha = \frac{\Delta d\omega^2 a^3}{2\gamma} = 2ca^3 , \tag{10}$$

$$c = \frac{\Delta d\omega^2}{4\gamma} . \tag{11}$$

Thus, the shape of the drop is determined by the dimensionless parameter α.

Equation (9) can be integrated to give

$$\sin\theta = Y\left(1 - \frac{\alpha Y^2}{4}\right) \tag{12}$$

or

$$\tan\theta = \frac{dX}{dY} = \frac{Y\left(1 - \frac{\alpha Y^2}{4}\right)}{\left[1 - Y^2\left(1 - \frac{\alpha Y^2}{4}\right)^2\right]^{1/2}} , \tag{13}$$

where $X = x/a$.

Several useful relations follow readily:

1) When $Y = Y_o$, $\sin\theta = 1$, hence from (12)

$$\alpha Y_o^3 - 4Y_o + 4 = 0 , \tag{14}$$

one of whose roots gives Y_o as a function of α.

2) Differentiating (12) yields

$$d\sin\theta = (1 - \frac{3\alpha Y^2}{4})dY \ , \qquad (15)$$

which when multiplied on the left-hand side by $\tan\theta$ and the right-hand side by dX/dY, and integrated between the origin and (X_o, Y_o) yields

$$1 = X_o - \frac{3\alpha}{4}\int_o^{X_o} Y^2 dX \ . \qquad (16)$$

Since

$$\frac{V}{a^3} = 2\pi \int_o^{X_o} Y^2 dX \ ,$$

where V is the volume of the drop, one finds from (16)

$$\frac{V}{a^3} = \frac{4\pi}{3}(\frac{r}{a})^3 = \frac{8\pi}{3\alpha}(X_o - 1) \ , \qquad (17)$$

where r is the radius of a sphere of the same volume as the drop. Equation (17) reduces to a useful form to convert a to r

$$\frac{r}{a} = \left[\frac{2(X_o - 1)}{\alpha}\right]^{1/3} . \qquad (18)$$

3) At high ω the drop is closely approximated by a cylinder with rounded ends. In the cylindrical part $d\sin\theta/dY = 0$, $\theta = 90°$ and $Y = Y_o$ and (9) becomes

$$\alpha Y_o^3 - 2Y_o + 1 = 0 \ . \qquad (19)$$

Combining (19) and (14) yields for a long cylindrical drop:

$$Y_o = 3/2 \ , \qquad (20)$$

and the highest possible value

$$\alpha = 16/27 \ . \qquad (21)$$

Combining (10), (20) and (21) leads to Vonnegut's equation[1]

$$\gamma = \frac{\Delta d \omega^2 y_o^3}{4} , \tag{22}$$

For the limiting value of α, (13) can be readily integrated to yield for the ends of the cylindrical drop:

$$X = \frac{\sqrt{3}}{2}\left[\ln\frac{2\sqrt{9 - Y^2} + 3\sqrt{3}}{2\sqrt{9 - Y^2} - 3\sqrt{3}} - \ln\frac{2 + \sqrt{3}}{2 - \sqrt{3}}\right] + 3 - \sqrt{9 - Y^2} . \tag{23}$$

Since $Y = y/a = 3y/2y_o$, this equation is identical to Vonnegut's equation (16)[1].

For $0 < \alpha < 16/27$, (13) can be integrated by making the substitution

$$q = 1 - \frac{\alpha Y^2}{4} , \tag{24}$$

to give

$$X = -\frac{1}{\sqrt{\alpha}}\int \frac{q\,dq}{(q^3 - q^2 + \frac{\alpha}{4})^{1/2}} + C . \tag{25}$$

If $q_1 > q_2 > q_3$ are the roots of the cubic term in the denominator it can be shown that

$$q_1 = 1 - \frac{\alpha}{4} Y_o^2 . \tag{26}$$

The three roots are always real over the possible range of α, and are conveniently evaluated trigonometrically[4] in the form

$$q_1 = \frac{2}{3}\cos\frac{\psi}{3} + \frac{1}{3} ,$$

$$q_2 = \frac{2}{3}\cos(\frac{\psi}{3} + 240°) + \frac{1}{3} ,$$

$$q_3 = \frac{2}{3}\cos(\frac{\psi}{3} + 120°) + \frac{1}{3} ,$$

where

$$\cos\psi = 1 - \frac{27}{8}\alpha .$$

Since the interval of q over which the integral (25) must be evaluated is $q_1 \leq q < 1$, the solution is[5)]

$$X = -\frac{2}{\sqrt{\alpha(q_1 - q_3)}}\left[q_1 F(k,\phi) - (q_1 - q_3)E(k,\phi) + (q_1 - q_3)\tan\phi\sqrt{1 - k^2\sin^2\phi}\right] + C \,, \tag{27}$$

where F and E are the elliptic integrals of the first and second kind,

$$k^2 = \frac{q_2 - q_3}{q_1 - q_3} \,,$$

and ϕ is defined by

$$q = \frac{q_1 - q_2\sin^2\phi}{1 - \sin^2\phi} \qquad (0 \leq \phi \leq \tfrac{\pi}{2}) \,. \tag{28}$$

At (X_o, Y_o), $q = q_1$ and $\phi = 0$, the bracketed term in (27) vanishes so that

$$C = X_o \,. \tag{29}$$

At the origin $X = 0$, $Y = 0$ and $q = 1$

$$X_o = \frac{2}{\sqrt{\alpha(q_1 - q_3)}}\left[q_1 F(k,\phi_1) - (q_1 - q_3)E(k,\phi_1) + (q_1 - q_3)\tan\phi_1\sqrt{1 - k^2\sin^2\phi_1}\right] \,, \tag{30}$$

where $\phi = \phi_1$ when $q = 1$.

These equations allow the drop shape to be computed for any value of α using tables of the elliptic integrals[6)]. Then all dimensions are known in units of a and can readily be expressed in terms of r using (18). Instead of α the more convenient shape-determining factor cr^3 can

be used by combining (10) and (18):

$$cr^3 = \frac{\alpha}{2}\left(\frac{r}{a}\right)^3 = X_o - 1 \ . \qquad (31)$$

Table I reports the values of the most important drop parameters for various values of α, while Fig. 2 shows the drop shape for several cases.*

At values of α greater than in Table I (when the central part of the drop is effectively cylindrical) the following equations apply with sufficient accuracy:

$$\alpha = 16/27 \ , \qquad (32)$$

and

$$Y_o = 3/2 \ . \qquad (33)$$

From (31):

$$X_o = cr^3 + 1 \ . \qquad (34)$$

From (31) and (32):

$$\frac{r}{a} = \frac{3}{2}(cr^3)^{1/3} \ . \qquad (35)$$

From (34) and (35):

$$\frac{x_o}{r} = \frac{2}{3}\,\frac{cr^3 + 1}{(cr^3)^{1/3}} \ . \qquad (36)$$

From (33) and (35):

$$\frac{y_o}{r} = (cr^3)^{-1/3} \quad \text{or} \quad y_o = c^{-1/3} \ . \qquad (37)$$

From (36) and (37):

$$\frac{x_o}{y_o} = \frac{2}{3}(cr^3 + 1) \ . \qquad (38)$$

Equation (37) is Vonnegut's[1], but for reasons stated earlier (36) is more useful in experimental work; Fig. 3 shows x_o/r and y_o/r as a function of the independent variable cr^3.

* For all but the last six values of α in Table I, the shape parameters were calculated by numerical integration of (9), using an IBM 1620 computer. For the highest values of α this procedure was too time-consuming and the table was completed by computing X_o, Y_o, r/a and cr^3 from (30), (26), (18) and (31), respectively.

TABLE I

Calculated Shape Parameters of a Rotating Drop.

α	r/a	σr^3	x_o/r	y_o/r	x_o/y_o
0	1.000	0	1.000	1.000	1.000
0.05	1.017	0.0263	1.009	0.996	1.013
0.10	1.037	0.0557	1.018	0.990	1.028
0.15	1.058	0.0888	1.029	0.985	1.044
0.20	1.081	0.1265	1.042	0.980	1.063
0.225	1.095	0.1476	1.048	0.976	1.074
0.250	1.108	0.1703	1.056	0.973	1.085
0.275	1.124	0.1951	1.063	0.969	1.098
0.300	1.140	0.2222	1.072	0.965	1.111
0.325	1.158	0.2521	1.082	0.960	1.126
0.350	1.177	0.2854	1.092	0.955	1.143
0.375	1.198	0.3227	1.104	0.950	1.162
0.400	1.222	0.3653	1.117	0.944	1.184
0.425	1.250	0.4146	1.132	0.937	1.209
0.450	1.281	0.4727	1.150	0.928	1.238
0.475	1.318	0.5435	1.171	0.919	1.275
0.500	1.363	0.6330	1.198	0.907	1.321
0.525	1.421	0.7536	1.234	0.892	1.384
0.550	1.504	0.9354	1.287	0.869	1.481
0.555	1.526	0.9854	1.301	0.863	1.508
0.560	1.550	1.043	1.318	0.857	1.539
0.565	1.578	1.111	1.338	0.849	1.576
0.570	1.611	1.192	1.361	0.840	1.621
0.575	1.652	1.296	1.390	0.828	1.678
0.580	1.704	1.435	1.429	0.814	1.756
0.5825	1.737	1.528	1.455	0.804	1.809
0.5850	1.779	1.648	1.488	0.792	1.878
0.5875	1.836	1.817	1.534	0.776	1.977
0.5900	1.925	2.105	1.613	0.751	2.148
0.5910	1.986	2.314	1.669	0.734	2.275
0.5920	2.099	2.739	1.781	0.702	2.538
0.5922	2.150	2.944	1.834	0.688	2.667
0.5924	2.217	3.227	1.907	0.670	2.846
0.5925	2.289	3.555	1.990	0.651	3.059
0.59255	2.355	3.869	2.068	0.634	3.261
0.59257	2.412	4.161	2.140	0.620	3.452
0.59258	2.468	4.463	2.209	0.606	3.645

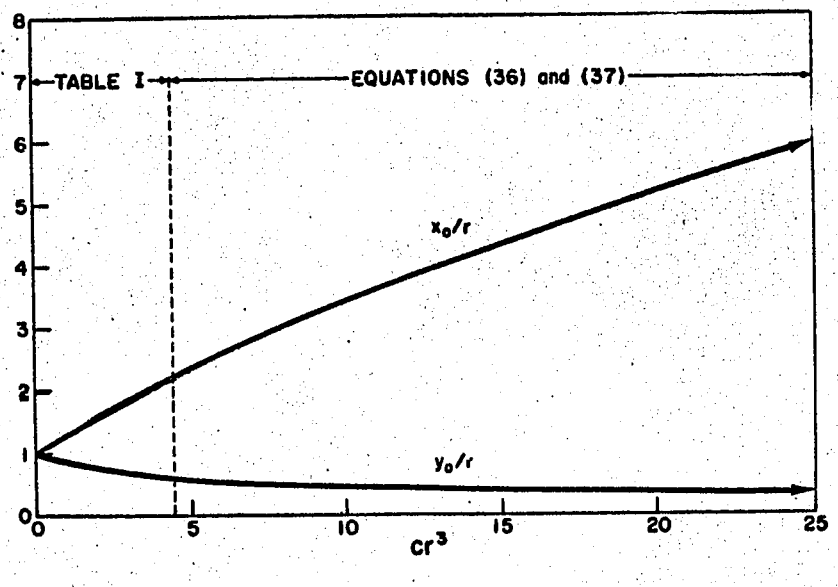

Figure 3 Variation of x_o/r and y_o/r with cr^3.

Silberberg[2] concluded that (37) is applicable when the axis ratio $x_o/y_o > 3.5$, in general agreement with the present calculations, although the choice of this critical value is arbitrary, and depends on the accuracy being sought.

3. EXPERIMENTAL PART

(a) Apparatus

The rotating cell used (Fig. 4) is driven by a 1/3 HP A.C. motor (Bodine Electric Co., Chicago) through two DYNA minidrives (Ontario Drive and Gear Ltd.) connected in series so that the speed of rotation of the apparatus is steady and can be varied continuously up to 10,000 RPM; the speed is measured to 1 RPM with a tachometer (Hasler Berne Ltd.). The clamp assembly on the left side of the photograph (Fig. 4a) holds the rotating tube securely.

The glass tube is 1 ± 0.001 cm. i.d. and approximately 22 cm. long. Since it is important to avoid vibration of the bubble, precision bore tubing is used to provide good balancing at all speeds. At each end of the tube there is a ground glass joint into one of which is fitted an ordinary stopper and into the other one with a 1.5 mm. capillary in the centre, both stoppers being spring loaded to provide a tight seal (Fig. 4b).

(b) Procedure

A critical step in the measurement is the introduction of a bubble of accurately known volume. After thoroughly cleaning the cell, the stopper with the capillary is wetted with the heavier (phase 2) liquid and inserted in one end of the tube. The tube is held vertically and filled completely and allowed to stand so that any trapped air bubbles

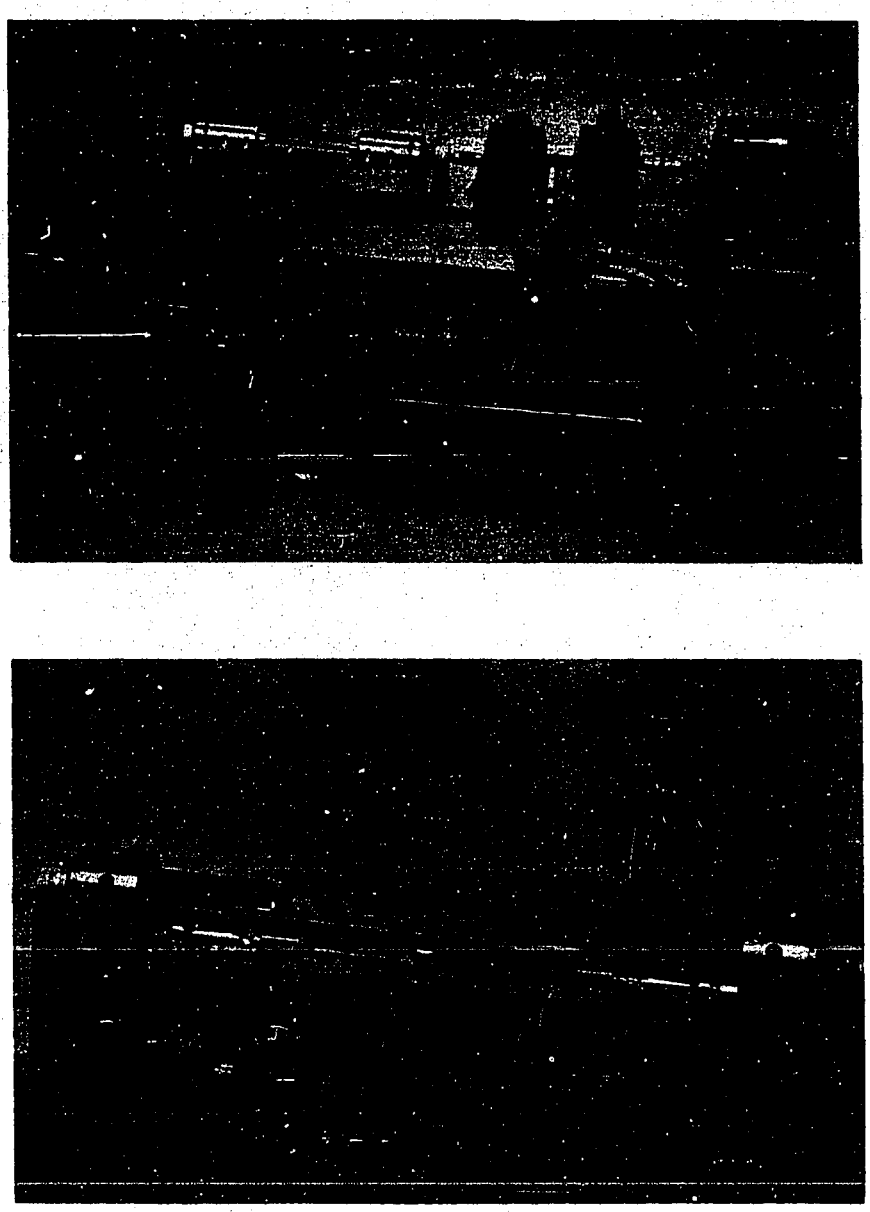

Figure 4(a) Photographs of rotating drop apparatus showing whole assembly and cathetometer for measuring drop length (top) and detail of glass tube and fixed part of clamp assembly (bottom).

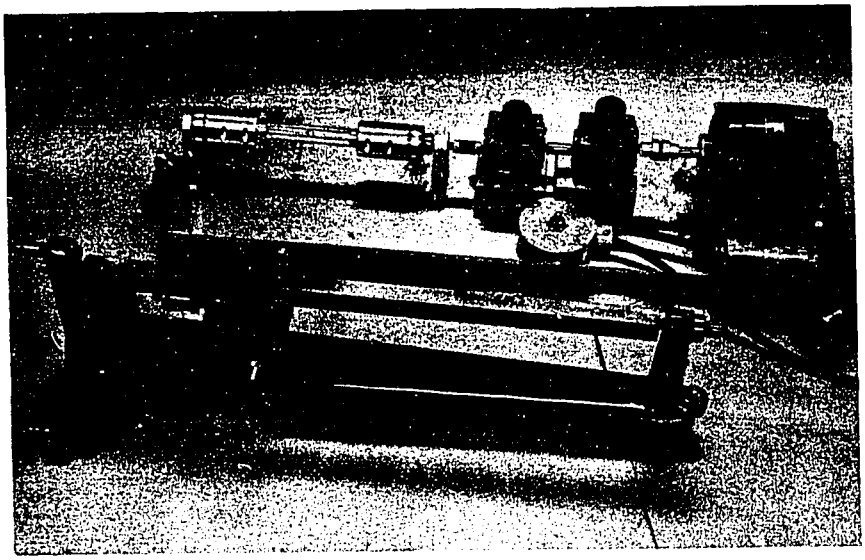

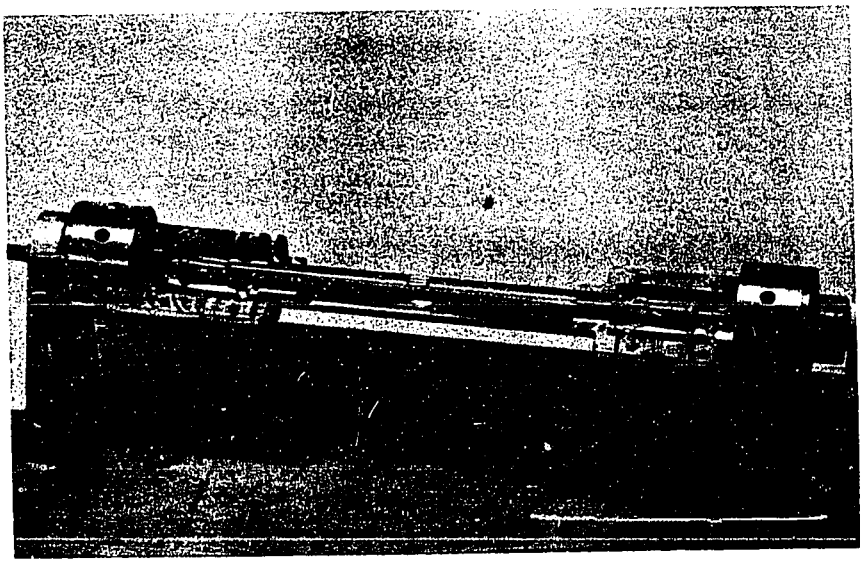

Figure 4(a) Photographs of rotating drop apparatus showing whole assembly and cathetometer for measuring drop length (top) and detail of glass tube and fixed part of clamp assembly (bottom).

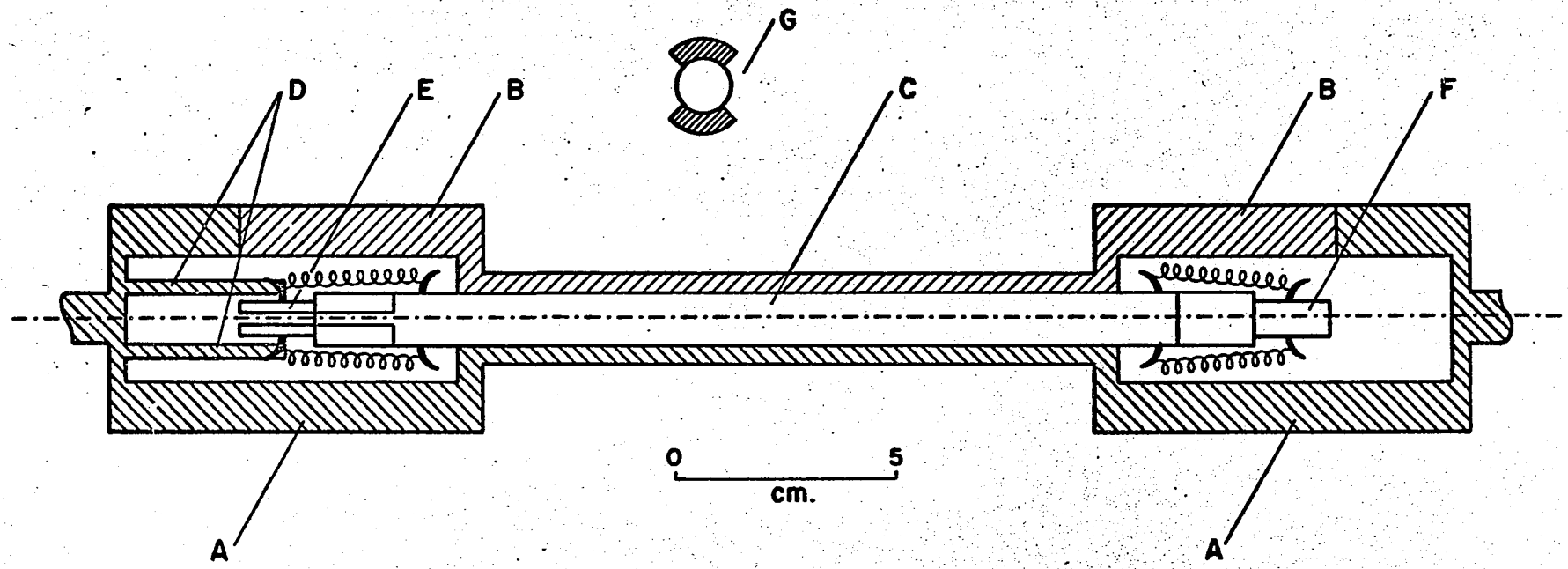

Figure 4(b) Rotating drop apparatus (schematic)
A - fixed part of clamp assembly, B - removable part of clamp assembly, C - glass tubing, D - two pins to prevent the slip between glass tubing and clamp assembly, E, F - ground glass stoppers; E has capillary at its center, G - cross section.

escape, after which it is inclined nearly horizontally with the open end up. A hypodermic needle fitted to a microburette is slowly inserted through the capillary at the lower end and a carefully measured (to 10^{-4}c.c.) volume of phase 1 is introduced which coalesced to form a single bubble. The needle is slowly withdrawn and the upper open end of the tube is closed with the other stopper, with the excess phase 2 being expelled through the capillary. In this way the drop was introduced under very little hydrostatic pressure. The tube is then inserted in the apparatus clamp.

The bubble length is measured using a horizontal cathetometer over a range of speeds of rotation. After reaching equilibrium the drop length from tip to tip is measured twice at each speed of rotation; from left to right and then in reverse. This reduces any error caused by any inclination of the tube.

4. RESULTS AND DISCUSSION

In all systems examined, except air and liquids of low viscosity such as water, the drops had very smooth surfaces and as predicted by the theory were elongated along the horizontal axis of rotation with increasing speed of rotation (Fig. 5). A typical set of results and calculations is given in Table II and shows that the method gives constant values of γ over a wide range of ω.

A summary of results for a variety of systems is given in Table III, and some comparisons with the pendant drop and ring tensiometer methods are given in Table IV.

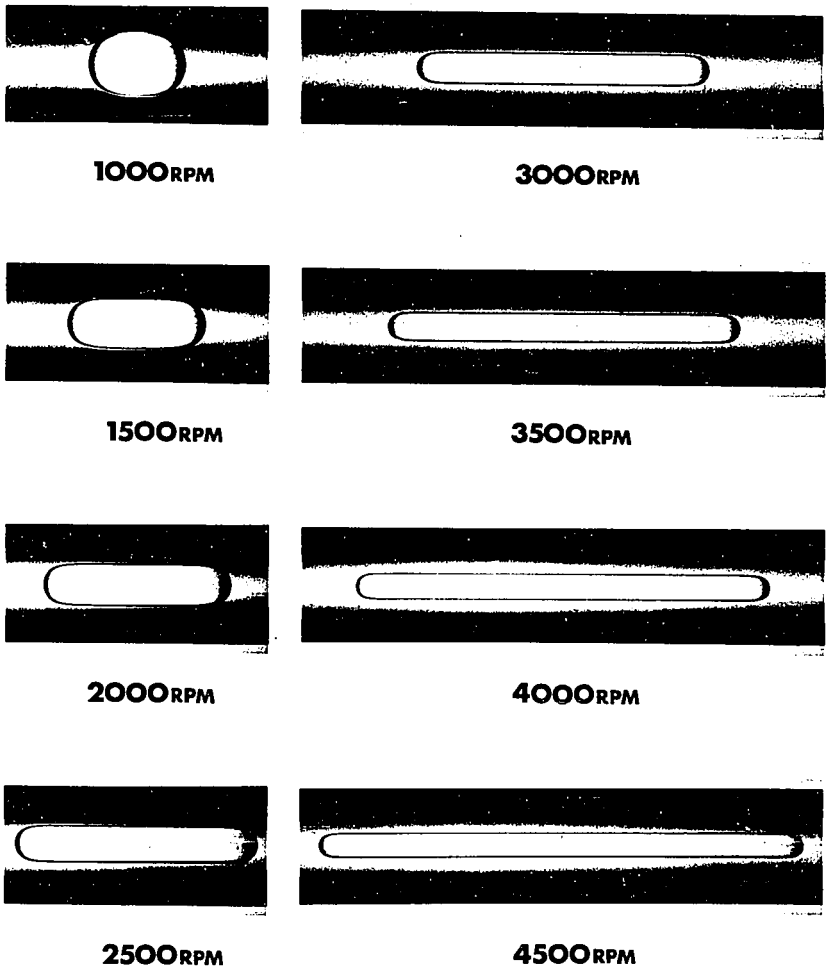

Figure 5 Photographs of a heptane drop (0.156 $cm.^3$) in glycerol rotating at various speeds.

TABLE II

Calculation and result of a typical experiment.

System: n-hexadecane/glycerol

$V = 0.1900$ cm.^{3} $\Delta d = 0.485$ g.cm.$^{-3}$ $r = 0.3567$ cm.

ω		$2x_o$	x_o/r	cr^3 [a]	c	γ [b]
RPM	rad.sec.$^{-1}$	cm.			cm.$^{-3}$	dyne.cm.$^{-1}$
859	89.9	1.048	1.469	1.580	34.84	28.14
1207	126.4	1.343	1.883	3.163	69.74	27.77
1629	170.6	1.786	2.504	5.72	126.1	27.97
1957	204.9	2.172	3.045	8.22	181.3	28.08
2160	226.2	2.433	3.411	10.05	221.6	27.99
2454	256.9	2.819	3.952	12.90	284.4	28.13
2644	276.8	3.091	4.334	15.05	331.9	27.99
2947	308.6	3.530	4.949	18.70	412.3	28.00
3285	343.9	4.062	5.695	23.47	517.5	27.71
3639	381.0	4.579	6.420	28.36	625.3	28.14
4020	420.9	5.200	7.290	34.65	764.0	28.12
4489	470.0	5.996	8.406	43.27	954.1	28.06

Mean = 28.0

S.D. = 0.6%

a) Interpolated values from x_o/r using Table I when $x_o/r < 2.209$. For greater values (36) is used.

b) Calculated from (11).

TABLE III

Interfacial tension and other physical properties of experimental systems

No.	Phase 1	Phase 2	Δd g.cm.$^{-3}$	η_2 poise	γ dyne.cm.$^{-1}$
1	Air	Glycerol	1.260	8	66.1
2	Heptane	Glycerol	0.576	8	28.4
3	n-Hexadecane	Glycerol	0.485	8	28.0
4	Water	Cyclohexanol phthalate	0.071	230	26.4
5	Water	Dow Corning fluorosilicone fluid FS-1265	0.302	130	40.3
6	Air	2% aqueous solution of Cyanamer P250 polyacrylamide	1.001		65.3

TABLE IV

Comparison of interfacial tension measurement by different methods

(Temperature: 21° ± 1°C)

System	γ (dyne.cm.$^{-1}$)			γ_1/γ_2
	Rotating drop (1)	Pendant drop (2)	Ring tensiometer	
Air/glycerol	66.1	64.6	63.4	1.02
Heptane/glycerol	28.4	27.8	27.7	1.02
n-Hexadecane/glycerol	28.0	27.2	27.3	1.03

Accurate measurements of ω and V are essential for this method, since γ varies as $\omega^2 V^n$, with $n \geq 3/2$. Of the two requirements the more difficult to meet is the second and it is the reason for the care taken in introducing the bubble into the cell. With a gas bubble, care must be taken to prevent any change of V from variations in temperature and pressure. Although V changes with ω, it is readily shown in bubbles at atmospheric pressure that the variation in V from the centrifugal field is negligible.

It is theoretically possible to determine γ without measuring V, since at high ω (36) is applicable. Substituting (11) into (36) leads to

$$G\left(\frac{1}{\gamma}\right)^{1/3} = H\left(\frac{r^3}{\gamma}\right) + 1 , \tag{39}$$

where

$$G = \frac{3x_o}{2}\left(\frac{\Delta d\omega^2}{4}\right)^{1/3} , \tag{40}$$

and

$$H = \frac{\Delta d\omega^2}{4} . \tag{41}$$

If the drop length is measured at two or more speeds, both the V and γ can be calculated from simultaneous equations such as

$$\left.\begin{aligned} G_1\left(\frac{1}{\gamma}\right)^{1/3} &= H_1\left(\frac{r^3}{\gamma}\right) + 1 \\ G_2\left(\frac{1}{\gamma}\right)^{1/3} &= H_2\left(\frac{r^3}{\gamma}\right) + 1 \end{aligned}\right\} . \tag{42}$$

It can easily be shown that the solutions of (42) are

$$\gamma = \left[G_1 - H_1\left(\frac{G_1 - G_2}{H_1 - H_2}\right)\right]^3 , \tag{43}$$

and

$$r^3 = \left(\frac{G_1 - G_2}{H_1 - H_2}\right)\left[G_1 - H_1\left(\frac{G_1 - G_2}{H_1 - H_2}\right)\right]^2 = \left(\frac{G_1 - G_2}{H_1 - H_2}\right)\gamma^{2/3} . \tag{44}$$

However this method was found to be impractical, because the ratio $G_1(H_1 - H_2)/H_1(G_1 - G_2)$ was never much greater than unity. Thus, a small error in ω, and hence G and H, lead to a large error in γ.

In accord with Vonnegut's observation[1] an air bubble in water had a rippled surface. Although the exact cause of the ripples is not known, it only occurred with systems of low viscosity and was probably due to the vibration from the motor drive.

Rayleigh[7] showed that in a non-rotating field a cylindrical drop developes axisymmetric standing waves of length exceeding the circumference with an accompanying decrease in interfacial area. More closely related to present work is the investigation by Rosenthal[3] who found that a long bubble subjected to small axisymmetric disturbances in the axial direction is stable at all wave-lengths if the ratio $\left[(y_o)_a/(y_o)_b\right] \geq 0.63$, where $(y_o)_a$ is the actual radius of the cylinder and $(y_o)_b$ is the equilibrium value given by (37). It then follows readily from (37) that if there is a sudden change from ω_1 to ω_2 the bubble will not break up provided that $\omega_2/\omega_1 \geq 0.50$. In our experiments no instability was observed when ω was changed gradually or kept constant. A sudden stop of the apparatus, however, often resulted in the break-up of the cylinder into two or more smaller drops in accordance with Rayleigh's theory[7, 8].

It should be remembered that ω is the speed of rotation of the drop. Because of buoyancy, the drop axis does not coincide exactly with the axis of rotation so that ω of the drop may be slightly less than that of the tube. Thus, by assuming $\omega_{drop} = \omega_{tube}$ an error may be introduced to yield a higher value of γ, which may explain why the values obtained were consistently higher than those by the ring and

pendant drop methods (Table IV). One would expect, however, that this error would disappear at high ω and/or η_2.

It should be pointed out that viscosity does not enter into the theory, although in a very viscous system it takes longer for the drop to reach its equilibrium shape. Thus this method is particularly useful for viscous systems where, by contrast, the more conventional techniques may not be applicable.

Two non-Newtonian aqueous systems, one pseudoplastic and the other viscoelastic, were briefly examined. After three hours' rotation at 2025 RPM an air bubble in a 0.1% solution of Carbopol 940 (Goodrich Chemical) reached a steady but not an equilibrium x_o which depended upon whether the final speed was reached by increasing or decreasing ω; this is presumably due to the high yield value of the pseudoplastic Carbopol solution. However, an air bubble in a viscoelastic polyacrylamide solution (2% Cyanamer P250, American Cyanamid) after three hours' rotation at 1530 RPM reached an equilibrium x_o from which γ was evaluated (Table III). Thus, this method may be applicable to viscoelastic molten polymer systems.

5. CONCLUDING REMARKS

Vonnegut[1] suggested that the method might be used to measure surface pressure-area curves of insoluble monolayers, since the surface area A of the drop given by

$$\frac{A}{a^2} = 4\pi \int_0^{Y_o} Y\sqrt{1 + (dX/dY)^2}\, dY \,, \qquad (45)$$

can be controlled by changing ω.

Substituting for dX/dY from (13) yields,

$$\frac{A}{a^2} = 4\pi \int_0^{Y_o} \frac{Y dY}{\left[1 - Y^2\left(1 - \frac{\alpha Y^2}{4}\right)^2\right]^{1/2}} \qquad (46)$$

and making the substitution

$$q = 1 - \frac{\alpha Y^2}{4} ,$$

one obtains

$$\frac{A}{a^2} = -\frac{4\pi}{\sqrt{\alpha}} \int_1^{q_1} \frac{dq}{(q^3 - q^2 + \frac{\alpha}{4})^{1/2}} , \qquad (47)$$

which integrates to[5]

$$\frac{A}{a^2} = \frac{8\pi}{\sqrt{\alpha(q_1 - q_3)}} F(k, \phi_1) , \qquad (48)$$

where the symbols have the same meaning as in (30).

When $cr^3 = 0$, the drop is spherical and $A/r^2 = 4\pi = 12.57$. For much higher values of cr^3 the area of the cylindrical drop is given approximately by

$$\frac{A}{r^2} = \frac{8\pi}{3} \frac{cr^3 + 1}{(cr^3)^{2/3}} . \qquad (49)$$

Thus, at $cr^3 = 29$, axis ratio x_o/y_o is 20, but the surface area has only doubled. The variation in surface area produced by changing the speed of rotation is therefore too small to be used in evaluating a surface pressure-area isotherm.

REFERENCES

1. Vonnegut, B., Rev. Sci. Instr. 13, 6 (1942).
2. Silberberg, A., Ph.D. Thesis, Basel University (1952).
3. Rosenthal, D.K., J. Fluid Mech. 12, 358 (1962).
4. Handbook of Chemistry and Physics, 40th Edition, Chemical Rubber Publishing Co., Cleveland (1958), p. 259.
5. Grobner, W. and Hofreiter, N., Integraltafel, Vol. I, p. 78, 3rd Edition, Springer Verlag, Vienna (1961).
6. Emde, F., A. M. Legendres Taflen der Elliptichen Normalintegrale, Konrad Wittwer, Stuttgart (1931).
7. Rayleigh, Lord, Proc. London Math. Soc. 10, 4 (1879).
8. Rumscheidt, F.D. and Mason, S.G., J. Colloid Sci. 17, 260 (1962).

LIST OF SYMBOLS

a	=	radius of curvature of the drop surface at the origin
A	=	surface area of the drop
c	=	a parameter defined by (11)
d_1, d_2	=	density of phase 1 (drop) and phase 2
Δd	=	$d_2 - d_1$
E, F	=	elliptic integral of the second and first kinds
G, H	=	defined by (40) and (41)
k	=	modulus of elliptic integral
p , p_o	=	pressure outside the drop; at $y = 0$
p' , p'_o	=	pressure inside the drop; at $y = 0$
q_1, q_2, q_3	=	roots of cubic equation (see 47)
r	=	radius of a sphere of the same volume as the drop
x, x_o	=	cylindrical coordinate; semi major axis
X	=	x/a
y, y_o	=	cylindrical coordinate; semi minor axis
Y	=	y/a
V	=	volume of drop
α	=	parameter defined by (10)
γ	=	interfacial tension
η	=	viscosity
θ	=	the angle between the normal of the interface at (x,y) and the negative x-direction
ρ_1, ρ_2	=	principal radii of curvature of drop surface
ϕ	=	amplitude of elliptic integral
ω	=	angular velocity